Semi-automated generation of personalised finite element lumbar spine models: a step towards a pre-surgery planning tool for spinal fusion

Nikita Ghosh

Supervised by Julie Choisne, Justin Fernandez, Peter Robertson

A thesis submitted in the fulfilment of the requirements for the degree of

Doctor of Philosophy

in

Bioengineering

Auckland Bioengineering Institute

The University of Auckland

Auckland, New Zealand

April 2024

Abstract

Degenerative Disc Disease is a musculoskeletal disorder often surgically operated using fusion implants and associated with high failure rates. Population based models can predict patient-specific bone geometry to better predict clinical outcomes. The lumbar spines (L1-L5), sacrum and pelvic surfaces were segmented from 100 healthy adult participants aged 16-84 years. A principal component analysis was performed on individual vertebrae (L1-L5), sacrum, pelvis, combined sacrum and pelvis and whole lumbar spine to capture the main modes of shape variation within the population. Consequently, a shape model was developed (for the individual vertebrae, sacrum, pelvis, and whole lumbar spine) to predict the bone geometry from the anthropometric and bone measurements. The predictive capability of statistical shape model (SSM) was computed with leave one-out- analysis. The results showed that the, SSM can predict the bone shapes with root mean squared error of 1.92 ± 0.68 mm (average across all the individual vertebrae), 4.28 ± 1.29 mm in the sacrum, 5.75 ± 1.76 mm in the pelvis and 9.21 ± 4.55 mm in the whole lumbar spine. The dice scores of the SSMs were 0.89 (average across all the individual vertebrae), 0.78 in the sacrum, 0.74 in the pelvis and 0.63 in the whole lumbar spine. The shape models developed in our study can characterize the bone shape variation and predict the personalized bone shape geometry within an adult healthy population without segmenting the bones manually.

The International Spine Study Group has reported that the success of the fusion surgery relies on maintaining the optimal values of spinopelvic parameters. Most spinopelvic parameters are measured on 2D sagittal/frontal X-rays pre-surgery. The information obtained from the projection of 2D angles is supposedly limited compared to the parameters calculated in 3D. Therefore, in our research also explored the difference between spinopelvic parameters measured on CT scans from 2D slices and the 3D reconstruction of the spine. Our results indicated that the calculated 3D angles were not statistically different to the 2D measured angles. Although the distances calculated from a 3D perspective were statistically different to the ones measured in 2D. Our study demonstrates the reliability of 2D measures from the surgeons when compared with the 3D reconstructions.

Since spinal fusion surgery is performed to restore the spine's natural curvature, we also wanted to investigate the correlation of sacrum, pelvis, combined pelvis and sacrum and whole lumbar spine shape with the 3D spinopelvic parameters. Our findings between the 3D sacropelvic parameter and sacrum shape suggest that sacrum width is moderately correlated with pelvic incidence (PI) angle and anterior

pelvic angle (APA). It was also found out that there is a moderate correlation between lumbar spine shape and sacropelvic parameters due to the structural complexity of the spine.

Our work also investigated the sex-related changes in the 3D spinopelvic parameters. The simple main effects analysis performed on our population indicated that sex did not have a statistically significant difference ($p = 0.909$) on all the spinopelvic parameters. However, statistically significant differences were found in APA, PI, and lumbar lordosis (LL) measurements between sexes.

We also developed a computationally time efficient 3D lumbar spine FE model which could help the surgeons in understanding the stress distribution in whole lumbar spine before surgery. Our model was validated in terms of bone, ligament, and intervertebral disc material property to provide a trade-off between accuracy and computational time. Moreover, the average Von Mises stress and stress pattern observed in our simplified FE model is consistent with the results observed in the detailed FE model. Therefore, our FE model has a good potential for clinical use.

Finally, in this thesis we developed a personalized, computational-time efficient 3D lumbar spine FE model from CT scans. This study will allow clinicians to investigate the detailed complex morphology and stress distribution in the patient's lumbar spine before surgery.

Acknowledgements

First and foremost, I would like to express my deepest gratitude towards my thesis supervisors Dr. Julie Choisne, Associate Professor Justin Fernandez, and Dr. Peter Robertson, for their valuable suggestion and guidance throughout my PhD journey. I am also highly indebted to my advisory committee, Dr. Joe Baker and Dr. Ju Zhang, for their invaluable advice, support, and encouragement.

I would also like to thank my co-workers in Musculoskeletal Modelling Group for lending their helping hand whenever needed. A huge thanks to all my friends – Amelia, Dwaipayan, Kiran, Kuntal, Poulamee, Joyce, Saheli, Nima, Haniye, Shima, Leyla, Ali, Vijaya, Kunal, Arpita for cheering me up whenever I felt exhausted, listening to all the presentations numerous times, and keeping me motivated.

I am also very grateful to each and every staff of Auckland Bioengineering Institute for helping me in each and every step of my PhD journey. I am very thankful to Callaghan Innovation, MedTech Center of Research Excellence, University of Auckland, and Auckland Bioengineering Institute for generously funding this project. I would also like to thank Mercy Hospital, Waikato Hospital, Wishbone Orthopaedic Research Foundation and Formus Labs for providing me with their datasets.

Finally, I would like to give my special thanks to my husband Kazem and my mom, dad and sisters for their love, care, tireless motivation, endless support, and patience throughout the process.

Contents

List of Figures

8

9

List of Tables

11

Chapter 1: Introduction

This thesis focuses on developing personalised 3D lumbar spine models by selecting bone landmarks from medical imaging and fitting a statistical shape model to generate a personalised spine finite element model without the need for lengthy bone segmentation. In the future, this work could be augmented to allow clinicians to visualise the detailed 3D morphology and stress distribution of the spine from CT scans before surgery.

Degenerative Disc Disorder (DDD) is a debilitating condition of the spine where patients usually suffer from chronic low back pain (LBP) and instability. The latest Global Burden of Disease Study reported that low back pain is the leading cause of living a disability-adjusted life (Murrie et al. 2003). According to research published in Annals of Translational Medicine (Wu et al. 2020), 7.5% of the world's population is affected by LBP. Almost 5-8% of community dwellers and 19% of working adults suffer from chronic Low Back Pain (Andersson 1999; Cassidy, Carroll, and Côté 1998; Elliott et al. 1999). Across all socioeconomic levels in New Zealand, this is one of the primary causes of health loss, an excess of 130 million is spent by the Accident Compensation Corporation (ACC). National Institutes of Health estimated that the total cost associated with this disease in the US is between $560- $635 billion annually (Institute of Medicine (U.S.), Committee on Advancing Pain Research 2011).

Common surgical treatment consists of replacing the degenerative disc with a fusion implant. Incorrect placement of the implant and inability of restoring the patients' natural lumbar spine curvature (lordosis) can lead to patients continuing to experience significant pain and failure of the adjacent discs due to changes in the axial loading of the spine (Ghiselli et al. 2003; Okuda et al. 2004; Rothenfluh et al. 2015). Spinal fusion has a relatively high failure rate (reportedly up to 40%), although only 25% of failures may be revised (Martin et al. 2013). Patients with unrevised failed surgery face long term health issues, with associated economic burdens (Farcy and Schwab 1997; Martin et al. 2013; Pekkanen et al. 2013).

Computational modelling can predict clinical and functional outcomes but is highly dependent on the complex geometry of the musculoskeletal system and the ability to describe patient-specific loads and boundary conditions.

Finite element modelling is an attractive alternative to in-vitro experimentation and an accepted method in evaluating medical implant performance, and surgery planning and carrying out fundamental research (Guan et al. 2006; Shirazi-Adl, Shrivastava, and Ahmed 1984). Some researchers previously developed FE models using a generic model which supposedly represents every individual (Charriere, Sirey, and Zysset 2003; Guan et al. 2006; Haq et al. 2020; Nicolella and Bredbenner 2012). However, the spine geometry varies significantly among people (Vresilovic et al. 2012, Rohling et al. 2013, Campbell et al. 2016). To overcome the issue of one size fits all, other researchers have developed patient-specific detailed FE models from patient medical images (mainly for research purposes) which can become very time-consuming and expensive to use in the clinic. To address the issue of manually segmenting bone for every patient within a population, probabilistic methods such as Statistical Shape Modelling (SSM) may be employed to characterize the shape variations described by a set of landmark points (Campbell and Petrella 2015, 2016).

SSM has great potential for characterizing different anatomical variations in many parts of the body (Bischoff et al. 2014). SSM has been extensively applied to the femur (Zhang et al. 2014), knee (Baldwin et al. 2010), pelvis (Meller et al. 2004), tibia and fibula (Nolte et al. 2020) with an average Root mean square error (RMSE) ranging from 0.52 to 2.95mm. Similarly, in the lumbar spine some SSM were developed to 1) provide detailed 3D anatomical variation of the intervertebral lumbar disc shape (Vresilovic et al. 2012), 2) characterize the lumbar spine curvature in the sagittal plane (Boisvert et al. 2008, Ali et al. 2012), 3) accelerate the medical imaging segmentation process (Rasoulian et al. 2013) and 4) characterize the 3D lumbar shape and alignment variability (Hollenbeck et al. 2018). Hollenbeck et al. (2018) performed a SSM separately on each lumbar vertebrae on 11 healthy participants aged 20 to 58. In this study, the shape of the entire lumbar spine (L1-S1) and functional spinal units (L4- L5 and L5-S1) were also characterized. They obtained a root mean square error of 1.06 ± 0.19 mm for the SSM of individual bones and 1.42 ± 0.27 mm for the whole lumbar spine. The main limitation of their study was the limited number of participants and the age restriction which was not representative of the population who would usually receive surgery.

Lumbar lordosis, pelvic incidence and other sacropelvic parameters are quantitatively measured by clinicians on 2D sagittal and frontal X-rays before surgery. The information obtained from the projection of 2D angles are supposedly limited compared to the parameters calculated in 3D. Moreover, the success of the surgery depends on restoration of global sagittal balance (Farcy et al. 1997). Some studies (Schmidt et al. 1992; Vialle et al. 2005) have reported that the global sagittal balance is highly correlated with the optimal values of the patient-specific spinopelvic parameters. Prior works (Boulay et al. 2006; Janssen et al. 2009; Mac-Thiong et al. 2011) have also investigated the influence of sex on the spinopelvic parameters. Therefore, one aim of our study was to understand the difference between 2D and 3D sacropelvic parameters. Another aim of our study was to understand the influence of lumbar spine shape in the 3D spinopelvic parameters. Consequently, we also quantified the sex differences in the 3D spinopelvic parameters. Finally, we predicted the whole lumbar spine personalized shape integrating 3D spinopelvic parameters which can be used for finite element simulations later.

The overall aim of this project was to develop a personalized, computational-time-efficient 3D lumbar spine FE model from CT scans. This study will allow clinicians to investigate the detailed complex morphology and stress distribution in the patient's lumbar spine before spinal fusion surgery.

To achieve this aim, the objectives of this research are:

- Objective 1: To create a personalized, automated and population based whole lumbar spine model from an adult healthy population.

    o Objective a): To characterize the anatomical bone shape variation in a population-based model for the
        - individual vertebrae (L1-L5), sacrum and pelvis
        - the combined sacrum and pelvis
        - the whole lumbar spine

    o Objective b): To understand the accuracy of a population-based model for predicting the personalized bone shape for the
        - individual vertebrae (L1-L5), sacrum and pelvis
        - and the whole lumbar spine

14

- o Objective c): To investigate the differences between the spinopelvic parameters measured on CT scans from 2D slices and the 3D reconstruction of the spine.

- o Objective d): To understand the correlation between the 3D spinopelvic parameters and the
  - ▪ sacrum
  - ▪ pelvis
  - ▪ combined sacrum and pelvis
  - ▪ whole lumbar spine bone shape.

- o Objective e): To understand the effect of sex on the 3D spinopelvic parameters.

- • Objective 2: To create a computationally time efficient lumbar spine finite element model which could be used for clinical purposes.

  - o Objective a): To investigate the effect of vertebrae material property to provide a trade-off between accuracy and computational time.

  - o Objective b): To understand the influence of linear spring ligaments, non-linear connector ligaments and no ligament in our FE model.

  - o Objective c): To understand the implication of our FE model with and without modelling the intervertebral disc.

Chapter 2: Literature Review

This chapter focuses on outlining a detailed overview of lumbar spine anatomy, degenerative disc disease, treatment options for degenerative disc disease, population based modelling, and finite element modelling. The chapter also provides a summary of the current literature.

2.1. Lumbar spine anatomy

The human spine is an essential anatomical structure of our body which is composed of seven cervical vertebrae, twelve thoracic vertebrae, five lumbar vertebrae, and one sacrum vertebrae (five fused bones), and three to four fused coccygeal segments. It acts as a load-bearing structure and transfers load from the upper part of the body to the lower end with the help of the sacrum and pelvis. Each vertebral body is connected with spinal ligaments and intervertebral discs (Bogduk et al. 1991, Taylor et al. 2020).

The human lumbar spine is composed of five vertebrae (Gilchrist et al. 2003, Waxenbaum et al. 2023). Due to the wide range of motion in this area, the lumbar spine bears the majority of the upper body's weight, which can subsequently create stress on the structures and lead to chronic low back pain (Jayson et al. 1980, Adams et al. 2004).

The lumbar vertebrae consist of various components (Figure 1). In the anterior part of the vertebrae, the vertebral body is divided into the trabecular and the cortical bone. The cortical bone is stiff and dense, whereas the trabecular bone is composed of a sponge-like porous structure. The posterior part of the vertebrae consists of pedicle, lamina, transverse process and spinous process. From either side of the body, the pedicle projects backward. The laminae project backward from the pedicles and meet in the posterior part completing the vertebral foramen. The spinous process acts as a muscle attachment site, and it projects backward from the junction of the laminae. The transverse process projects laterally from the pedicles. The facet joints exist at the junction of pedicles and laminae. There are four facet joints located on the superior and inferior processes to the left and right of the vertebral body on each vertebra. The facet joints articulate with the adjacent vertebrae. The intervertebral discs are spongy cartilaginous pads. These connect the adjacent vertebrae and act like a shock absorber throughout the spinal column

16

(Figure 2). Spinal ligaments also play a significant role in the mobility of spinal motion (Kirby et al. 1989, Vaccaro et al. 2002).
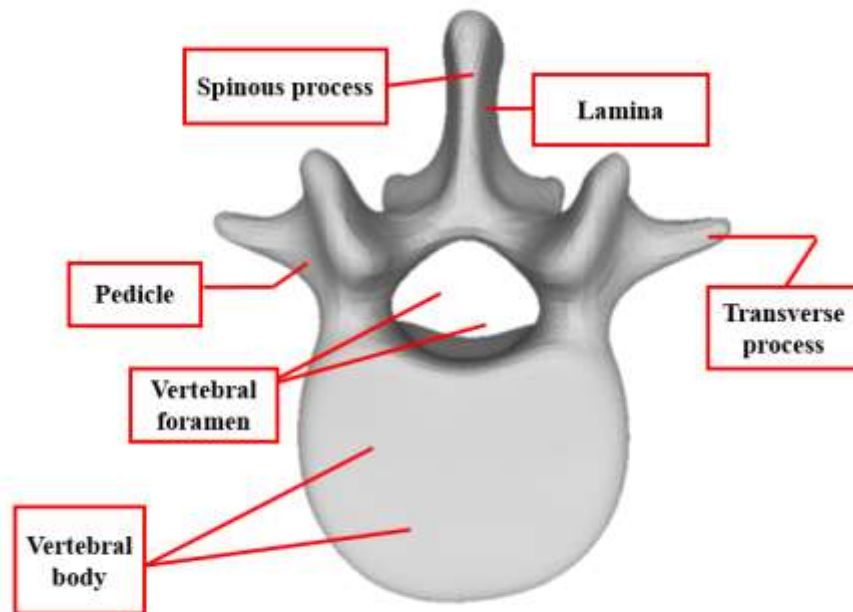
Figure 1:Superior view of human lumbar vertebrae (L1)
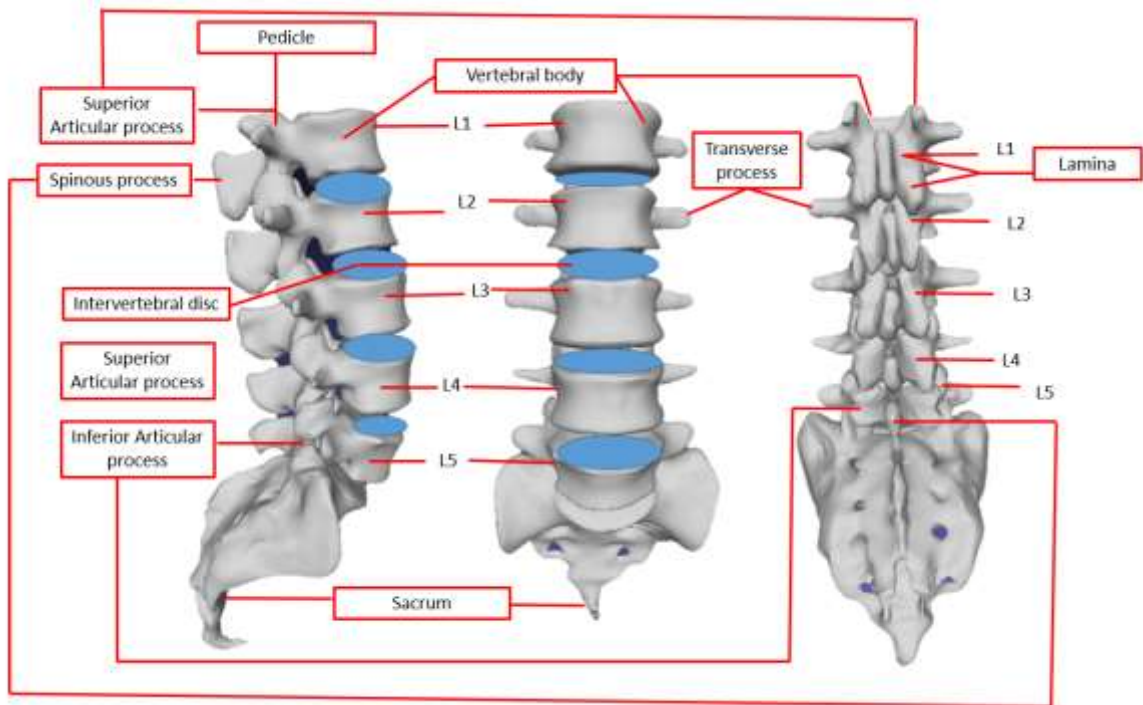
Figure 2: The sagittal, frontal, and posterior views of the lumbar spine (left to right)

2.2 Degenerative Disc Disease (DDD)

According to the North American Spine Society, degenerative disc disease is a clinical condition characterized by the manifestation of disc degeneration greater than expected, considering the age of the patient. The impacts of DDD and aging on the intervertebral disc are analogous. In the elderly population, the declination in the mechanical properties of the discs is very common. Ex-vivo experiments have shown that under the influence of excessive loading, the vertebral endplates collapse first rather than the intervertebral disc (Adams et al. 2004). So, a healthy disc can only be degenerated (fissures and herniation) under the combined application of excess compressive loads and bending (Adams et al. 1985).

During the early stages of disc degeneration, herniation occurs due to the decreased strength of the annulus fibrosis. The bulging of the nucleus pulposus and annulus tears through the annulus fibrosis wall can result in more pressure being applied to surrounding spinal nerves (Noailly et al. 2012). This "nerve pinching" mechanism is the primary cause of low back pain and it can be treated surgically. If the annulus tear is not too severe, then the nucleus pulposus can be substituted with a hydrogel substance which can

preserve the intradiscal pressure (Bernick et al. 1982; Adams et al.1985; Prescher et al. 1998). However, the use of artificial discs is becoming more common nowadays because of their ability to restore relatively more mobility compared to fusion.

2.2.1 Pathology of disc degeneration

The underlying mechanism and mechanical progression of disc degeneration are unknown. But some studies (Adams et al. 1985; Prescher et al. 1998, Meakin et al. 2001) have demonstrated that abnormal motion patterns and excessive loads accelerate the process. The pathological discs are classified according to the different grades depending on the severity of the disc degeneration. The most commonly used grading scale for the assessment of degeneration is the "Thompson Scale." This scale groups the progression of the morphological changes in the disc into four stages.

At Grade I, the nucleus pulposus exists as a bright viscous fluid at the centre of the disc, the annulus fibrous layers are clear and organized and the permeability of the cartilaginous endplates is high. Overall, it represents all the features of a healthy disc. In Grade II discs, in the nucleus, a slight discolouration is prominent. In Grade III discs, the boundary between the nucleus and the annulus cannot be observed, the endplates become calcified, and the annulus discs are disorganized and ruptured. In Grade IV, the different layers of annulus are non-identifiable, the nucleus and the annulus are unclear, and the height of the disc is also reduced significantly (Thompson et al. 1990).

The largest avascular tissue in the human body is the intervertebral disc. Therefore, slight disruptions to the tissue components can become very severe in the long-term due to healing difficulties. While fissures in annular lamellae are more common during the late degeneration stage, the mechanical strength reduction can cause herniation even at an earlier stage of disc degeneration. Osteophyte formation, progressive height declination of disc height and loss of integrity across the endplates can also be observed. Therefore, there is a high correlation between the morphological changes and mechanical behaviour of intervertebral discs.

2.2.2 Morphological changes in the intervertebral discs

The degeneration of the disc is initiated within the nucleus pulposus. Generally, the water content starts to decrease at the site of the nucleus, subsequently affecting the other parts of the intervertebral disc. In degenerated nucleus pulposus there are more metalloproteinases (MMPs), which enhances the breakdown of proteoglycans. Additionally, Type I collagen content increases and Type II collagen content decreases (Prescher et al.1998). Due to these significant changes, the nucleus resembles solid tissue. In the subsequent stages of degeneration, the difference between nucleus and annulus becomes indistinct.

The cartilaginous endplates are exposed to progressive calcification and also the function reduces to a drastic level. Fissures and cracks are observed along the end-plate surface. Nerve endings and blood vessels start to grow inside the disc due to limited osmotic transportation through the endplates (Bernick et al. 1982).

The water level in the annulus reduces in addition to enhanced cross-linking in collagen fibres. The reduction of water content and the breakdown of proteoglycans lead to loss of hydrostatic pressurization in the nucleus. As a result, the circumferential tension in the lamellae also reduces (Meakin et al. 2001). In the later degeneration stages, the annular lamellae disintegrate with rupture and buckling of the collagen fibre bundles. Moreover, the space between the discs becomes narrower due to the enhanced axial deformation.

Disc degeneration is often accompanied by osteophyte formation around the end-plate rim. Adams et al. (2011) mentioned this as a remodelling mechanism where these changes expand the end-plate's cross-sectional area and distribute the loads to a wider area. However, no consistent pattern can be observed by these mineralized tissues. Under compressive loads, these mineralized tissues aid in global resistance.

In summary, patients with DDD suffer from unstable motion, reduced disc height, herniation and bulging of the nucleus pulposus and nerve roots or spinal cord compression. For treating DDD the majority of patients are recommended to undergo non-invasive and traditional treatment options such as nonsteroidal

and analgesic medications and physiotherapy. However, if the low back pain persists and the quality of life of the patient is not improved, surgical interventions are needed.

2.3. Treatment

The most common surgical procedures for treating DDD are total disc replacement (TDR), dynamic stabilization and fusion (Don et al. 2008; Galbusera et al. 2011; Sengupta et al. 2004). Depending on the procedure, the disc is partially or fully removed and substituted with a bone cage to relieve the pressure on the spinal nerves and reduce pain. If the degeneration and instability are less severe, then a dynamic stabilization device is added to the disc to add some stability and unload the facet to minimize pain (Sengupta et al. 2004). Mostly the treatments are successful, but some complications can occur post-surgery.

2.3.1. Total Disc Replacement

The application of TDR has increased significantly over recent years because of its ability to restore the mechanical function of the disc. This allows the degenerated segment to return to its normal intervertebral space and range of motion. Currently, the best available ball on socket market designs is ProDisc (DePuy Synthes, Indiana, United States) and Charite (Johnson & Johnson, New Jersey, United States) (Dmitriev et al. 2008; Sinigaglia et al. 2009). These discs are made up of a polyethylene core which articulates with two metallic endplates. Several studies report that the efficacy of TDR is better than fusion (Tropiano et al. 2003, Huec et al. 2005; Shim et al. 2007; Bertagnoli et al. 2011). The Adjacent Segment Degeneration (ASD) occurrence after fusion surgery is also reported less in TDR (Dmitriev et al. 2008).

However, this approach has some limitations. A healthy IVD exhibits some axial compression properties, but the available implants used for this procedure have very high axial stiffness which can cause excessive compressive loading in the adjacent segments. Moreover, due to the free sliding of the articulating endplates over the core, bony endplates are prone to damage. It can also lead to over flexibility at the treated degenerated segment (Sinigaglia et al. 2009). The other most common complications are vertebral body damage, facet degeneration, pain at the facet joint and prosthesis migration. The over flexibility of the device can cause increasing loading at facets. Therefore, the location and proper size of the device

21

according to the patient-specific bone geometry is very important to minimize future complications (Siepe et al. 2006).

2.3.2. Spinal Fusion and Dynamic Stabilization Devices

TDR tries to restore the normal mobility of the spine but sometimes the instability in the degenerated section (pinched nerve, abnormal facet) of the spine causes excessive mobility. In this case, stability is provided to the affected area using fusion or dynamic stabilization devices (Bertagnoli et al. 2011; Bono et al. 2004, 2005).

For the last few decades in treating DDD, spinal fusion surgery has remained the gold standard with respect to surgical treatment options (Bertagnoli et al. 2011). The aim of this surgery is to add stability to the injured spinal segment using fusion devices. Currently, there are mainly two spinal fusion surgery approaches: posterolateral fusion and interbody fusion.

2.3.2.1. Posterolateral Fusion

 In the posterolateral approach, the posterior elements are targeted through a midline skin incision. Then the damaged portion which is putting pressure on spinal nerves is removed. This process is known as decompression. Finally, a graft from the iliac crest or allograft is placed over the intertransverse membrane and facet joint of the vertebrae. Titanium rods and screws are used to provide stability. Previously, posterolateral fusion was achieved without instrumentation, but current research shows that use of instrumentation promotes fusion (Bono et al. 2004, 2005).

2.3.2.2. Interbody Fusion

Interbody fusion, either posterior lumbar interbody fusion (PLIF) or transforaminal interbody fusion (TLIF), has few advantages over posterolateral fusion. PLIF or TLIF fuses the anterior column of the spine which supports 80% of the body load. Therefore, it can enhance the fusion rate compared to
22

posterolateral fusion. Additionally, this approach substitutes the IVD with a fusion implant which contains bone grafts to promote bone formation between the two vertebrae in order to fuse them, alleviating potential discogenic pain. This approach aids in indirect foraminal decompression, restoration of intervertebral disc height and preservation of lordosis to some extent.

A dynamic stabilization device is used to treat a segment having minor instability. Dynamic rods are made up of stainless steel, titanium or some flexible materials like polycarbonate-urethane to provide flexibility to the rod (Schmidt et al. 2010). These devices unload the discs and the facet joint which helps in relieving pain (Sengupta et al. 2004; Wilke et al. 2009). During the procedure, the IVD is replaced with a fusion implant. The dynamic cord joins the dynamic screws and limits spinal flexion, while the dynamic spacer limits spinal extension.

Over the past 15 years, spinal fusion devices have proven to be efficient in minimizing spinal pathologies. Some systematic reviews (Ghiselli et al. 2003; Adams et al. 2004; Pekkanen et al. 2013) show that patient-reported outcomes for fusion and structured rehabilitation are similar due to disc degeneration. One study showed (Mobbs et al. 2013) a rapid increase in lumbar spine fusion rates (336%) from 1996 to 2001 in the United States of America. Sinigagalia et al. (2009) also reported 49-88% good outcomes from fusion. The Swedish Lumbar Spine Study Group (SLSSG) showed that fusion patients had a 33% reduction in back pain score and a 25% decrease in disability measured using the Oswestry disability index (ODI) whilst the non-surgical group had 3-7% reduction in pain. Furthermore, the economic cost has also been lowered in the operative group when compared to long-term non-surgical treatment (Fritzell et al. 2001, 2004).

Even with these numbers, there is still disagreement about the spinal fusion surgery's efficiency based on reports on Adjacent Segment Degeneration (ASD) (Goel et al. 2005; Panjabi et al. 2007; Serhan et al. 2008). Lumbar fusion can reduce the range of motion in the degenerated segment and puts more stress on adjacent discs and facets which can lead to ASD. Some studies showed that the single level of posterior fusion accelerates the degeneration of adjacent segments (Okuda et al. 2004; Hyun et al. 2010; Rothenfluh et al. 2015). The occurrence of ASD depends on several factors such as fusion cage length, age of the patient and the condition of the adjacent segments.

The other complications are loosening of the cage, broken screws, improper placement of the cage, and number of fused segments, enhanced postoperative disc height and failure to restore the lordotic curve. Gillet et al. (2003) reported that in a population of 106 patients with a 2 to 15-year follow-up, 20% rate of ASD leads to revision surgery. The re-operation rate for 215 patients was 27.4% with a 6.7-year follow-up.

Spinal fusion with preserved sagittal balance has minimal complications during long-term follow-up (Hyun et al. 2010; Schwab et al. 2013). The efficacy of the surgery depends on the optimal values of sacropelvic parameters (Figure 3) such as pelvic tilt (PT), the sagittal vertical axis (SVA), sacral slope (SS), and the difference between pelvic incidence and lumbar lordosis angles (PI-LL) (Kim et al. 2007). It has been reported by the International Spine Study Group that the mismatch of these parameters leads to disability and high back pain scores. The patients who have PI-LL mismatch of more than 10 degrees are 10-times more prone to develop ASD. Therefore, Schwab et al. (2013) mentioned from their observation that restoration of the PI-LL mismatch should be the primary objective in the surgical management of adult deformity. If these factors are not considered during a fusion procedure, the patients are at greater risk of developing ASD.
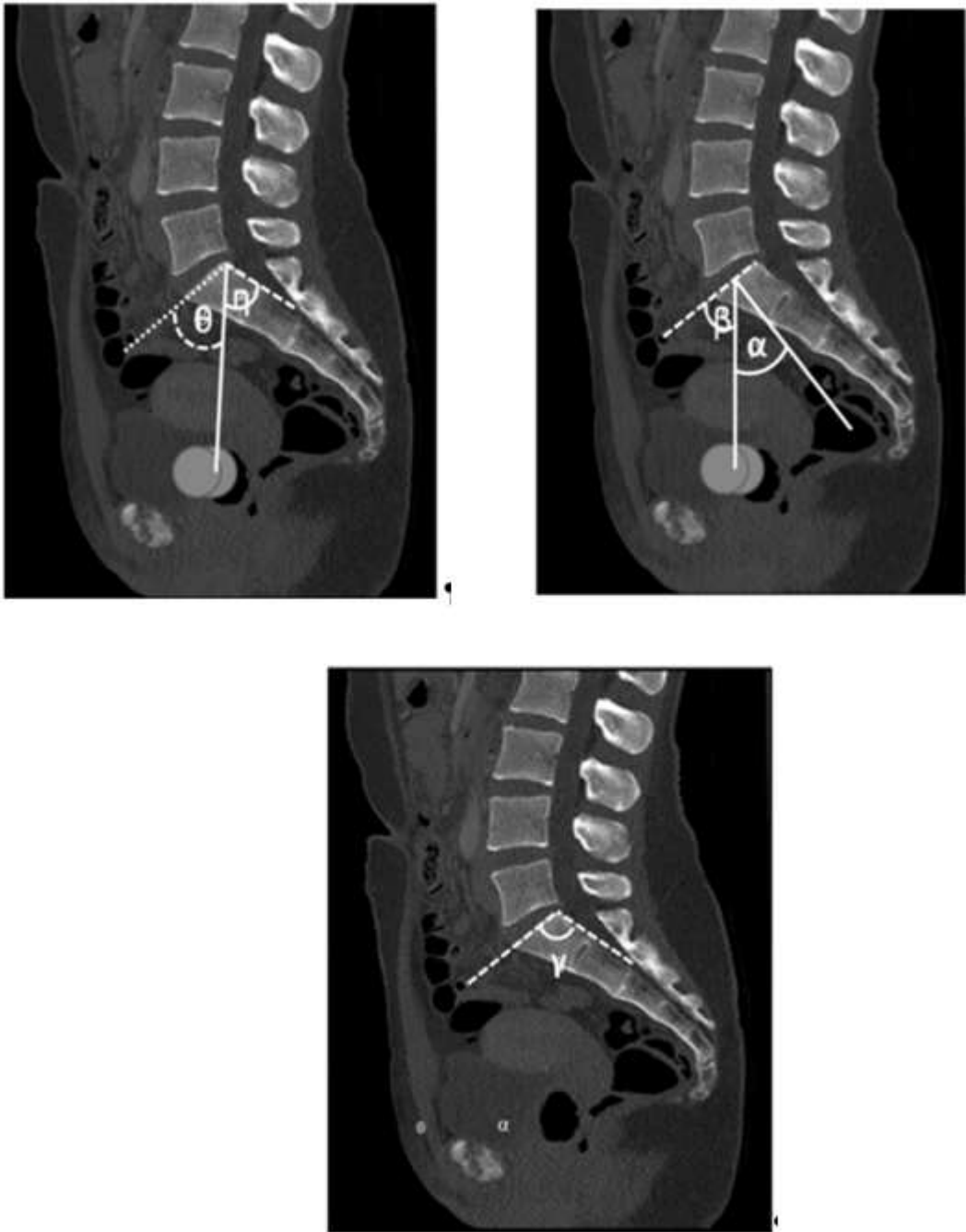
Figure 3: Sacropelvic parameters such as Sacropelvic angle (Ө), Femorosacropelvic angle (ŋ) Pelvic incidence (α), Pelvisacral angle (β) and Sacral table angle (Ɣ)

2.4. Sacropelvic angle and distances measurement

Generally, orthopaedic surgeons measure sacropelvic parameters such as PI, LL, PT, SS from two-dimensional (2D) sagittal/frontal X-rays in weight-bearing conditions before surgery. During 2D imaging, the sacropelvic angle measurements (pelvic incidence, sacral slope, acetabular inclination, introversion, and pelvic tilt) are majorly influenced by participant positioning and rotation of the radiographs. Due to a lack of standard pelvic positioning, participant mispositioning can lead to improper measurement of pelvic tilt or obliquity. Generally, in 2D radiographs, a point X-ray source is used for generating the projected image. The anteroposterior projection is often sensitive to rotation on the longitudinal and transverse axis. As a result, the lower part of the acetabulum is often misinterpreted as the posterior wall of the pelvis. Hence the determination of anteversion and retroversion angles becomes challenging (Janssen et al. 2009; Mellano et al. 2015). Through CT scans, it is possible to eliminate all the errors and quantify the detailed 3D structure of the pelvis and sacrum. Some studies were performed to find the correlation between the clinical parameters measured in 2D and 3D. Jozwiak et al. (2015) compared the 2D and 3D measurements of anteversion angle, inclination angle, and tilt angle in normal and spastic hip joints and found a negative correlation between 2D anteversion angle and 3D acetabular tilt angle. However, no correlation was observed between the 3D tilt and adduction angle measured on the 2D. This study compared the 3D measurements only with 2D angles in the frontal and horizontal planes. Since they could not find the 2D angle corresponding to the 3D inclination angle, the 3D inclination angle was compared with a 2D angle in the frontal plane. Therefore, the correlation was affected by the different axes of the angles. Imai et al. (2020) investigated the correlation between spinopelvic parameters and sacral slope in female patients with developmental hip dysplasia and concluded that the measurements were similar in 2D and 3D. Hu et al. (2021) analyzed the quasi-automatic 3D and 2D spinopelvic measurements in a large cohort and revealed the manual 2D measurements were consistent with 3D measurements. Hence the accurate characterization of the sacropelvic parameters according to each patient's geometry is vital to predict the surgical outcome (Jóźwiak et al. 2015; Rothenfluh et al. 2015, Imai et al. 2020). For quantifying the variability of the anatomical structure among a population, personalised models are developed.

2.5. Personalised Models

Traditionally most of the models developed in the literature use a generic patient model, which assumes one size fits all. However, these models are unable to capture the detailed complex biological structural information, and thus cannot make predictions about each and every patient (Sigal et al. 2010). There is an increasing need to analyze the variability of bone shape across the population due to age, ethnicity, gender, health condition, and other essential factors that can strongly influence pre-operative planning, diagnosis, postoperative care, and patient monitoring. Along with providing clinical insight, these models can also provide three-dimensional information about the bones. A personalised musculoskeletal model can be developed from CT or MRI images. However, generation of a personalised model is very time consuming and arduous. Statistical shape models (SSM) can produce an average shape along with the population's main modes of shape variation rapidly and accurately. By utilizing SSM, the shape of every individual within that population can be acquired by adding the contributions of the principal modes of variation to the average shape distribution (Cootes et al. 1995; Merck et al. 2008; Sigal et al. 2010).

2.6. Statistical shape models

SSMs were first introduced by Kendall (1977) and Bookstein (2006) that represent geometric objects in Euclidean space. Later Cootes et al. (1995) used landmarks to generate SSMs, which are widely used in medical image segmentation. SSM has excellent potential for characterizing different anatomical variations in many body parts. SSM has been extensively applied to the pelvis (Meller et al. 2004), knee (Baldwin et al. 2010), femur (Bryan et al. 2010; Nicolella et al. 2012), clavicle (Lu et al. 2013), cervical spine (Bredbenner et al. 2014), scaphoid (Bevers et al. 2021), thoracic spine (Wai et al. 2022), tibia, and fibula (Bruce et al. 2022) to predict these bone shapes within a population (average predictive root mean square error = 0.52-2.95mm) (Nolte et al. 2020). SSMs can be also used in organ tracking during surgery, orthopaedics implant designing (Cootes et al. 1995), finding the relationship between the function and the anatomical structures (Thompson et al. 2001, Merck et al. 2008) and finite element modelling (Campbell and Petrella 2015).

In the lumbar spine, some of the SSM models are developed to assess the effects of degeneration on the pre-testing of clinical devices (Sprent et al. 2006), to characterize the lumbar spine curvature in the sagittal

27

plane (Boisvert et al. 2008; Meakin et al. 2009), to provide intervertebral lumbar disc shape (Vresilovic et al. 2012), to accelerate the medical imaging segmentation process (Rasoulian et al. 2013), to generate a subject-specific Finite element (FE) model of the lumbar spine (Campbell et al. 2016), to characterize the 3D lumbar shape and alignment variability (Hollenbeck et al. 2018) and to provide detailed 3D anatomical variations of individual lumbar vertebrae (Haq et al. 2020).

In previous studies (Campbell et al. 2016; Haq et al. 2020; Klop et al. 2021, Kassab-Bachi et al. 2022), statistical shape models developed for the clavicle, knee, pelvis, femur, tibia, fibula, patella, talus, calcaneum and spine were evaluated for accuracy based on model compactness, generalization, and specificity.

In the SSM studies, model compactness was estimated by analysing the ability of the model to describe shape instances by a minimum number of principal component (PC) modes. An ideal SSM generates large cumulative variance with very few PC modes. Meller et al. (2004) demonstrated that 95% variance of pelvis shapes could be obtained with the first 24 PC modes out of 39. Baldwin et al. (2010) reported that 96% of shape variations in the knee was described by the first five out of 10 modes. Rasoulian et al. (2013) found that out of 31 modes, 25 modes were adequate to capture 95% of shape variations in L1-L5 vertebrae. Peloquin et al. (2014) reported that six PCs out of 12 were sufficient to accurately capture the shape variations of the L3-L4 IVD. Campbell et al. (2016) demonstrated 12 modes were sufficient to describe 95% of variations in L1-L5 out of 17 modes. Haq et al. (2020) observed in combined L2-L3 and L4-L5 vertebrae 95% variation described by the first 12 modes out of 20 modes. This study (Haq et al. 2020) also reported that 95% intervertebral disc (combined IVD at each level) variation shapes were captured by first 11 modes out of 40 modes. Klop et al. (2021) found out that the first 10 modes out of 25 modes captured 95% of the total variations of clavicle shapes. Bachi et al. (2022) investigated that first 64 PCs out of 152, describing 95% variation of L4-L5 segments.

Model generalization describes the ability of SSM to produce new shapes, which were not included in the SSM model. The model generalization was measured using leave-one-out cross-validation (Lorenz et al. 2000, Lamecker et al. 2004). For this type of validation, one training set observation was removed, and the model was recalculated with the other training sets. The new reconstructed model was then fitted to the left-out training set with an optimization method, and the Root Mean Square Error (RMSE) was calculated. In a study conducted by Rasoulin et al. (2013), the RMSE value of 1.4 mm for a L1-L5 model,

while using 10 modes was observed. Peloquin et al.(2014) reported RMSE value of 0.10 for the L3-L4 disc using 13 modes. Campbell et al. (2016) found that the RMSE value for a L1-L5 model was reduced from 3.65 ± 0.63 mm to 2.78 ± 0.45 mm while using 1 PC to 16 PCs. Haq et al. (2020) showed the RMSE value converged to 0.4 mm using 4 modes for L1, 0.58 mm using 17 modes for a L2-L3 model, 6.7 mm using 17 PCs for a L4-L5 model and 0.18 mm using 35 PCs for IVD. Bachi et al. (2022) demonstrated for a L4-L5 segment, with 30 PCs the RMSE value was 1.60 ± 0.34 mm.

Model specificity is the ability of SSM to produce valid shape instances. SSM model specificity was computed by measuring the RMSE between the randomly generated shape by the shape model and its closest training samples. Campbell et al. (2016) found the specificity value of a L1-L5 SSM model was 3.76 mm with 17 PCs and 3.11mm with 1PC. Audenaert et al. (2019) reported the specificity value of the pelvis, femur, tibia and patella were 2.05 ± 0.35 mm, 1.91 ± 0.28 mm, 1.36 ± 0.21 mm and 0.71 ± 0.11 mm, respectively. In the study of Haq et al. (2020) the specificity value of L1 was 1.43 mm with negligible standard deviation error. Bachi et al. (2022) obtained a specificity error of 3.00 ± 0.29 mm with 30 modes for a L4-L5 segment.

Prior works on the lumbar spine used SSM for characterising the variation in whole lumbar spine curvature (Meakin et al. 2001, Ali et al. 2012; Campbell et al. 2016) and individual vertebrae (Hollenbeck et al. 2018). However, these studies used a small sample size, a limited number of healthy participants and a restricted age range. An inadequate sample size might reflect an inaccurate representation of segment morphology variation. A small sample size can be more prone to sampling bias where specific subgroups can be overrepresented or underrepresented. Therefore, a power analysis should be performed for drawing any robust conclusion about the morphology differences. All of these studies on the lumbar spine SSM, required the prior identification of landmarks, which is labour-intensive. These limitations may lead to an inaccurate representation of morphological variations of the lumbar spine.

For restoring the sagittal alignment of the spine (after spinal fusion surgery), the relationship between pelvic incidence and lumbar lordosis is extensively studied in the literature (Hyun et al. 2010; Schwab et al. 2013, Aoki et al. 2015). To our knowledge, none of the previous works have focused on investigating the effect of other sacropelvic parameters on the lumbar spine shape. Previous studies have quantified the sex difference in lumbar lordosis (Murrie et al. 2003; Hegazy et al. 2014; Sudhir et al. 2015, Bailey et al. 2016) and some spinopelvic parameters (pelvic incidence, sacral slope, pelvic tilt, sacral orientation).

29

However, no studies have investigated the sex differences in femorosacropelvic angle, anterior pelvic angle, projection angle, pelvisacral angle, crest pubic, crest sacrum, inlet and outlet distances in adult healthy participants. Characterising the sex differences in the aforementioned spinopelvic parameters might provide detailed information about surgery planning.

In the lumbar spine, SSM is used to provide detailed information about the variation of bone morphology, lumbar shape, curvature, and intervertebral disc shape and it is used to generate 3D virtual geometry for Finite element analysis (Hollenbeck et al. 2018). Due to the complexity of the shape in the lumbar spine, developing a fully parametrized model has been always challenging (Dreischarf et al. 2014).

If a fully parameterized model of the lumbar spine can be developed with SSM, which can be used efficiently in a population-based simulation framework such as FE modelling, then it can help us analyze the relationship between shape variations and biomechanical function.

2.7. Finite Element Modelling

Finite element (FE) modelling of the spine is an attractive alternative to in-vitro experimentation and an accepted method in the evaluation of medical implant performance, surgery planning, and carrying out fundamental research (Shirazi-Adl et al. 1984, Rohlmann et al. 2006, Meijer et al. 2011). FE Modelling can help us to predict some important biomechanical parameters (internal stress within the tissues and implants) that cannot be measured directly by experimentation.

Previous studies-built FE models (Más et al. 2017) representing either a functional spinal unit (FSU) or a full lumbar spine depending on the model's purpose (Maurel et al. 1997; Wang et al. 2005, Rohlmann et al. 2006; Guan et al. 2006). Some FE models were developed to measure the range of motion of healthy lumbar vertebrae at different levels during flexion, extension, bending, and axial rotation (Mellano et al. 2015). Other FE models (L3-L5) were developed to investigate the difference in biomechanical effects between the healthy lumbar spine and a spine with dynamic fixation/PLIF/COFLEX on adjacent segments (Más et al. 2017, Fan et al. 2019). Different FE models analyzed the intradiscal pressure at the right and left facet joint force under different movements for exploring the effect of fusion on the adjacent intervertebral disc (Kuo et al. 2010). FE models also investigated the maximum displacement and stress-strain relation in the osteoporotic vertebral body and fractures on a single lumbar vertebral body (Chiang

et al. 2006). FEM was used to understand the effects of stress-strain distribution in the lumbar spine during fusion surgery with one vs. two cages (Chiang et al. 2006).

2.7.1. FE model of the lumbar spine

Several vital factors, i.e., spine geometry, bone mineral density and disc material property, boundary conditions, joint contact and load distribution need to be considered while developing an FE model. Creating a highly detailed finite element (FE) model of the lumbar spine involves managing a larger number of parameters and leads to increased model runtime. In response to this, we developed a lumbar spine FE model that balances simplicity with accuracy, ensuring computational efficiency and suitability for clinical applications. This was achieved by incorporating a less detailed FE model with more focus on the accurate prediction of stress-strain distribution in the lumbar vertebrae and behavior of intervertebral disc and lumbar ligaments, contributing to reduced computational time.

2.7.1.1. Meshing

In previous research, the different structures of the lumbar spine (vertebrae, endplates, and discs) were usually meshed using hexahedral (Buckley et al. 2007, Cells et al. 2016) or tetrahedral elements (Park et al. 2013, Coogan et al. 2016; Fan et al. 2019). Tetrahedral meshing is more automated and easier to generate, whereas hexahedral meshing requires manual intervention (Mathur et al. 2012). Tetrahedral mesh is more suitable for meshing complex structures with higher accuracy. However, linear tetrahedral elements are stiffer and more sensitive to volumetric and shear locking. In terms of convergence rate and computational cost, hexahedral elements are superior for simpler structures (Benzley et al. 1995; Tadepalli et al. 2011). Yet, hexahedral meshes are less accurate in terms of discretization of complex geometry. Mesh sensitivity analysis is important to understand the effect of different mesh nodes and element numbers in the simulation of the FE model. Previous researchers (Campbell et al. 2016; Fan et al. 2019) performed a mesh convergence study to examine the accurate mesh density. From convergence study, the mesh density was selected in such a manner that the disc pressure and facet force were not primarily impacted during flexion, extension, rotation, and bending.

For providing a quantitative comparison between hexahedral and tetrahedral meshing, studies have employed metrics such as mesh quality, element aspect ratio, and convergence rate (Campbell et al. 2016;

Fan et al. 2019). For instance, hexahedral meshes typically yield higher-quality elements with lower aspect ratios, leading to more stable simulations. However, tetrahedral meshes may exhibit higher element aspect ratios, indicating potential issues with element quality and simulation accuracy. Convergence rate, determined through mesh sensitivity analysis, also serves as a metric for assessing the effectiveness of each mesh type in capturing the mechanical behaviour of the lumbar spine under various loading conditions. By comparing these metrics between hexahedral and tetrahedral meshing approaches, researchers can determine the most suitable mesh type for their specific biomechanical modelling needs.

2.7.1.2. Material property assignment of the lumbar spine structure

2.7.1.2.1. Vertebrae

Vertebrae consist of two parts: cortical and trabecular bone. The cortical bone consists of the outer part of the vertebral body. Cortical bone is usually dense and has a material property typically ranging from 10,000 to 14,500 MPa with a Poisson's ratio of 0.3 (Nguyen et al. 2018; Park et al. 2013). Trabecular bone is made of a sponge-like porous structure. Various models have defined cancellous bone with a Young's modulus between 100 to 450 Mpa and a Poisson's ratio ranging from 0.2 to 0.3 (Nabhani et al. 2002, Jovanovic et al. 2010, Ayturk et al 2011). Depending on the application, previous studies have used different modelling approaches to model the vertebrae.

2.7.1.2.1.1. Homogenous material property assignment to the whole vertebrae

The primary challenge of assigning heterogenous material property to the vertebrae is meshing the cortical thickness, which is usually less than 0.4 mm (Goel et al. 1995). For the simplicity of modelling, Nabhani et al. (2002) and Shin et al. (2018) modelled the whole vertebrae with a homogenous bone material property (Young's modulus and Poisson's ratio).

2.7.1.2.1.2. Heterogenous material property assignment to the vertebrae

 The bony vertebrae are generally subjected to relatively minuscule strains (Dooris et al. 2001). Therefore, cortical and trabecular bone are modelled with either linearly elastic isotropic or poroelastic, material,

having different Young's modulus and Poisson's ratio (Charriere et al. 2003; Schmidt et al. 2007). The values used for Young's modulus ranging from 10,000 to 14,500 MPa for the cortical Bone and 100 to 450 Mpa for the cancellous bone (Harrysson et al. 2007; Mazzoli et al. 2009, Más et al. 2017). The Poisson's ratio is usually 0.3 to 0.45 and 0.2 to 0.3, respectively (Haddas et al. 2018).

2.7.1.2.1.3. CT-based material property assignment to the vertebrae

In previous studies, vertebral bodies were represented as material-mapped subject-specific bones from CT scans (Keyak et al. 1990, Crawford et al. 2003). In some studies, the Hounsfield unit (HU) is converted to bone mineral density using a density phantom. For assigning the material property of heterogeneous bone tissue from CT, an average value is computed at each element. Then the HU within the element volume is averaged. Then for each element, the value is obtained by converting the CT number to density and density to the Young's modulus relationship by Crawford et al. (2003).

2.7.1.2.2. Intervertebral discs

Intervertebral discs are made up of the nucleus pulposus and annulus fibrosus. Researchers have modelled the intervertebral disc in many ways. In some studies, the annulus fibrosus was modelled as a combination of annulus fibres and matrix in a composite structure. In these works, the annulus fibres are an anisotropic structure modelled either by truss elements or rebar elements with 8-16 layers of a criss-cross pattern at an angle ± 35 (Goel et al. 1995; Noailly et al. 2005, Jones et al. 2008). The ground substance of the annulus is either modelled by the Hyperelastic Mooney Rivlin (Noailly et al. 2005; Schmidt et al. 2007), Yeoh (Ayturk et al. 2011), Neo-Hookean (Rohlmann et al. 2009, Moramarco et al. 2010), or linear hypo elastic approach (Shirazi-Adl et al. 1994). On the other hand, the nucleus pulposus is generally represented by an incompressible fluid-filled cavity or linear elastic fluid. Shahkari et al. (2015) used the Holzapfel-Gasser-Odgen method to consider the hyperelastic anisotropic property of the disc. For understanding the effect of disc mechanics, disc degeneration, and intradiscal pressure changes, these models were developed.

2.7.1.2.3. Ligaments

Ligaments provide stability during wide-range movements of the spine. The lumbar spine includes seven ligaments: 1) the anterior longitudinal ligament (ALL), 2) the posterior longitudinal ligament (PLL), 3) the intertransverse ligament (ITL), 4) the interspinous ligament (ISL), 5) the supraspinous ligament (SSL), 6) the ligamentum flavum (LF), and 7) the facet capsulary ligament (FCL) (Figure 4). Among all these ligaments, the ITL does not have clear lateral and medial borders, and the collagen fibre of the ITL is not densely packed or oriented as the fibres of other ligaments (Shirazi-Adl et al. 1994). Consequently, the ITL is not usually considered as a true ligament and is rarely modelled.
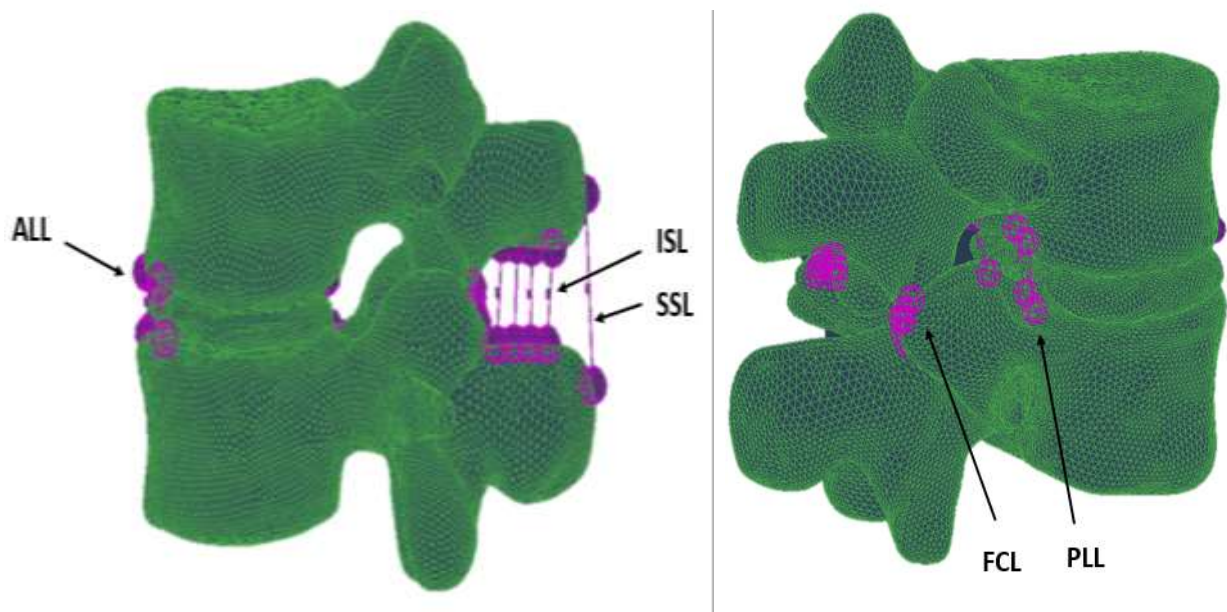
Figure 4:Lumbar spinal ligaments

2.7.1.2.3.1. Nonlinear spring/connector elements

In previous studies, the lumbar ligaments were modelled with uniaxial nonlinear tension only springs (Putzer et al. 2016, Fan et al. 2019) or connector elements (Guan et al. 2006, And et al. 2016). Based on the in-vitro experiments of the isolated ligaments and FSU, it is known that ligaments have a nonlinear toe zone following a nonlinear-linear transition in larger strains (Panjabi et al. 1982; Chazal et al. 1985,

Pintar et al. 1992). The material properties of the ligaments were obtained from the nonlinear force-displacement relationship of the ligaments. The force (F) in the ligaments can be obtained using the equation 1.

$$F = a \times \left(e^{(b \times (\in -c))}\right) - 1 \qquad (1)$$

where a, b and c values were experimentally obtained, and € indicates engineering strain.

The a, b, and c values for each ligament can be found in the Nolte et al. study (1990). Various groups (Panjabi et al. 1982, Chazal et al. 1985) frequently used these values to simulate the nonlinear property of ligaments during flexion, extension, rotation, and lateral bending.

2.7.1.2.3.2. Tension only truss elements

In some models, the lumbar ligaments were modelled using tension-only truss elements (Shirazi-Adl et al. 1984, Ayturk et al. 2011). The material properties were either nonlinear force-displacement or piecewise linear functions. Heuer et al. (2007) performed a stepwise reduction experiment to understand the effect of different bending moments on the range of motion on L4-L5 FSU by gradually removing the disc, facet joints, and ligament connections. Damm et al. (2020) followed the equation of Brown et al. (1996) to represent the nonlinear force-strain value (equation 2).

$$F(\in) = a \cdot \ln\left(e^{\frac{\in + b}{d}} + 1\right) \qquad (2)$$

where d = damping constant

Damm et al. (2020) performed a backward calibration of the stepwise reduction experiment to obtain the least square fit values of the ligaments.

2.7.1.3. Loading and Boundary conditions

During the modelling of the spinal segment, different loading and boundary conditions were applied according to the purpose of the model.

In some works, (Nabhani et al. 2002, Jovanovic et al. 2010; Hatira et al. 2012, Nguyen et al. 2018; Shin et al. 2018), a static axial compressive load is generally applied to the upper part of the individual vertebral body to replicate the upper body weight and muscle force (70% upper endplate, 30% upper articular facets). These studies mainly investigated the static stress-strain distribution in the lumbar spine. Under the load of 400N, Nguyen et al. (2018) reported that the maximum Von Mises stress obtained from L1, L2, L3, L4, L5 were 4.4., 4.77, 5, 3.77 and 2.75 Mpa, respectively. Under 450N load, Nabhani et al. (2002) found out that the maximum Von Mises stress in L5 was 1.92 and 1.91 Mpa, respectively. The highest displacements observed at L1, L2, L3, L4 & L5 were 0.01. 0.01, 0.0087, 0.0055 and 0.0045mm, respectively.

Also, in some previous studies (Shirazi-Adl et al. 1984, Puttlitz et al. 2011; Hatira et al. 2012; Park et al. 2013) a combination of moment and compressive load is also applied at the upper part of the vertebral body to investigate the range of motion throughout the whole lumbar spine during flexion, extension, left and right axial rotation and bending.

During these FE simulations, the lower part of the vertebral body is constrained in all six degrees of freedom. The sacrum is either constrained in all directions or acts as a rigid body. Kuo et al. (2010) demonstrated that during standing, under a load of 460N in L1, the Von Mises stress was increased steadily along L1-L5. The maximum Von Mises stress reported in L5 was 9.82 Mpa.

.

2.7.1.4. Validation of lumbar spine FE Models

Validation of lumbar spine FE models is a crucial step to assess the model's accuracy and reliability. Many researchers have validated their FE models prediction against the appropriate published experimental results. Driescharf et al. (2014) has compared the results of range of motion, facet force and intradiscal pressure from eight different published lumbar spine FE models against the experimental data. The median range of motion, facet forces and intradiscal pressures for all of these eight models were in good agreement with the ex-vivo studies. However, the maximum and minimum intradiscal pressure (IDP) and facet joint forces were not in the range of the published FE studies. Charles et al. (2013) have

validated their auxiliary facet system model's segmental range of motion, facet joint forces and Von Mises stress at the annulus with the experimental values. Chagnon et al. (2010) has validated the disc properties of their FE model against ex-vivo creep experiments to analyse different level of disc degeneration. Rohlmann et al. (2001) has validated the IDP in L1-L5 finite element models under the application of pure moments and a 280N follower load with the ex-vivo studies. Wilke et al. (2008) and Heuer et al. (2008) has validated the IDP obtained from the FSU sample with the ex-vivo values. The researchers concluded that the IDP obtained from the L1-L5 models and FSU samples are not similar. The mean IDP during flexion (7.5 NM) calculated from the FSU (Wilke et al. 2008) and from the L4-L5 from the whole lumbar spine FEM (Rohlmann et al. 2001) were 0.4 Mpa and .0.8 Mpa.

The previous studies (Boisvert et al. 2008, Ali et al. 2012, Hollenbeck et al. 2018) on SSM have characterized the shape and alignment variability of lumbar spines on a limited number of participants and their age range might not be representative of the population who would usually receive spinal fusion surgery. Therefore, our thesis aimed to develop a statistical shape model of each lumbar vertebrae, sacrum and pelvis individually and then combined lumbar spine shape to characterize the bone shape variation in a large number of healthy adult population. Moreover, this population-based framework can be used in Finite element study to understand the biomechanical behaviour of the spine. Detailed FE modelling of the lumbar spine translates to a larger number of parameters and enhanced model runtime.

In light of all these, we understand the need for developing a parameterized, robust, computationally time-efficient FE model and suitable for clinical use by modelling the intervertebral disc used to reduce computational time. In clinical applications such as surgical planning, time efficiency is vital since surgeons rely on accurate simulations to plan interventions. Therefore, the time efficient FE model allows for more dynamic and responsive planning. It will also facilitate computing the optimal spinopelvic parameters that need to be restored for pre-planning spinal fusion surgery.

In conclusion, our literature review highlights several gaps in the field that correspond to the aims of our research project. Firstly, while previous studies have developed lumbar spine models, there is a lack of personalized, automated, and population-based computationally time-efficient FE models derived from CT scans, particularly focusing on the entire lumbar spine including individual vertebrae, sacrum, and pelvis. This gap underscores the need to characterize anatomical bone shape variation in a population-based model and evaluate its accuracy for predicting personalized bone shape. Additionally, there is a lack of understanding regarding the differences between spinopelvic parameters measured on CT scans from 2D slices and 3D reconstruction, as well as the correlation between 3D spinopelvic parameters and

bone shape. Furthermore, the influence of sex on 3D spinopelvic parameters remains understudied. Secondly, while computational lumbar spine finite element (FE) models exist, there is a need for more time-efficient models suitable for clinical purposes. This involves investigating the effect of vertebrae material properties, understanding the influence of different ligament modelling approaches, and assessing the implications of modelling the intervertebral disc in FE simulations. These gaps in the literature emphasize the importance of our research objectives in addressing key challenges and advancing knowledge in the field of lumbar spine modelling for clinical applications.

Chapter 3: Material and Methods

This chapter describes the detailed methodology of our work from 3D lumbar spine reconstruction to statistical shape modelling, 2D to 3D sacropelvic parameter comparison, the correlation between bone shape and spinopelvic parameters and development of Finite element model (Figure 5).
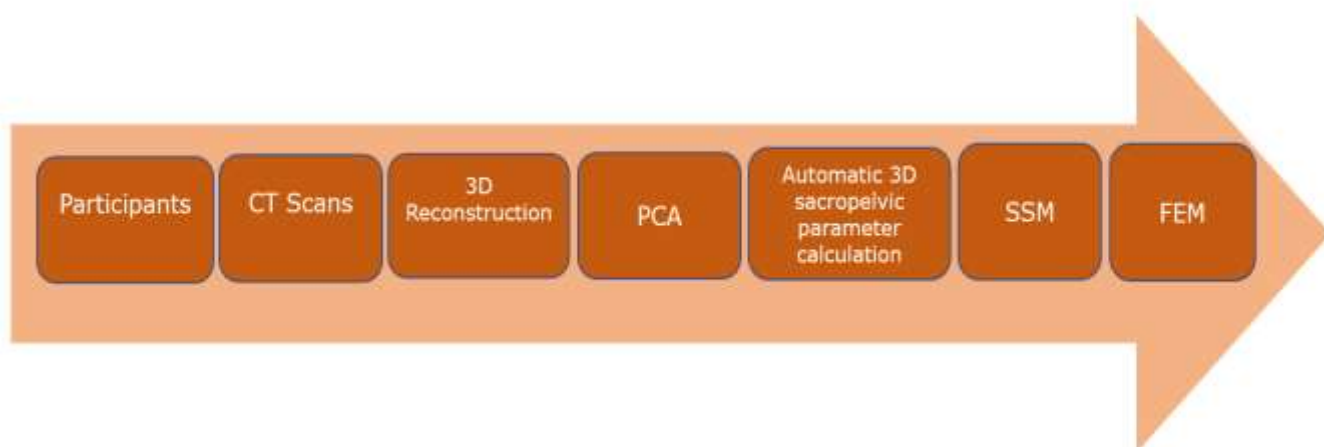
Figure 5: Workflow of the study

Where CT = Computed tomography, PCA = Principal component analysis, SSM = Statistical shape modelling, FEM = Finite element modelling

3.1. Participant Information

De-identified CT scans data from 100 healthy adult participants (64 males,36 female, age 16-84 years, 41 ± 16 years old) were collected at Waikato Hospital in New Zealand, with ethics approval (18/CEN/8) from Waikato hospital and the NZ Health and Disability Ethics Committee. CT scans for major trauma assessment were recorded with patients in supine positions. Only scans with intact spinal column and pelvis were included in the dataset. The scan range started from above L1 to mid-femur, including the

lumbar spine, the sacrum, and the pelvis. The slice thickness of each scan varied between 0.8 to 3 mm and the pixel spacing varied between 0.57*0.57mm to 1.27*1.27mm. An orthopaedic surgeon checked each CT scan and excluded patients with anatomical anomalies and previous surgeries from the analysis.

3.2. Lumbar spine reconstruction

A total of 40 healthy lumbar spines (L1-L5), sacrum, and pelvic surfaces were manually reconstructed from the participants CT scan dataset using Mimics (Version 21.0, Materialise, Inc., Leuven, Belgium). The rest of the participants (60) were segmented automatically by a machine learning algorithm (Deep Seg, developed in-house). The automatically segmented meshes were visually inspected and corrected, remeshed in case of abnormal bone reconstruction. Out of 480 automatically segmented bones, 352 were manually corrected in Mimics and remeshed in Materialise 3-Matic (Version 17.0, Materialise, Inc., Leuven, Belgium). To perform the manual segmentation in Mimics, several steps were taken. The segmentation process begins by loading the CT scan images in the Mimics software. Then. a grayscale threshold to the CT images were applied to separate bone pixels from other soft tissues and surrounding structures in the body (Figure 6A). Next, the mask created from the threshold was split into each specific bone, then manually edited in frontal (Figure 6B) or sagittal view (Figure 6C) to refine the segmentation boundaries and correct any artifacts. This involved removing unwanted regions and adjusting the boundary contours to better align with the anatomical structure of the desired region. With the interactive 2D views, in frontal sagittal and axial plane precise adjustment to the segmentation boundaries and structure were done more accurately. After the manual editing process the masks were smoothed and then wrapped to remove any holes in the mask and create a 3D surface (Figure 6D). Different smoothing and wrapping factors were used for each segmentation due to the varying CT scan parameters. However, it was ensured that every reconstructed bone was not very rough or over-smoothed, such that physiological features had not been neglected. Throughout the segmentation process each bone structure was visually inspected to identify any inconsistencies. Finally, the resulting 3D surface mesh built from Mimics provided detailed information about each structure.
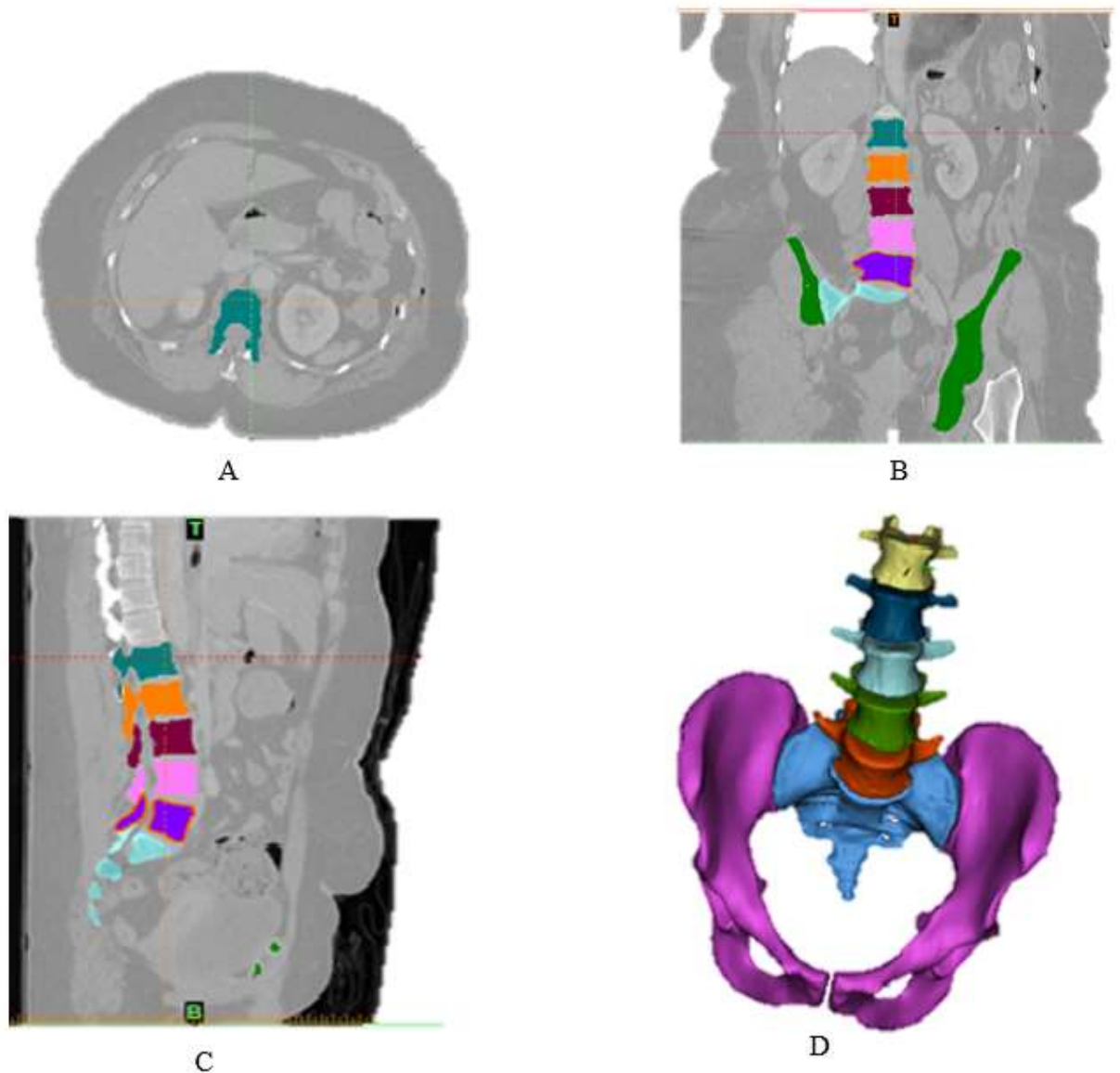
Figure 6: Segmentation of lumbar vertebrae and pelvis in Mimics 21.0

3.3. Template mesh generation and coordinate system assignment

The template meshes for each bone (L1 to Pelvis) were chosen as a mesh from all the participants in the dataset which has desired number of elements and node numbers. The template mesh is selected in such

a way that it can be fitted to a large range of meshes in our dataset. After the selection, the template meshes for each bone were converted to a 2D surface mesh of triangular elements of size 2mm (L1-L5, Figure 7) and 3mm (sacrum and pelvis, Figure 8) in Hypermesh (Version 17, Altair, Troy, MI). The element numbers of the L1 to L5 meshes were 7950, 8792, 8804, 9318 and 9786 respectively. The node numbers for the L1 to L5 meshes were 11318, 12449, 16629, 16363, and 17032 respectively. An example of the template mesh for L2 is shown in Figure 7. The element numbers for pelvis and sacrum were 32364 and 14926 respectively. The template pelvis and sacrum mesh are shown in Figure 8A, B, C and D. The fine template meshes ensured to capture the detailed anatomical complexity of the bones accurately.
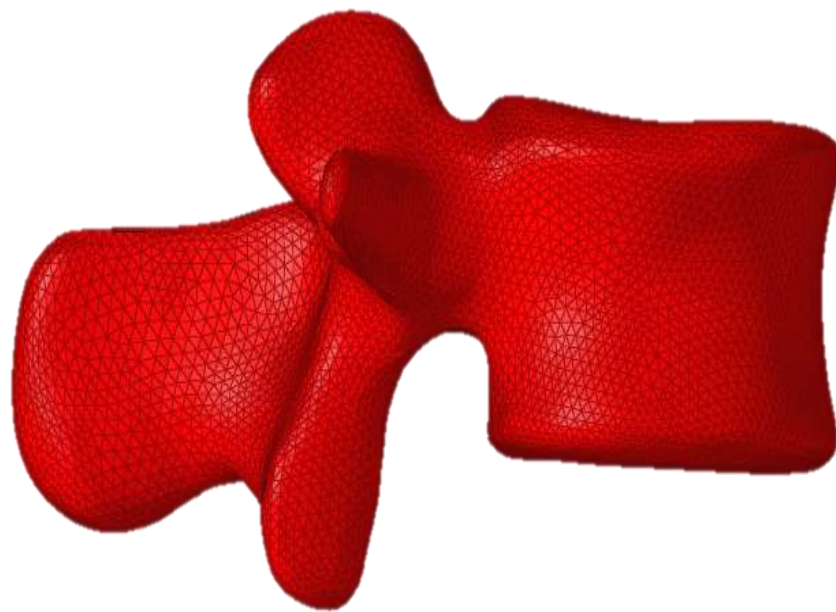
Figure 7: Remeshed fine template vertebrae (L2) in Hypermesh
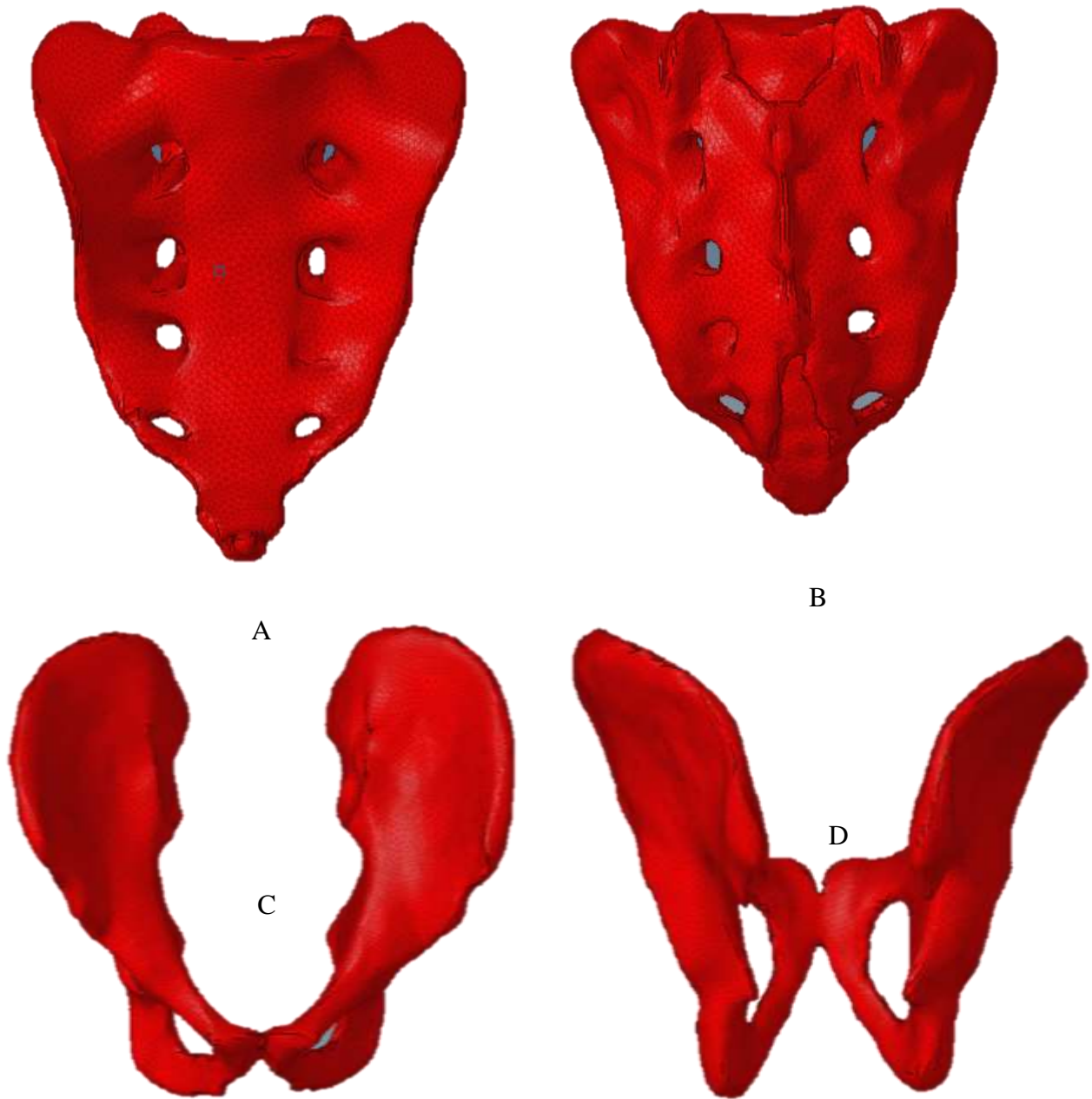
Figure 8: Template meshes of the sacrum anterior view (A), sacrum posterior view (B), pelvis anterior view (C) and pelvis posterior view (D) in Hypermesh where A-P = Anterior-posterior orientation, S-I = Superior-inferior, L-M = Lateral -medial orientation

For each template mesh, a bone coordinate system was assigned according to the International Society of Biomechanics (ISB) recommendation (Winther et al. 2002). For each vertebra, the origin of the coordinate system was fixed to the centre of the vertebral body. The Y-axis was built by creating a line joining the centre of the upper and lower plateau of the vertebrae, pointing superiorly. The centre of each plateau was found automatically with the help of a MATLAB (Version R2018A, MathWorks, Massachusetts, USA) script by fitting a circle in the upper and lower plateau. The Z-axis was developed by creating a vector passing through the centre of the left and right pedicles, pointing towards the right. The centre of each pedicle was found automatically with the help of a MATLAB script by fitting a cylinder in the pedicles. The X-axis was constructed by finding the cross product of the Y and Z-axis, pointing anteriorly (Figure 9A). For the sacrum, the origin of the coordinate system was fixed to the centre of the sacral endplate. The Z-axis was built parallel to the left and right posterior superior iliac spine (PSIS), pointing towards the right. The left and right PSIS landmarks were found automatically with the help of a Python, by obtaining the most superior left and right nodes in the PSIS region. The X axis was created by drawing a vector through the midpoints of the right and left PSIS and the sacral endplate centre, pointing anteriorly. The Y-axis was developed by computing the cross product of X and Z axis, pointing superiorly (Figure 9B). For the pelvis, the origin of the coordinate system was placed at the barycentre of the pelvis. The Z-axis was built parallel to the left and right anterior superior iliac spine (ASIS), pointing towards the right. The left and right ASIS landmarks were found automatically with the help of Python, by obtaining the most inferior left and right nodes in the ASIS region. For creating the X-axis, a vector was drawn through the midpoint of the left and right ASIS and the midpoint of the left and right posterior superior iliac spine (PSIS), pointing anteriorly. Similarly, the Y axis was built by calculating the cross product of X and Z axis, pointing superiorly (Figure 9C).
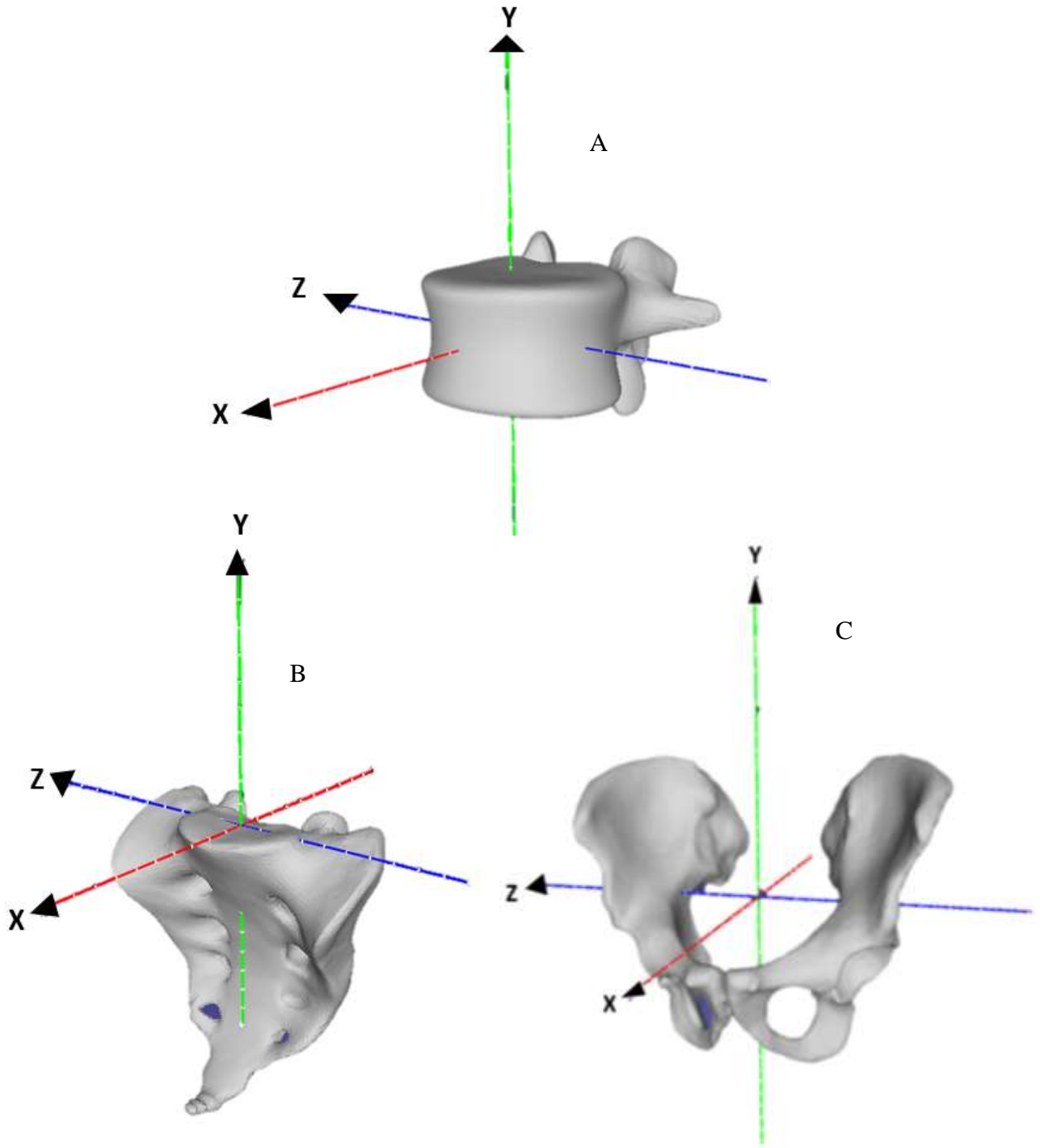
Figure 9: Template ISB bone coordinate system (Winther et al. 2002) vertebrae (A), sacrum (B), and pelvis (C) where A-P = Anterior-posterior, S-I = Superior-inferior, L-M = Lateral - medial orientation

3.4. Workflow of Principal Component Analysis (PCA)

Principal component analysis (PCA) is a statistical method, which is mainly used for dimensionality reduction. PCA converts a training set of shapes into a few important components called principal components (PC). The first PC accounts for the highest variability in the dataset, and each of the succeeding PC accounts for the lower variability than the preceding principal component. Therefore, any shape can be reconstructed by the combination of PCs. The main steps involved in PCA are:

1. Centering the Data: Before performing PCA, the mean of each feature (dimension) is subtracted from the data. This centers the data around the origin and ensures that the first principal component passes through the centroid of the data.
2. . Computing the Covariance Matrix: The covariance matrix is computed from the centered data. This matrix captures the relationships between different features in the dataset. The covariance between two features measures how they vary together.
3. Calculating Eigenvalues and Eigenvectors: The next step is to calculate the eigenvalues and eigenvectors of the covariance matrix. Eigenvectors represent the directions (principal components) along which the data varies the most, while eigenvalues indicate the amount of variance explained by each principal component.
4. Choosing Principal Components: The eigenvectors are ranked in descending order of their corresponding eigenvalues. The principal components are then selected based on the proportion of variance they explain. Typically, only a subset of the principal components (those with the highest eigenvalues) are retained, leading to dimensionality reduction.
5. Transforming the Data: Finally, the original data is projected onto the subspace spanned by the selected principal components. This transformation results in a lower-dimensional representation of the data, where the new axes (principal components) capture most of the variance in the original dataset.

For performing a PCA, an in-house open-source python library GIAS2 (Zhang et al. 2014) was used. PCA was performed first on each vertebra (L1-L5), sacrum and pelvis separately and second, on the whole lumbar spine and sacropelvic (L1-Pelvis) to quantify the shape variation among an adult healthy population.

3.4.1. Mesh fitting

The first step in the PCA was to non-rigidly register all the bone meshes (source mesh) to the template meshes (target mesh). After segmentation, the meshes obtained from Mimics were in each participant CT scan coordinate system. The template mesh was assigned to ISB coordinate system (Refer to Section 3.3). In order to bring the participant meshes and template meshes to a common coordinate system for analysis, mesh correspondence between source and target meshes was required. Therefore, a non-rigid registration in GIAS2 was achieved using the radial basis function (RBF). RBF is a meshless deformation technique where the registration error between the source and target meshes can be minimized using iterative knot placement (Zhang et al. 2018).

3.4.2. Alignment

The second step was to rigidly align all the source meshes to the template mesh coordinate system by aligning the meshes at their barycentre. For the whole lumbar spine, all the source meshes were aligned to L1's upper plateau 's center. Then, to reduce the translational and rotational variance between the template and target meshes, the rigid registration was performed in GIAS2.

3.4.3. Principal component analysis (PCA)

The last step was to perform the PCA on the aligned and fitted meshes. The PCA generates the mean shape of the bones, the percentage variation in each PC, and each participant's projected weights for each PC. The projected weights were later used as input to the statistical shape model.

3.4.4. Procrustes analysis

For removing the size variation in bone shape, we also performed a Procrustes analysis in the whole lumbar spine model using GIAS2. This analysis was carried out by isometrically scaling all the bones,

along the three axes. Then, a PCA was performed on the scaled bones. Procrustes analysis aids us in better understanding bone shape variation without considering the differences in bone size.

3.5. Statistical Shape Modelling (SSM)

After performing the PCA, we created a statistical shape model (SSM) for predicting bone shape geometry in our dataset.

3.5.1. Partial least square regression (PLSR)

A PLSR was used to predict the shape using demographic information to generate the SSM. PLSR is initially used for principal component regression in statistics. PLSR requires predictors to create a set of responses that provide the relationship between the predictors and the responses. For comparing the predictive capability of bone shapes with and without bone measurements for each bone, we developed two sets of SSMs (one with bone measurements and other without bone measurements). For the first set of SSMs, the predictors (input to the PLSR) were the demographic information of the participants (sex, age). For the second set of SSMs, the predictors were demographic information and bone measurements. The bone measurements included vertebral height, length, and width (for L1 to L5), the sacrum's S1 upper plateau length and width, and pelvic ASIS and PSIS distances. The vertebral length was measured with the help of a python script by computing the distance between the anterior and posterior points of the X-axis in upper and lower plateau of fitted meshless of each vertebra. The width of the upper and lower plateau was computed automatically from the fitted meshes by measuring the distance between the most medial and lateral point of the Z -axis. The height of the vertebral upper and lower plateau was obtained from the fitted meshes automatically by computing the distance between the midpoint of upper and lower plateau's center. For the sacrum, the sacral endplate length was obtained automatically from the fitted meshes by calculating the distance between the most anterior and posterior point in the X-axis. The width was obtained from the fitted meshes 'most lateral and medial point in the Z-axis. The left and right PSIS were computed automatically by obtaining the mot superior point in the Y axis of the fitted meshes. For the pelvis, the left PSIS and ASIS were automatically computed from the fitted meshes by obtaining the most inferior points of the left and right PSIS region in the Y axis (Refer to section 3.3). The responses (output of PLSR) to both set of SSMs were the participant-specific weights in each principal component's

direction. The predicted surface bone geometry was generated with the participant-specific weights (PLSR output) and the mean mesh (obtained from PCA).

3.5.2. Accuracy of SSM

To measure the accuracy of the SSM with bone measurements, we have computed the compactness, specificity, generality, and fitting error, adapted from Audenaert et al. (2019).

Compactness: This analysis determines how well the model can specify the maximum variation in the dataset while retaining the minimum number of principal components.

Fitting error: This analysis calculates the surface distance between the manually segmented and non-rigidly registered meshes.

Generalization: This analysis determines how well the model can predict the bone geometry outside the dataset. A Leave one out analysis (LOO) was used for this analysis. In each iteration, the shape model was trained using N-1 participants (N= total no. of the participants), and the model predicted the bone geometry of that left-out participant. Then, the node-to-node distance between the predicted and the aligned meshes were determined.

A root mean squared error (RMSE) was determined to measure the node-to-node distances. Also, the DICE score was used for the volume similarity comparison between the manually reconstructed and predicted shape (where zero means no similarity and one mean maximum similarity). A custom python script was used to compute these metrics.

3.5.3. Shape prediction of whole lumbar spine

3.5.3.1. Prediction using mean lumbar spine PCA, 3PCs and CT scan landmarks

In this method, we predicted the whole lumbar spine shape from mean lumbar spine shape along with 3 Pcs obtained from the PCA (Refer to section 3.4.3). In this process, the mean lumbar spine model's point cloud (source data) was fitted to participant's 3D anatomical landmarks (target data) along the first 3 Pcs. The 3D anatomical landmarks were the most anterior, posterior, lateral and medial points in the upper and lower plateau of each vertebra obtained from CT scans. The first three Pcs were selected (Grant et al. 2020) as it captures the maximum number of the unique weightings in the whole lumbar spine shape. During this process the distance between the source and target point clouds were reduced using the rigid body translation, rotation of GIA2. In this process, the whole lumbar spine shape was predicted from the mean point clouds and 3 PCs, without requiring the segmentation of the whole bone shapes. The predicted shape of whole lumbar spine was compared with the CT reconstructed whole lumbar spine in Cloud Compare (Version 2.6.1, Électricité de France, France).

3.5.3.2. Prediction using participant-specific bone measurements and lumbosacral angles obtained from landmarks

In this method, we predicted the whole lumbar spine with participant-specific bone measurements (upper and lower plateau length, width, height of each single bone) and lumbosacral angles (monosegmental lumbar lordosis angle, pelvic incidence angle and L5-sacrum angle) taken from the previous landmarks. In this process, PLSR was used to predict the whole lumbar spine shape. The input to the PLSR were the patient-specific bone measurements, lumbosacral angles, age, and gender of the participant. The output of the PLSR were the participant-specific weights in each principal component's direction. The predicted surface bone geometry was generated with the participant-specific weights (PLSR output) and the mean mesh (obtained from PCA). Then the predicted whole lumbar spine shape was again compared with the CT reconstructed shape in Cloud Compare.

3.6. 2D and 3D Sacropelvic parameters comparison:

3.6.1. 2D sacropelvic parameters

An orthopaedic fellowship-trained spine surgeon measured each participants' 2D sacropelvic parameters from their CT scan images such as anterior pelvic angle (APA), pelvic incidence (PI), sacral table angle (STA), projection angle (PA), femorosacral pelvic angle (FSPA), sacropelvic angle (PRS1), pelvisacral angle (PSA), crest-to-pubis distance (CPD), crest-to-sacral distance (CSD), inlet (ID) distance, outlet distance (OD) and inlet-outlet angle on the sagittal slices of the CT scan images (Figures 6-12). The 2D sacropelvic parameters were measured in Intellispace PACS Enterprise (Version 4.4, Philips, Amsterdam, Netherlands). The angles and distances were calculated on the midline sagittal image to identify the best-required landmarks. The centre of the femoral head or the anterior superior iliac spine was identified from the midpoint between the two lateral sagittal images and used to compute the required angles and distances. After measuring all the parameters, 20 scans were randomly measured again in a blinded fashion. To determine the reliability of the measurements, Cronbach's alpha was used. The sacropelvic parameters are defined below (Anon et al. 2016).

3.6.1.1. Bicoxofemoral axis: The line formed between the centres of both femoral heads.

3.6.1.2. Anterior Pelvic angle (APA): The angle (ψ) formed between the lines connecting the midpoint of the sacral endplate, bicoxofemoral axis, and the superior margin of the pubic symphysis (Figure 10).
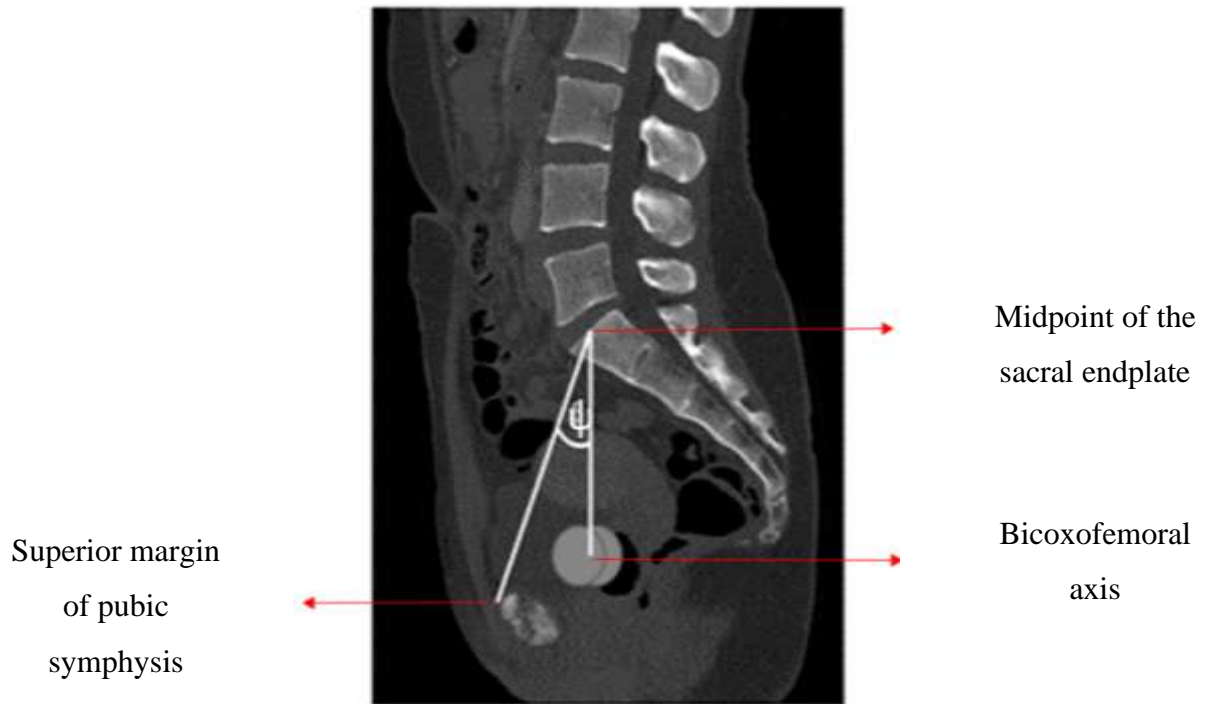
Figure 10: Anterior Pelvic angle is defined as ψ

3.6.1.3. Pelvic Incidence (PI): The angle (α) formed between the line perpendicular to the midpoint of the sacral endplate and the bicoxofemoral axis (Figure 10).

3.6.1.4. Pelvisacral angle (PSA): The angle (β) formed between a line tangent to the sacral endplate and the line through the bicoxofemoral axis and the middle of the sacral endplate (Figure 11).

Figure 11: Pelvic incidence (α) and Pelvisacral angle (β)

The sum of pelvic incidence and pelvisacral angle is always 90 degrees.

3.6.1.5. Sacropelvic angle (PRS1): The angle (θ) formed between the line joining the bicoxofemoral axis and the posterior corner of the S1 Vertebral body and the line running along the sacral endplate (Figure 12).

3.6.1.6. Femorosacral pelvic angle (FSPA): The angle (η) formed between the line running along the posterior corner of the S1 vertebral body and the bicoxofemoral axis (Figure 12).

Figure 12: Sacropelvic and Femorosacral pelvic angle

3.6.1.7. Sacral Table angle (STA): The angle (γ) formed between the line tangent to the sacral endplate and the posterior side of the S1 vertebral body (Figure 13).
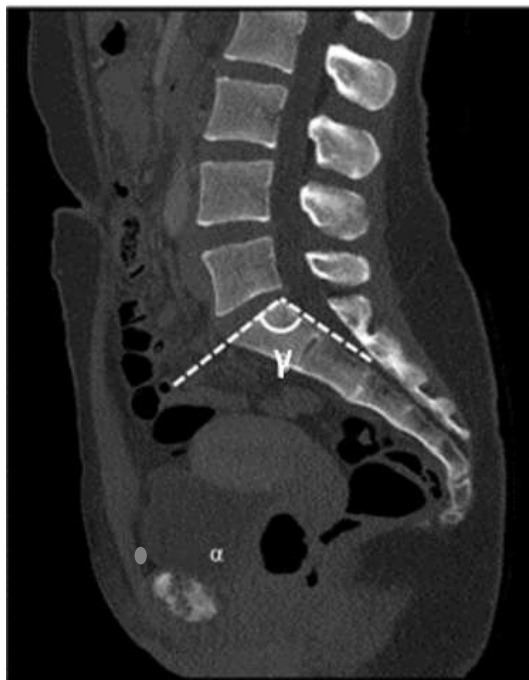
Figure 13: Sacral Table angle

3.6.1.8. Projection angle (PA): The angle (δ) formed by a line drawn from the apex of the pubic symphysis to the sacral promontory and a line drawn along the sacral endplate. A positive value is obtained when the line from the endplate is superior to the symphysis (Figure 14).
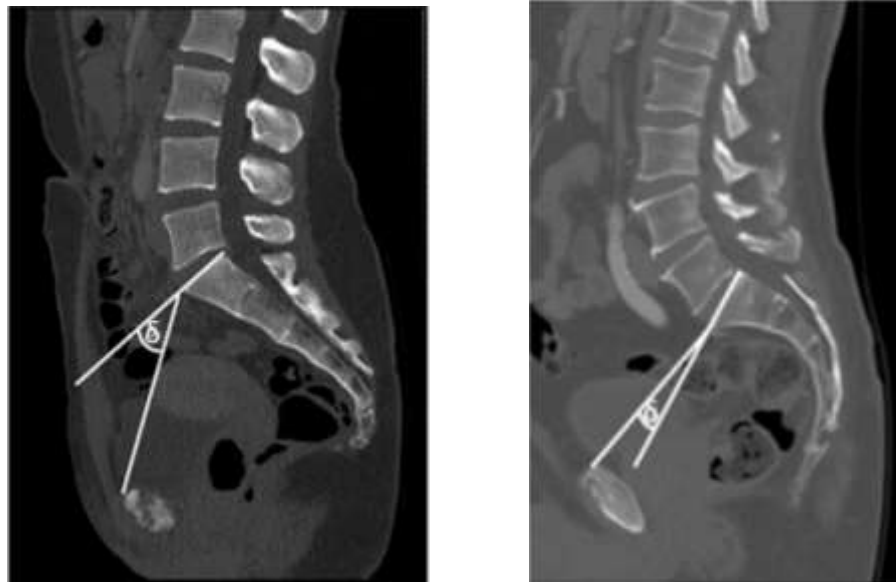
Figure 14: Projection angle positive value (left), negative value (right)

3.6.1.9. Crest-to-sacral distance (CSD): The distance (dashed line in Figure 15) from the anterior superior iliac spine (ASIS) to the posterosuperior corner of the S1 vertebral endplate.

3.6.1.10. Crest-to-pubis distance (CPD): The distance (solid line in Figure 15) from ASIS to the superior midpoint of the pubic symphysis. CSD and CPD are novel measures using ASIS as marker in the anterosuperior direction. The surgeon measured these angles to obtain an insight of pelvic depth in superoinferior and anteroposterior direction.

Figure 15: Crest pubic distance (dashed line) and crest sacrum distance (solid line)

3.6.1.11. Inlet distance (ID): The distance (solid line in Figure 16) from the anterior edge of the S1 vertebral endplate to the anterior edge of the pubic symphysis.

3.6.1.12. Outlet distance (OD): The distance (dashed line in Figure 16) from the anterior-superior edge of the apex of the sacrum to the anterior-inferior edge of the pubic symphysis.

Figure 16: Inlet distance (solid line) and outlet distance (dashed line)

3.6.1.13. Inlet-Outlet angle: The angle (£) formed by inlet and outlet distances (Figure 16). This angle is measured to understand the spatial orientation of pelvis in the sagittal plane.

3.6.2. Automatic landmark selection and the angle and distances calculation

Each manually reconstructed bone surface was fitted to template meshes and assigned the ISB coordinate system [2] (Section 2.3). For calculating the aforementioned sacropelvic angles and distances in 3-Dimension, the nodes corresponding to anatomical landmarks on the meshes were automatically selected. The template meshes of each bone (L1-pelvis) was split into different anatomical regions to find the anatomical landmarks needed to calculate the angles and distances. The manual selection of the nodes from the selected anatomical region (required to calculate the sacropelvic parameters) was performed in Blender (3.1, Amsterdam, Netherlands). The nodes number from the selected regions were then exported in a txt file. After that, a customized Python code was used to find each pelvic and sacrum landmark needed to automatically calculate the 3D aforementioned sacropelvic parameters from the fitted

participant meshes. Then, the angles and the distances were also calculated automatically from the obtained landmarks. Finally, the 3D measurements obtained from the code were compared with the 2D angles measured by the orthopaedic surgeon. Therefore, the aim of this study was to compare the sacropelvic parameters measured in 2D by the orthopaedic surgeon and 3D measured from the CT scan of the fitted meshes. The comparison was made using a paired t-test on each angle and distance using IBM SPSS Statistics 27 (Chicago, IL). Before performing the t-test, the required assumptions, such as continuity and normality of the variables, were satisfied by the Shapiro-Wilk test.

3.7. Understanding the correlation of pelvis, sacrum, combined pelvis and sacrum and whole lumbar spine shape with 3D sacropelvic parameters

De-identified CT scans from 100 healthy adult participants' (36 female, age 16-84 years, 41 ± 16 years old) whole lumbar spine (L1-pelvis) were collected and subsequently segmented using Mimics (Materialise, Belgium). Each bone surfaces were non-rigidly aligned to a template mesh's centre of mass and subsequently fitted to the same mesh. A Python code was developed to obtain the landmarks needed to calculate 3D SP parameters such Anterior Pelvic angle (APA), PI, LL, Projection angle (PA), Femorosacropelvic angle (FSPA), Pelvisacral angle, Crest Pubic distance (CPD), Crest Sacrum distance (CSD), Pelvic thickness (PTH), In-out angle, L5-Sacrum and Inlet, Outlet distances automatically from the fitted meshes. The projected weights from the PCA of individual sacrum, pelvis, combined sacrum and pelvis and whole lumbar spine were obtained (Refer to Section 3.4.3).

- o Sacrum: For understanding the correlation between sacrum shapes and 3D sacropelvic parameters a Pearson correlation coefficient (R) was determined from the PCA projected weights of the sacrum model and the calculated 3D sacropelvic parameters.

- o Pelvis: Similarly, a Pearson correlation coefficient (R) was determined from the PCA projected weights of the pelvis model and the calculated 3D sacropelvic parameters.

- o Combined Sacrum and pelvis: Moreover, a Pearson correlation coefficient (R) was determined from the PCA projected weights of the combined sacrum and pelvis model and the calculated 3D sacropelvic parameters.

   Since, the clinicians were interested to understand the correlation of the pelvis, sacrum and combined pelvis and sacrum bone shape with the 3D sacropelvic parameters, we obtained the R value for the statistical analysis.

- o Whole lumbar spine: For the whole lumbar spine, an unscaled model was developed previously (Refer to section 3.5.3.2). To neglect the size variation in the bone shape, a Procrustes analysis was also performed in the whole lumbar spine. Then, for obtaining a better insight of the influence of the 3D sacropelvic parameters on the whole lumbar spine shape (scaled and unscaled), a Coefficient of determination (R^2) were computed from the PCA projected weights from both models (scaled and unscaled) and the calculated 3D sacropelvic parameters.

3.8. Understanding the effect of gender differences in 3D sacropelvic parameters

The participants' CT scans of the lumbar spine (L1-Pelvis) was reconstructed using Mimics (Materialise, Belgium). Each bone surface was fitted to template meshes for nodal correspondence. Then, bone landmarks were automatically obtained from the fitted meshes by a python code and used these landmarks to calculate each participant's 3-Dimensional spinopelvic parameters. Spinopelvic parameters studied included: Anterior Pelvic angle (APA), Pelvic Incidence, (PI), Lumbar lordosis (LL), Projection angle (PA), Femorosacropelvic angle (FSPA), Pelvisacral angle, Crest Pubic distance (CPD), Crest Sacrum distance (CSD), Pelvic thickness (PTH), In-out angle, L5-Sacrum and Inlet, Outlet distances. To analyse the effect of sex on spinopelvic parameters, a one-way ANOVA test was performed between male and female 3D spinopelvic parameters.

3.9. Finite Element model (FEM)

The aim of this FEM study was to develop a personalised FE model of the lumbar spine. This model could be implemented in the clinic to determine vertebral stress distribution for pre-planning fusion surgery.

3.9.1 Finite Element Model Development

A 3D finite element lumbar spine (L1-pelvis) model of a 40-year-old healthy male subject was developed in ABAQUS® (Version 6.14-2; Abaqus, Inc., Providence, RI, USA). Each 2D template surface mesh (Section 2.3) from this participant was converted to solid volumetric tetrahedral mesh in Hypermesh (Altair, Troy, MI). Finally, the 3D meshes of the whole spine, pelvis, and sacrum were imported into ABAQUS® (Version 6.14-2, Abaqus, Inc., Providence, RI, USA) in an ABAQUS input file (.inp) format.

For our research, two FE models were compared in terms of average Von Mises stress, stress pattern and computational time. The first model (Model 1) consisted of L1-L2 functional spinal unit (FSU), intervertebral disc (IVD) and lumbar ligaments. Whereas the second model (Model 2) was constructed by removing the IVD to reduce computational time and replaced with contact-pressure overclosure relationship.

Each FE modelling components such as bone material property, ligament property and IVD was validated against the literature.

3.9.2. Bone material property validation

We used the participant's L2 geometry to validate the bone material property. We decided to use L2 for the bone material property validation as it was commonly used in previous studies (Jovanovic et al. 2010; Nabhani et al. 2002; Nguyen et al. 2018).

60

3.9.2.1. Material property:

For our FE modelling, we applied a linear isotropic elastic homogeneous material property of cortical bone where Young's modulus (E) value is 12 GPA, and the Poisson's ratio (v) value is 0.3 (Nguyen et al. 2018, Shin et al. 2018). Due to the absence of density phantom while obtaining the data, instead of dividing the vertebral body into cortical and trabecular bone, we assigned cortical bone material properties to the whole bone for simplicity and time efficiency.

3.9.2.2. Loading and Boundary conditions:

To represent the half upper body weight of a healthy adult subject of 100kg, an axial load of 400N was applied on the upper plateau of L2 and superior articular processes. Physiologically, the facet joints can withstand between 10% - 40% of the compressive load which is applied to the vertebrae (J.E. Crouch et al. 1978, Dunlop et al. 1984; Lavaste et al. 1992; Hall et al. 1995) . Therefore, to mimic a more realistic loading condition, 80% of the load was subjected to the L2 upper plateau, and 20% was subjected to the L2 superior articular facets. The lower plateau of L2 was constrained in all six directions (Figure 17). The loading and boundary condition was replicated from the literature (Nguyen et al. 2018).
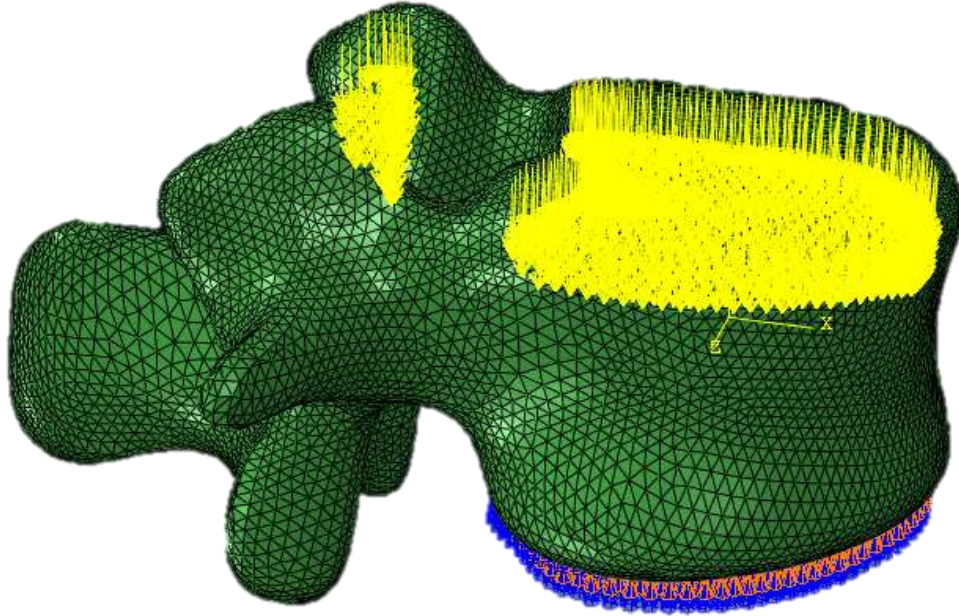
Figure 17: Loading & boundary condition of the individual vertebrae (L2) FE model

After carrying out all the previous steps, maximum Von Mises (VM) stress was extracted from L2, with the help of a python code and compared with the literature (Nabhani et al. 2002, Jovanovic et al. 2010; Nguyen et al. 2018).

3.9.3. Intervertebral disc validation

Regarding IVD validation, we built an FSU which consisted of L1-L2 including an IVD.

3.9.3.1. Material property:

In this work, the lumbar vertebral body was assigned to the same material property as above (Refer to Section 3.9.2.1). For modelling the IVD, the annulus fibrosis (AF), nucleus pulposus (NP) and endplates (L1 lower & L2 upper) were modelled separately (Kuo et al. 2010). The material properties of each component are listed in Table 1.

Table 1: Material properties of the FE model components

Components	Young's modulus (Mpa)	Poisson's ratio	Values taken from literature
Bone	12,000	0.3	Nguyen et al. 2018, Shin et al. 2018
Endplate	4000	0.3	Kuo et al. 2010
AF	4.2	0.45	Kuo et al. 2010
NP	1	0.49	Kuo et al. 2010

Where AF = Annulus fibrosis, NP = Nucleus pulposus

3.9.3.2. Interaction:

To analyze the accurate stress distribution between the vertebrae, accurate physiological interaction conditions were assigned between each bone. Since two adjacent vertebrae articulate with each other at the facet joint's junction, each vertebra's junction was specified as a surface in ABAQUS. To model the frictionless contact between the facet joints of each vertebra, surface-to-surface interaction was applied between them. The pressure-overclosure relationship defined the frictionless contact between the facet joints of L1 and L2 (Figure 16). For defining the surface-to-surface interaction between the L1-L2 facet joints, the right and left inferior articular surfaces of L1 were described as master surfaces and the right and left superior articular processes of L2 were defined as slave surfaces. For assigning the interaction between vertebrae endplates and IVD, the inferior endplate of L1 and superior surface of IVD and superior endplate of L2 and inferior surface of IVD were assigned to a 'Tie' constraint (Figure 18).
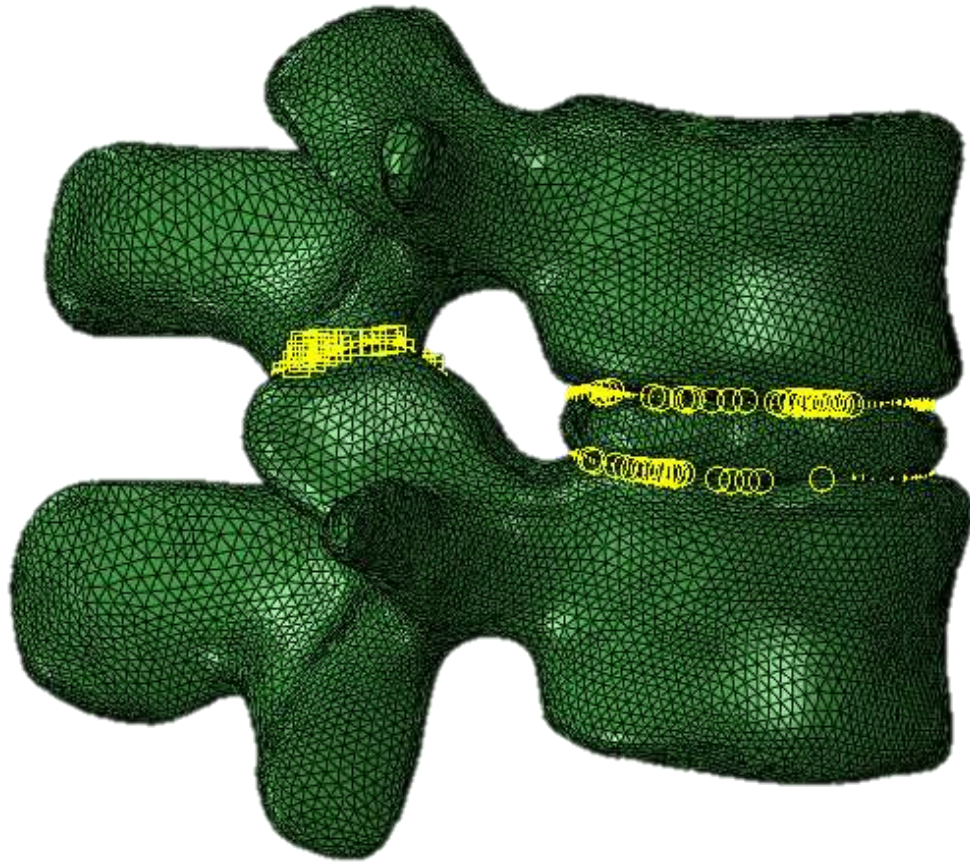
Figure 18: Interactions defined in IVD validation model

3.9.3.3. Loading and Boundary condition:

For evaluating the intradiscal pressures of L1-L2 disc in this study, the loading and boundary condition was replicated from the literature (Ranu et al. 1979, Shirazi-Adl et al. 1984, Kuo et al. 2010). An axial load of 300N, 460N and 600N is applied on the upper plateau of L1 to represent the upper body weight while standing. The lower plateau of L2 was constrained in all six directions (Figure 19).
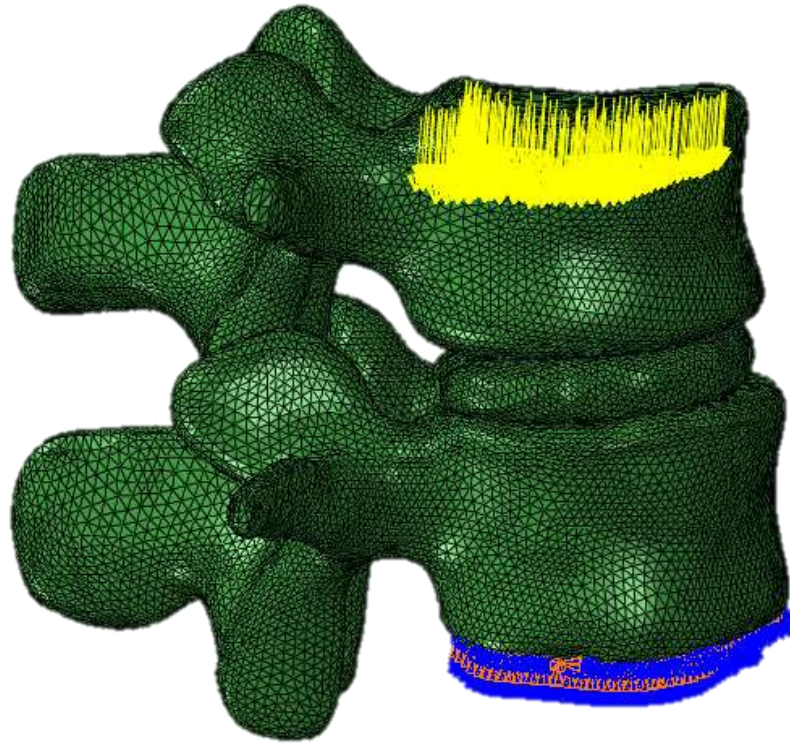
Figure 19: Loading and Boundary condition in IVD validation model

3.9.4. Lumbar ligaments validation

In our L1-L2 functional spinal unit, we have modelled the lumbar ligaments such as anterior longitudinal ligament (ALL), posterior longitudinal ligament (PLL), ligamentum flavum (LF), Interspinous ligament (ISL), and supraspinous ligament (SSL) at L1-L2 level (Devereaux et al. 2007). We did not include Intertransverse ligaments (ITL) in our FSU models, since it does not have distinct medial and lateral borders. Also, the collagen fibres in ITL are not oriented similarly to the other ligaments.

To understand the accurate behaviour of the lumbar ligaments, two different FE models were developed:

1. In the first model the ligaments were modelled as linear springs,
2. In the second model the ligaments were modelled as non-linear tension only connectors

3.9.4.1. Material property:

Both models were assigned the aforementioned bone and IVD material property (Refer to Table 1 in section 3.9.3.1).

Spring ligaments:

For this purpose, in one model the lumbar ligaments were modelled with linear springs (Pintar et al. 1992; Putzer et al. 2016). The ligament properties assigned to this model are described in Table 2.

Table 2: Lumbar Ligament's spring parameters at L1-L2 level

Ligaments	Stiffness at L1-L2 (N/mm)
Anterior longitudinal ligament	32.4 ± 13.0
Posterior longitudinal ligament	17.1 ± 9.6
Interspinous ligament	10.0 ± 5.0
Supraspinous ligament	23.0 ± 17.3
Ligamentum flavum	23.0 ± 7.8

Connector ligaments:

In the later model, the ligaments were modelled as tension only non-linear connectors. The properties of the ligaments (Table 3) were assigned according to the literature (Chazal et al. 1985). Physiologically, the ligaments' load-deformation curve has three distinct regions i.e., toe region, linear region and yield and failure region (Figure 20). In this connector model, we have considered the non-linear behaviour of ligaments to obtain more realistic outcome.
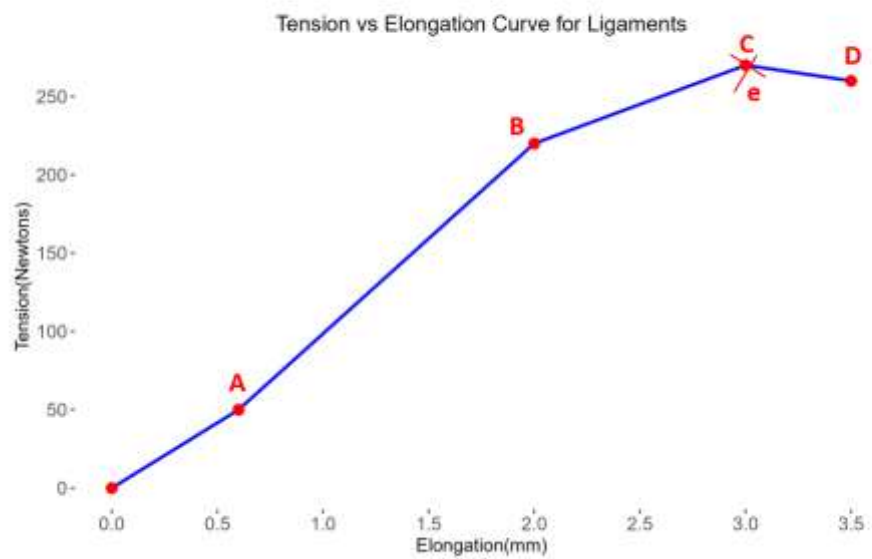
Where e= standard error

Figure 20: Tension elongation curve of lumbar ligaments

Table 3: Lumbar Ligament's connector parameters at L1-L2 level

Ligaments	Force at point A	Deformation at point A	Force at point B	Deformation at point B	Force at point C	Deformation at point C
Anterior longitudinal ligament	40	1	450	5.2	500	6
Posterior longitudinal ligament	30	0.8	360	3.6	390	5
Interspinous ligament	41	1	270	3.2	315	5.2
Supraspinous ligament	41	1	270	3.2	315	5.2

3.9.4.2. Interaction:

The interaction defined in these FE models (spring and connectors) were same as the IVD validation model (Refer to section 3.9.3.2). The only difference between these models is the ligament modelling approach as springs and connectors. (Figure 21 & Figure 22).
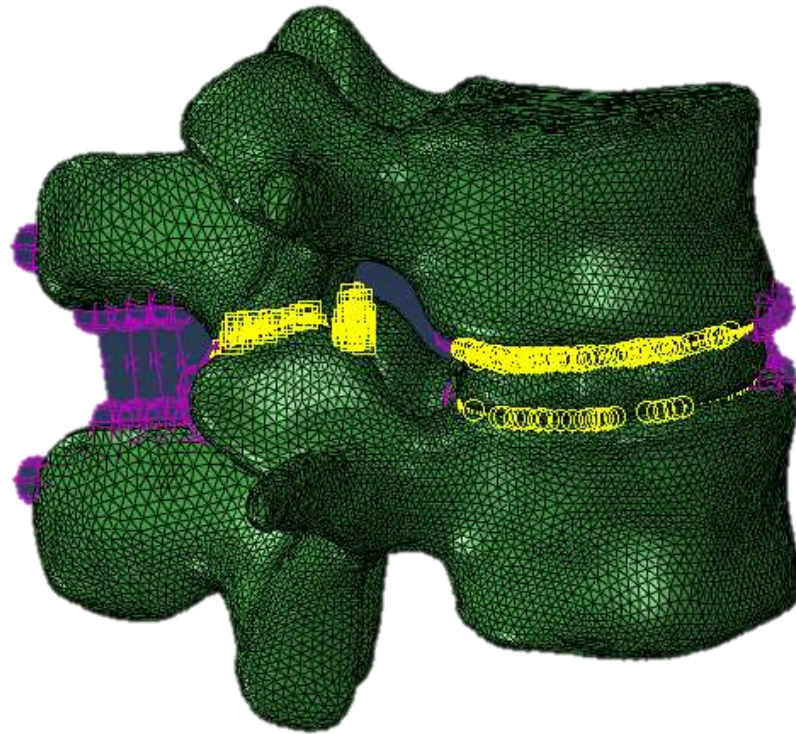
Figure 21: Interactions defined in linear spring ligament model
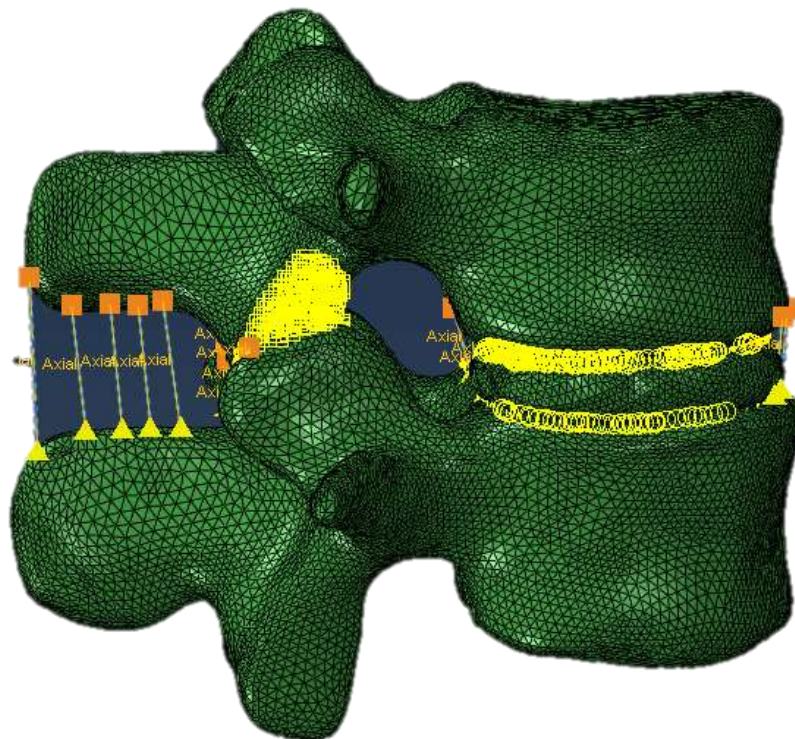
Figure 22: Interactions defined in non-linear connector ligament model

3.9.4.3. Loading and Boundary conditions:

For obtaining the accurate ligament property, the same loading and boundary condition was replicated described before (Refer to Section 4.2.2.3).

Finally, the intervertebral disc pressure (IDP) was calculated at L1-L2 level between the three models-

1. IVD validation model (without ligaments)
2. linear spring ligament model
3. non-linear connector ligament model

Then the IDP at these three models was computed with the help of a python script and were compared with the previous ex-vivo and FE studies (Ranu et al. 1979, Shirazi et al. 1994, Kuo et al. 2010).

3.9.5. Our Final validated FE model (L1-L2 FSU)

After validating the IVD and ligament property with previous studies (Ranu et al. 1979, Shirazi et al. 1994, Kuo et al. 2010). Model 1 was constructed with L1-L2 FSU, IVD, ligaments as connectors and Model 2 without the IVD and validated ligament property (Figure 23).
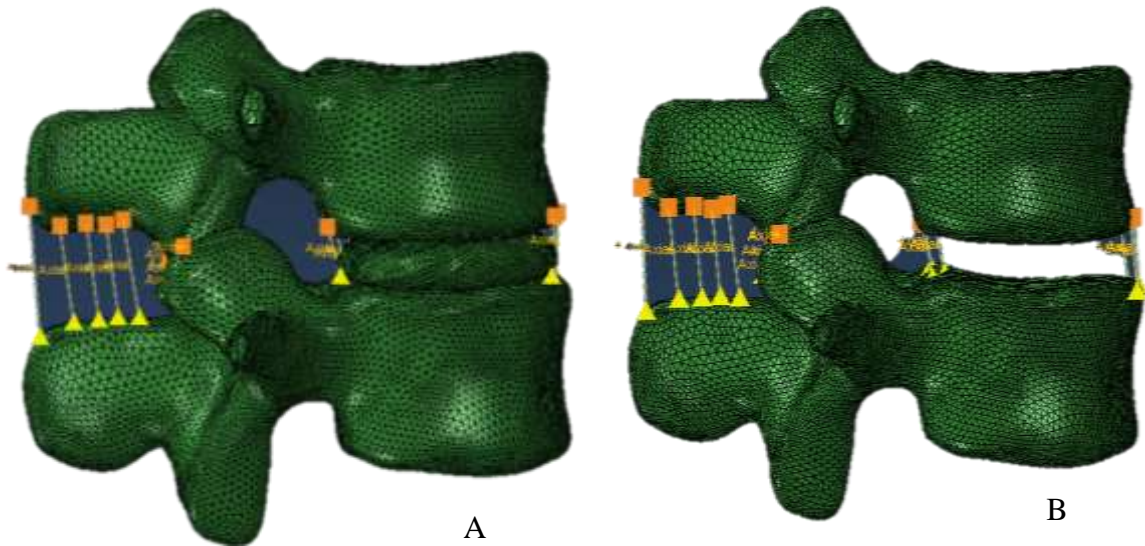
Figure 23: Geometry of Model 1 (A) and Model 2 (B)

3.9.5.1. Material Property:

In Model 1 and 2, the same material property was applied for the vertebral body and the lumbar ligaments modelled as connectors (Refer to section 3.9.2.1 & 3.9.4.1). In case of Model 1, the IVD was modelled similarly as described elsewhere (Refer to Section 3.9.3.1)

3.9.5.2. Interaction:

For Model 1 and 2, the interaction condition between the vertebrae facet joints were similar to previously described models developed for validation (Refer to section 3.9.3.2). In Model 2, instead of modelling the disc, we used the contact-pressure overclosure relationship between the inferior endplate of L1 and superior endplate of L2, to replicate the properties of IVD (Figure 24). A sensitivity study was performed to select the optimized stiffness and clearance parameters between each upper and lower endplate of vertebrae. This optimization was crucial for establishing a realistic contact pressure-overclosure relationship that accurately mimics the intervertebral disc (IVD) properties. The sensitivity study involved systematically varying the stiffness and clearance parameters while observing their impact on the contact pressure-overclosure relationship. This variation was performed in a controlled manner to assess how changes in these parameters influenced the model's response, particularly in replicating the

71

biomechanical behaviour of the IVD. The goal was to enhance the accuracy of the FE model by fine-tuning these parameters based on their sensitivity to variations, ultimately ensuring that the simulated behaviour aligns with the real-world physiological conditions.

<div align="center">A</div>
<div align="center">B</div>
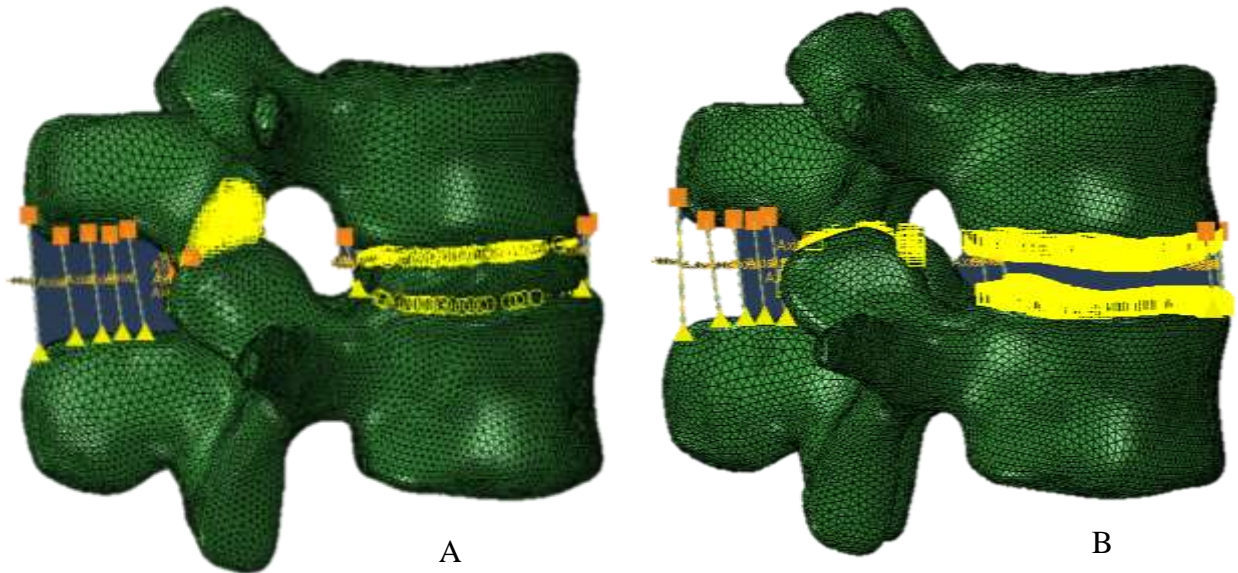
Figure 24: Interactions defined in Model 1 (A) and Model 2 (B)

3.9.5.3. Loading and Boundary conditions:

Then, the same loading and boundary condition was applied to both models (Model 1 and Model 2). For representing a subject with upper body weight of a 50kg, an axial load of 400N was applied on the upper plateau of L1 (80%) and superior articular processes (20%), which is aligned with the previous studies (Crouch et al.1978; Lavaste et al. 1992; Hall et al. 1995). To mimic a more realistic loading condition, 80% of the load was subjected to the L1 upper plateau, and 20% was subjected to the L1 superior articular facets. The lower plateau of L2 was constrained in all six directions (Figure 25).
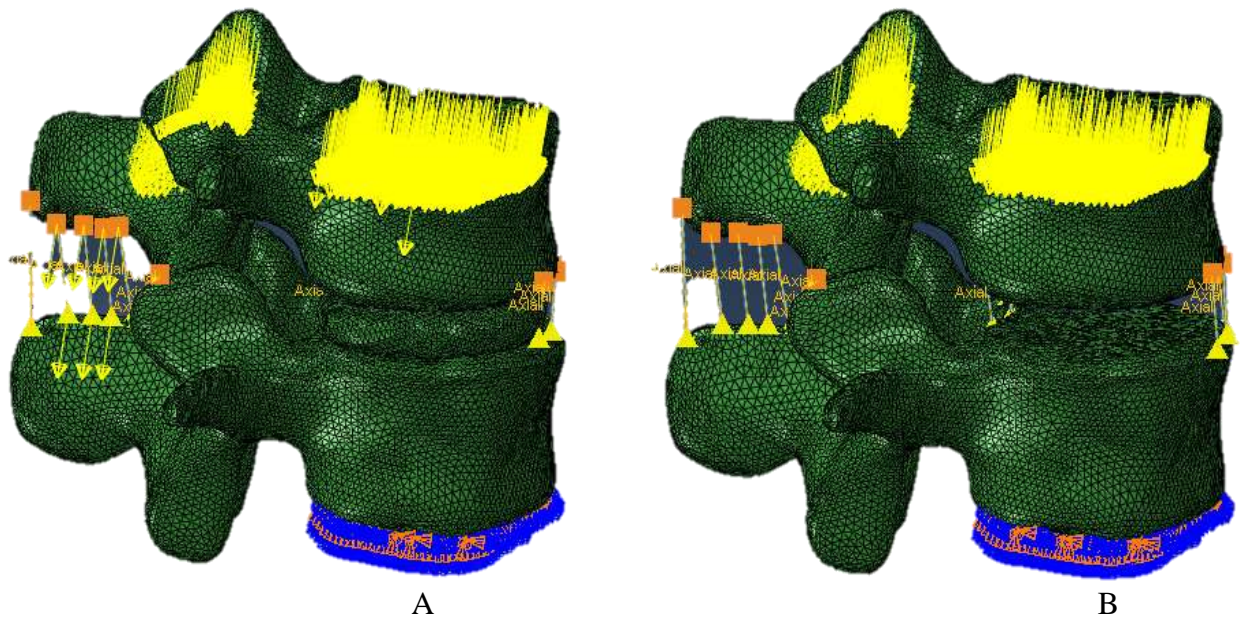
Figure 25: Loading and Boundary condition in Model 1 (A) & Model 2 (B)

Finally, the average and maximum Von Mises stress at L1 and L2 level from Model 1 and Model 2 were compared. Moreover, the displacement at a node in L1 and stress distribution at each vertebral level and computational time for running both models were also compared.

3.9.6. Whole lumbar spine FE model

Finally, Model 2 (without IVD) was extended by integrating L3, L4, L5, pelvis, sacrum, and all the lumbar and sacropelvic ligaments.

3.9.6.1. Material Property:

In this model, for the lumbar vertebrae, pelvis, and sacrum we applied the same property as mentioned before (Refer to Table 1 in Section 3.9.3.1). The lumbar ligaments were modelled with tension-only non-linear connectors (Chazal et al. 1985) (Table 3). The sacropelvic ligaments (anterior sacroiliac ligaments, short posterior sacroiliac ligaments, long posterior sacroiliac ligaments, sacrospinous ligaments,

73

sacrotuberous ligaments, illiolumbar ligaments) were modelled as linear springs as most of the studies in literature (Hao et al. 2011; Phillips et al. 2007) used linear springs for sacropelvic ligament modelling. The properties of the sacrolumbar ligaments were adapted from the literature (Hao et al. 2011; Phillips et al. 2007) and listed in Table 4.

Table 4: Sacropelvic ligament's spring parameters

Ligaments	Stiffness (N/mm)
Sacroiliac	5000
Sacrospinous	1500
Sacrotuberous	1500
Iliolumbar	1000

3.9.6.2. Interaction:

The interaction condition between the superior and inferior facet joints of L1-L2, L2-L3, L3-L4 and L4-L5 were described previously (Refer to Section 3.9.3.2). Moreover, the contact between L5 left and right inferior articular processes and sacrum superior articular processes and auricular surfaces of the sacrum and the pelvis's right and left iliac bone was also modelled similarly the interaction between the facet's joints were defined by nonlinear frictionless contact. Additionally, between the inferior endplate of L1, and superior endplate of L2, inferior endplate of L2 and superior endplate of L3, inferior endplate of L3 and superior endplate of L4, inferior endplate of L4 and superior endplate of L5, inferior endplate of L5 and sacral endplate the stiffness value of 50 N/mm and clearance value of 6 was applied to replicate the IVD properties (Figure 26).
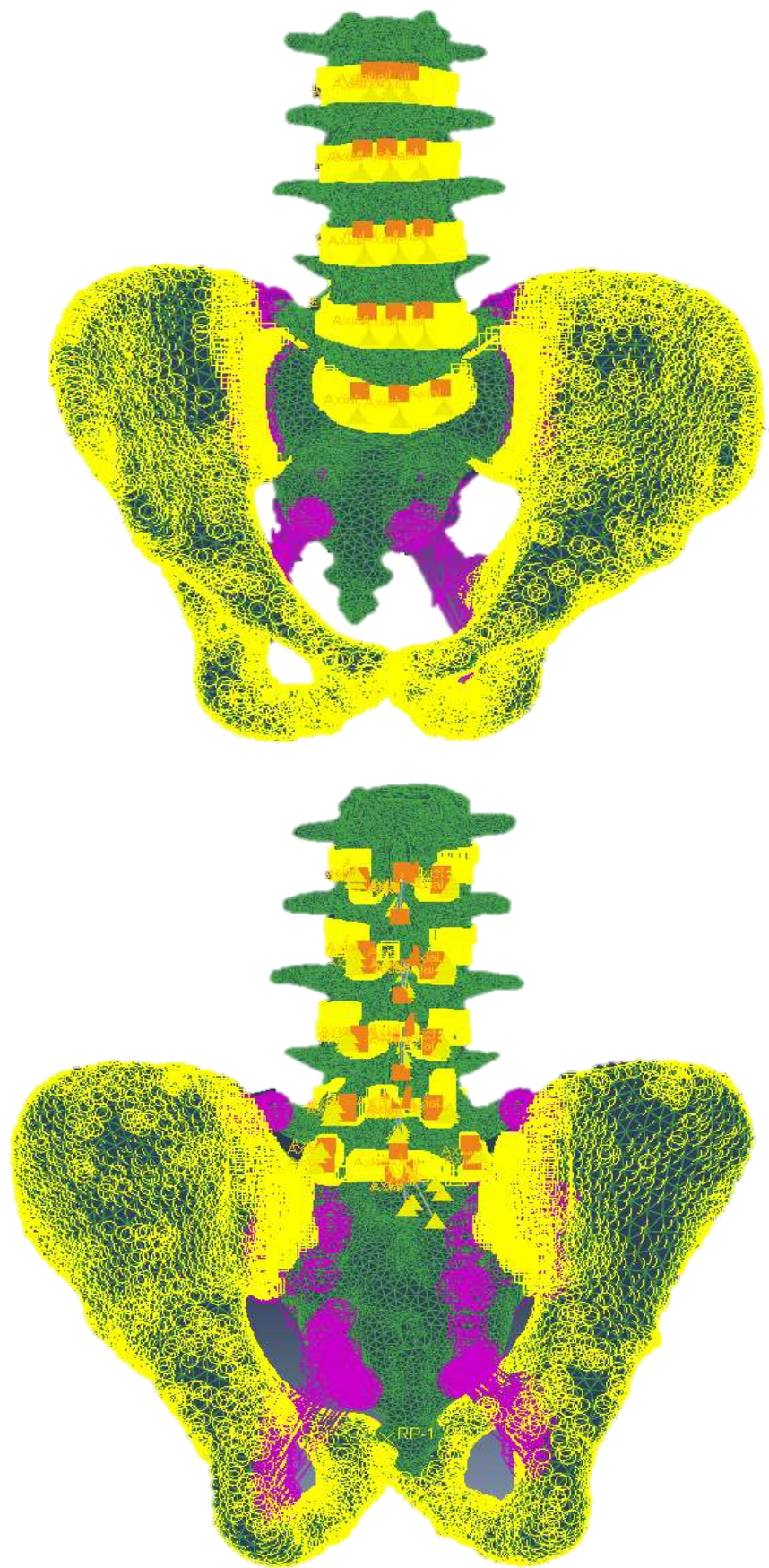
Figure 26: Anterior and posterior view of lumbar and sacropelvic ligaments

3.9.6.3. Loading and Boundary conditions:

In this model, a specific axial load of 400N was applied to the lumbar spine model for simulating the upper body weight. To mimic a more realistic loading scenario, 80% of the load was directed to the upper plateau of L1, and the remaining 20% was applied to the superior articular facets of L1. This distribution was based on established biomechanical principles and supported by references in the literature (Crouch et al. 1978; Lavaste et al. 1992; Hall et al. 1995). The pelvis was modelled as a rigid body to reduce computational time. Hence in our model, the motion of the pelvis was constrained in all 6 degrees of freedom (3 degrees in translation and 3 degrees in rotation) (Figure 27).

Figure 27: Loading and Boundary conditions applied in the whole lumbar FE model

After performing all the previous steps, ABAQUS/Standard solver was used to analyze the average and maximum Von Mises stress distribution in each vertebral level of this FE model. For a complete analysis, a 3.60 GHz Intel Core i7 CPU with 32 GB of RAM took 4 hours to process. The results were stored in an output file (.odb) for analysis.

Chapter 4: Results

This chapter represents the comprehensive results of statistical shape modelling, 2D to 3D sacropelvic parameter comparison, the correlation between bone shape and spinopelvic parameters and Finite Element modelling. The workflow of results obtained in our study is depicted in Figure 28.

Statistical shape modelling results	2D to 3D sacropelvic parameter comparison	Correlation between bone shape and spinopelvic parameters	Finite element modelling results
• Bone shape variation for single and combined bone • SSM prediction accuracy for single and combined bone	• Mean ± SD of sacropelvic angles (°) and distances (mm) calculated in 2D and 3D	• Correlation between sacropelvic parameters and individual pelvis, sacrum, fused pelvis and sacrum, whole lumbar spine bone shape	• Bone material property validation • Mesh convergence analysis • Disc material property validation • Lumbar ligament property validation • Functional spinal unit and whole lumbar spine validation (without IVD)

Figure 28: Workflow of results obtained in our study

4. Bone shape variation
4.1. Single bone analysis
4.1.1. Principal component analysis (PCA)

This study obtained the PCA for L1 – L5, sacrum, and pelvis bones. For L1, the first principal component (PC) (53 %) accounted for the vertebral body size and superior and inferior articular process variation. The second PC (6%) described the transverse process, mammillary process, and posterior part of the vertebral body width variation, and the third PC (5%) captured the superior and inferior articular and spinous process variations (Figure 29). The average shape ± 2SD, percentage variation in each direction for PC1, PC2 and PC3 in case of other vertebrae (L2, L3, L4 and L5) are illustrated in Appendix (Figure A1, A2, A3 and A4).
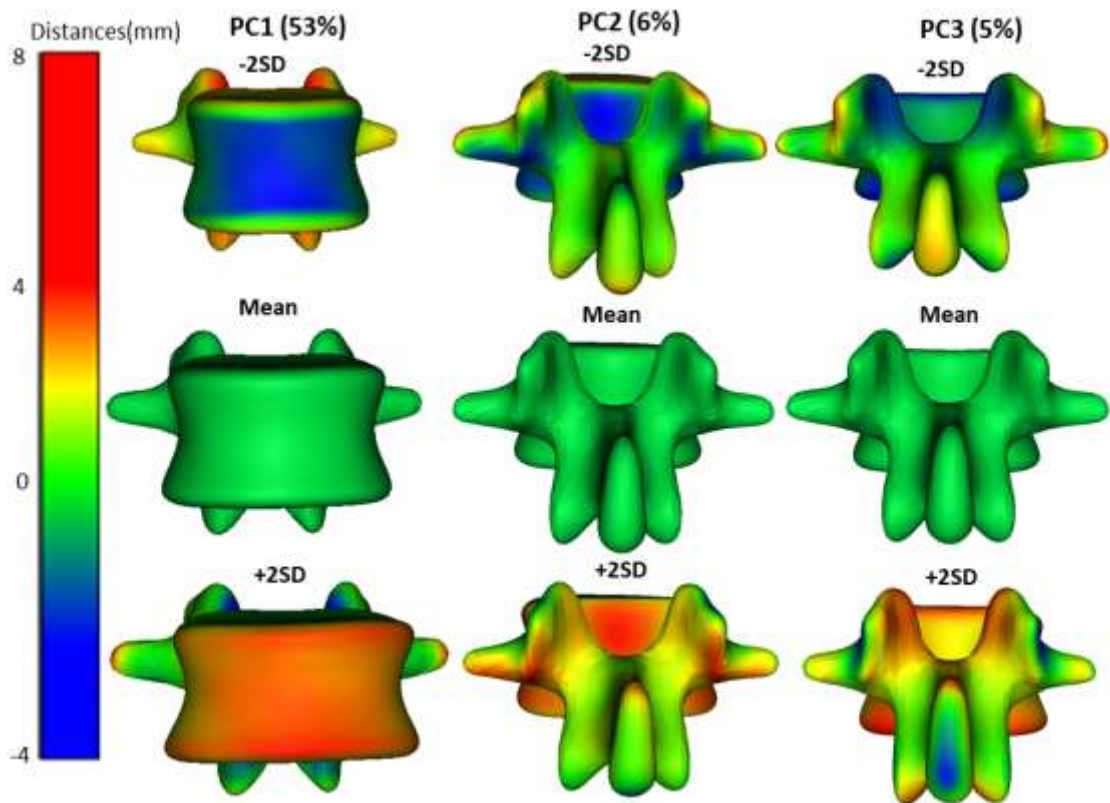
Figure 29: Average shape ± 2SD in each direction for PC1, PC2 and PC3 for L1, PC1 shows the anterior views of the vertebrae, PC2 and PC3 shows the posterior views of the vertebrae

For the sacrum, the first PC (34%) accounted for the sacrum height and coccyx inclination variation and the second PC (15%) represented sacral plateau width variation. The third PC (9%) captured the auricular process width variation (Figure 30).
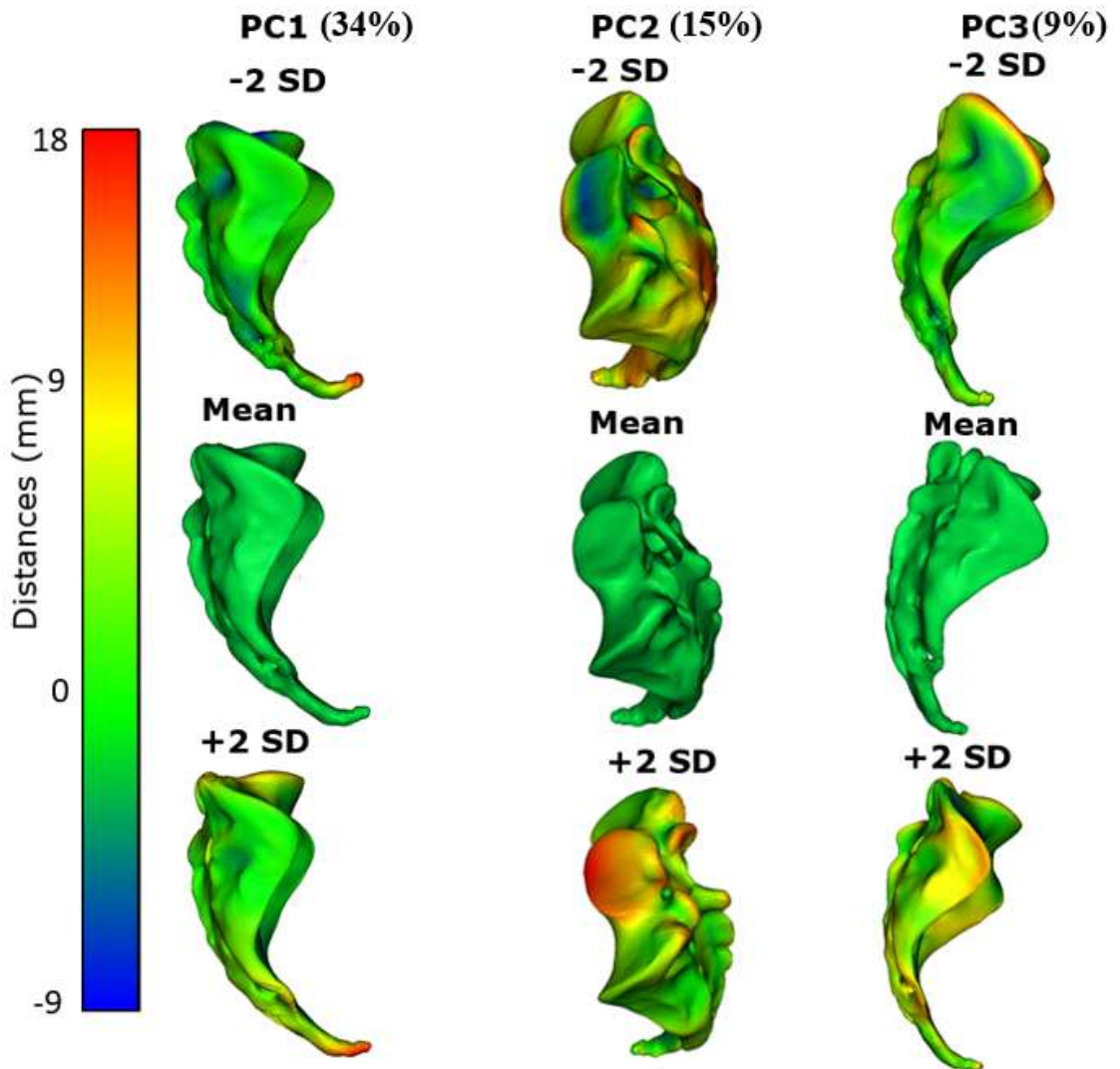
Figure 30: Mean ± 2SD meshes for PC1 to PC3 (sacrum) where PC1 and PC3 shows the lateral view of the sacrum where PC2 shows the superior view of the sacrum

For the pelvis, the first PC (39%) accounted for the bone height, and the second PC (16%) described the bone width variation. The third PC (10%) represented the iliac width variation (Figure 31).
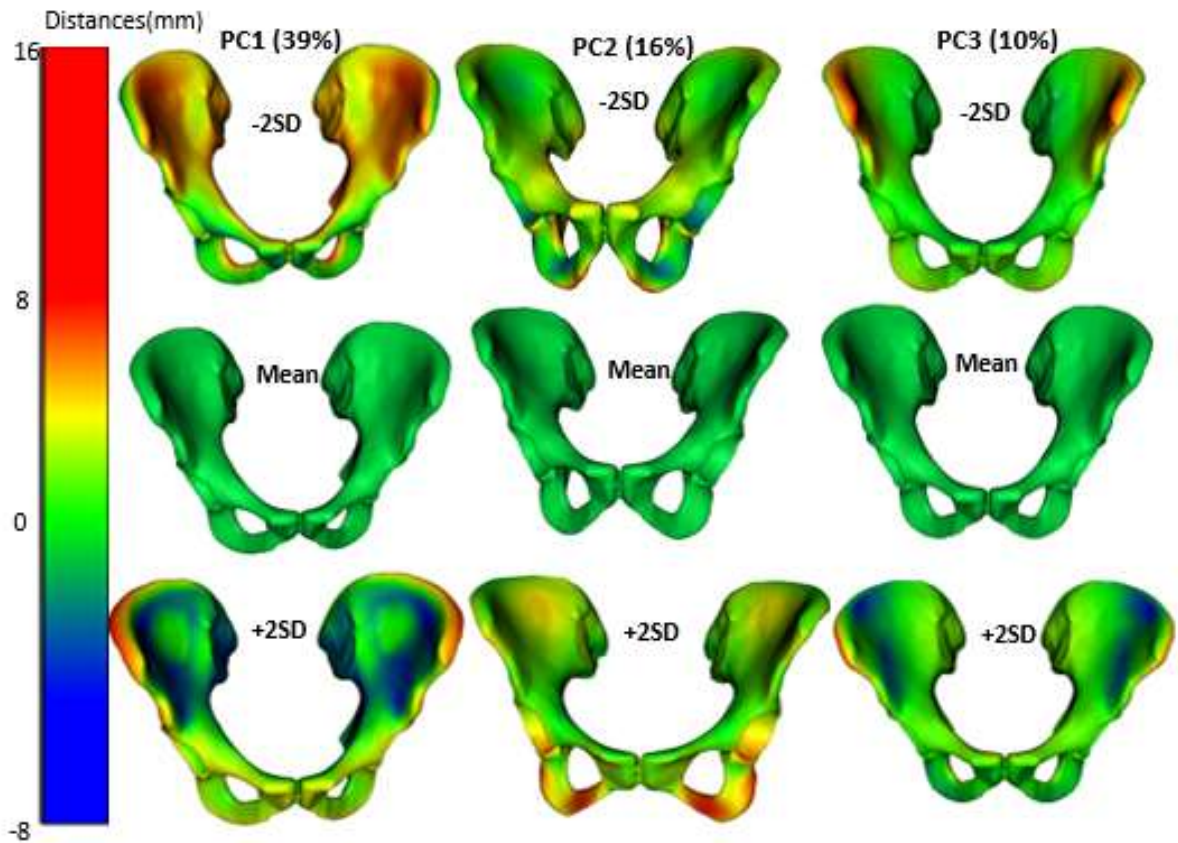
Figure 31: Mean ± 2SD meshes for PC1 to PC3 (pelvis) where PC1, PC2 and PC3 shows the anterior view of the pelvis

4.1.2. SSM prediction accuracy of individual vertebrae (L1-L5), pelvis, and sacrum SSM:

4.1.2.1. Fitting error:

The fitting error (Root mean square error for each bone was 0.11 mm for L1, 0.11 mm for L2, 0.12 mm for L3, 0.12 mm for L4, 0.13 mm for L5, 0.45 mm for the pelvis, and 0.47 mm for the sacrum.

4.1.2.2. Model Compactness:

The first and most predominant mode of every bone accounted for size variation. The First 39 PCs defined 95% of the data variation within the population; the first 39 PCs explained 95% of the data variation

81

within the population in L1, 37 PCs in L2, 38 PCs in L3, 43 PCs in L4, 41 PCs in L5 (Figure 32), 35 PCs in the pelvis, and 47 PCs in the sacrum (Figure 33).
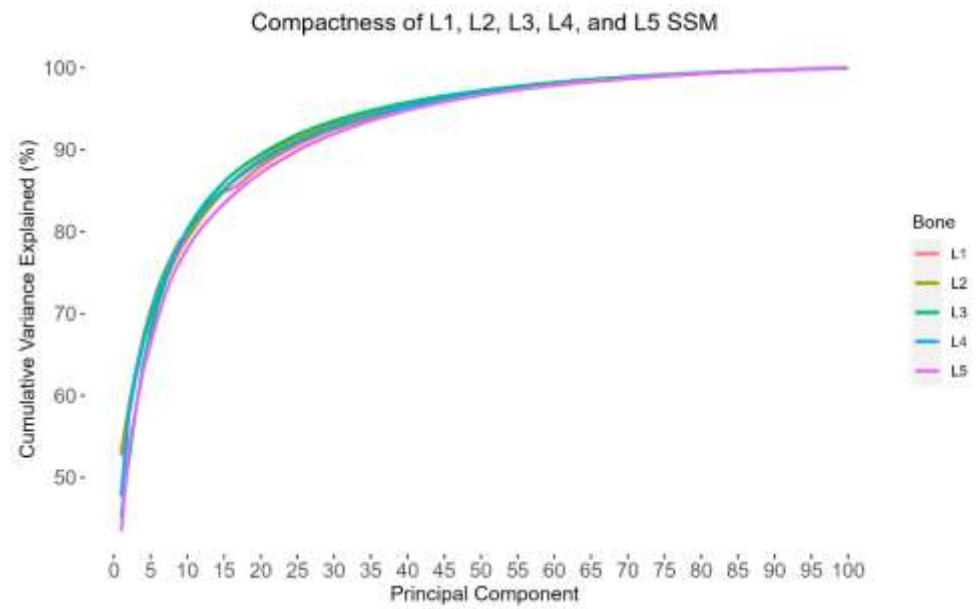
Figure 32: L1-L5 SSM compactness
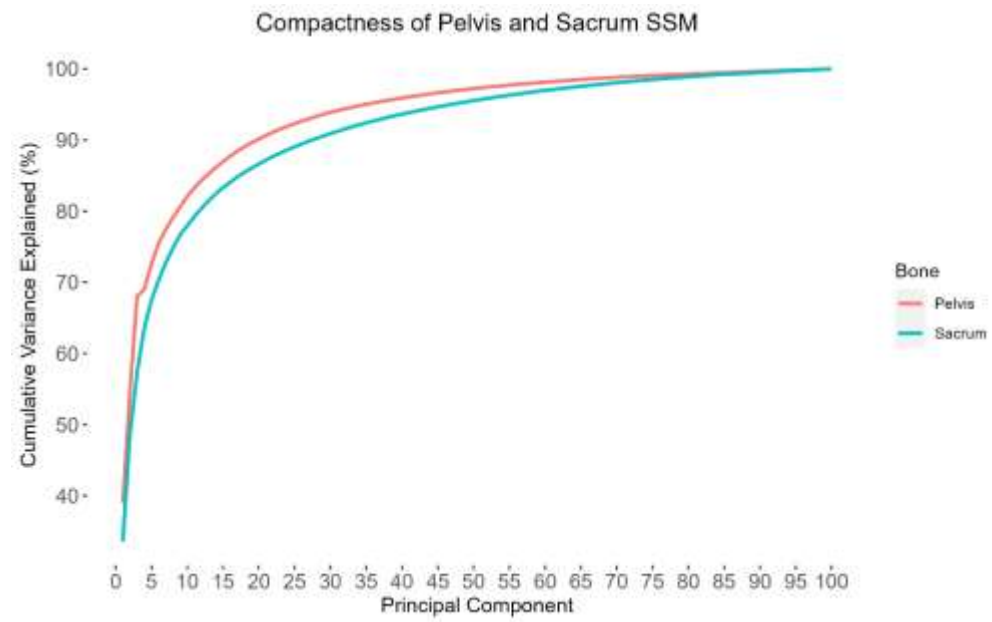
Figure 33: Pelvis and Sacrum SSM compactness

4.1.2.3. Model Specificity:

The specificity values for single bone SSMs are shown in Figure 33 and 34. The cut-off Root mean square error (RMSE) for each SSM model was defined as the number of PCs required to reach the RMSE value less than the fitting errors. Therefore, in the case of L1, the number of PCs needed to reach the RMSE less than 0.1 mm was 84 modes. In the case of L2, to reach the RMSE of less than 0.1 mm was 86 modes. The number of PCs required to reach the RMSE value less than 0.12 mm for L3 was 81 modes. The number needed to reach the RMSE value of less than 0.12 mm for L4 was 82 modes. In the case of L5 the number of PCs required to reach the RMSE less than 0.13 mm was 73 modes (Figure 34). In the pelvis the number of PCs required to reach the RMSE less than 0.45 mm was 83 modes. In the sacrum the number of PCs required to reach the RMSE less than 0.47 mm was 77 modes (Figure 35).
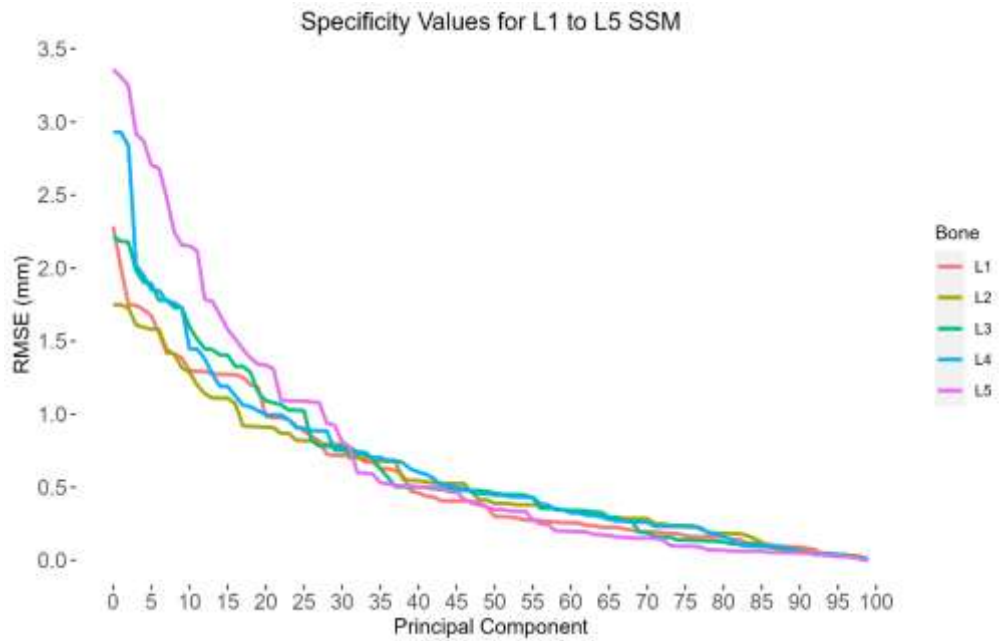
Figure 34: L1- L5 SSM specificity
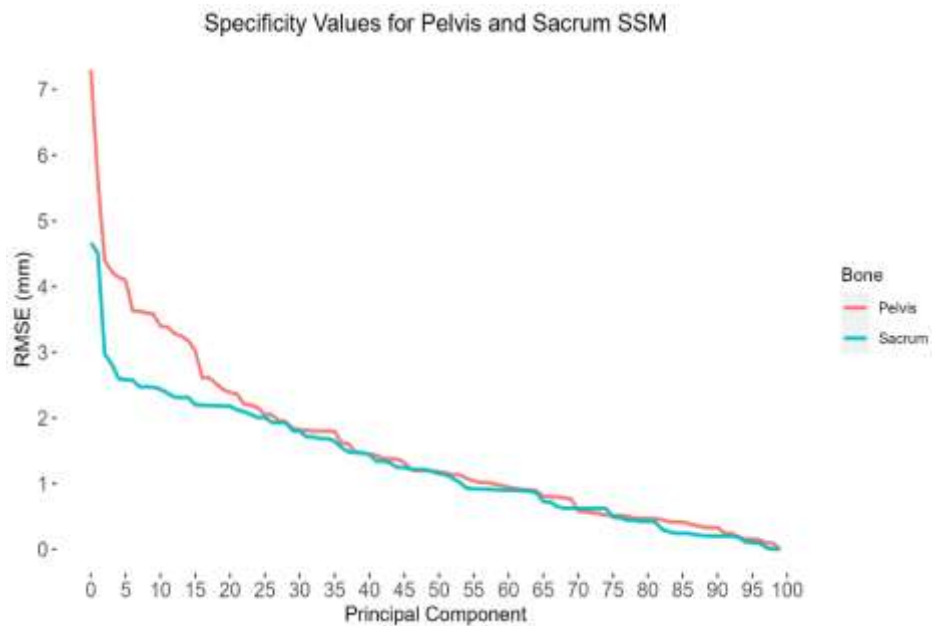
Figure 35: Pelvis and sacrum SSM specificity

4.1.2.4. Leave one out analysis

The predictive ability for single bone SSMs was quantified with the computation of RMSE value, and Dice score between the CT reconstructed and SSM predicted bones.

We evaluated the prediction accuracy using only demographics measurements (age + sex) and after adding the bone linear measurements for the individual bones (L1 to Pelvis). After integrating the bone measurements, the mean RMSE value was decreased by 17%, 15%, 13%, 14%, 12%, 6% and 5% for L1, L2, L3, L4, L5, sacrum and pelvis respectively (Figure 36). By the inclusion of the bone measurements the mean absolute error value was decreased by 0.33 mm, 0.31mm, 0.3 mm, 0.32mm, 0.31mm, 0.22mm and 0.27mm for L1, L2, L3, L4, L5, sacrum and pelvis respectively.

By considering bone measurements the dice score (between the CT reconstructed bones and the SSM predicted bones) was improved by 2-3% for each vertebra and 2% for sacrum and pelvis SSMs (Figure 37). After including the bone measurements, the mean absolute error dice score is improved by 0.02 for each vertebrae and 0.01 for sacrum and pelvis respectively.
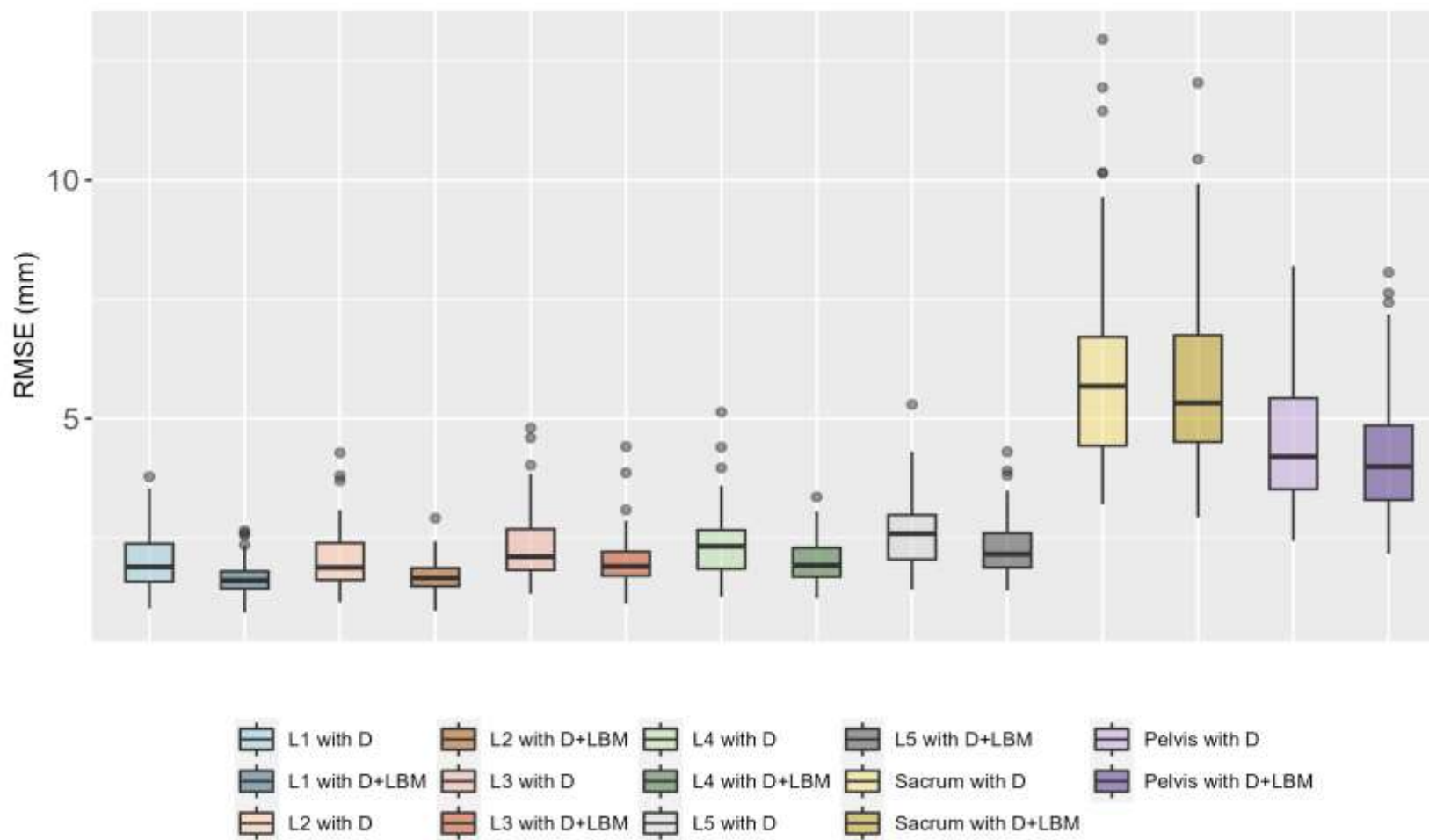
Figure 36: RMSE (mm) of Euclidian distances between CT reconstructed, and SSM predicted L1, L2, L3, L4, L5, pelvis and sacrum for only with demographics (D) and with demographic and linear bone measurements (D+LBM)
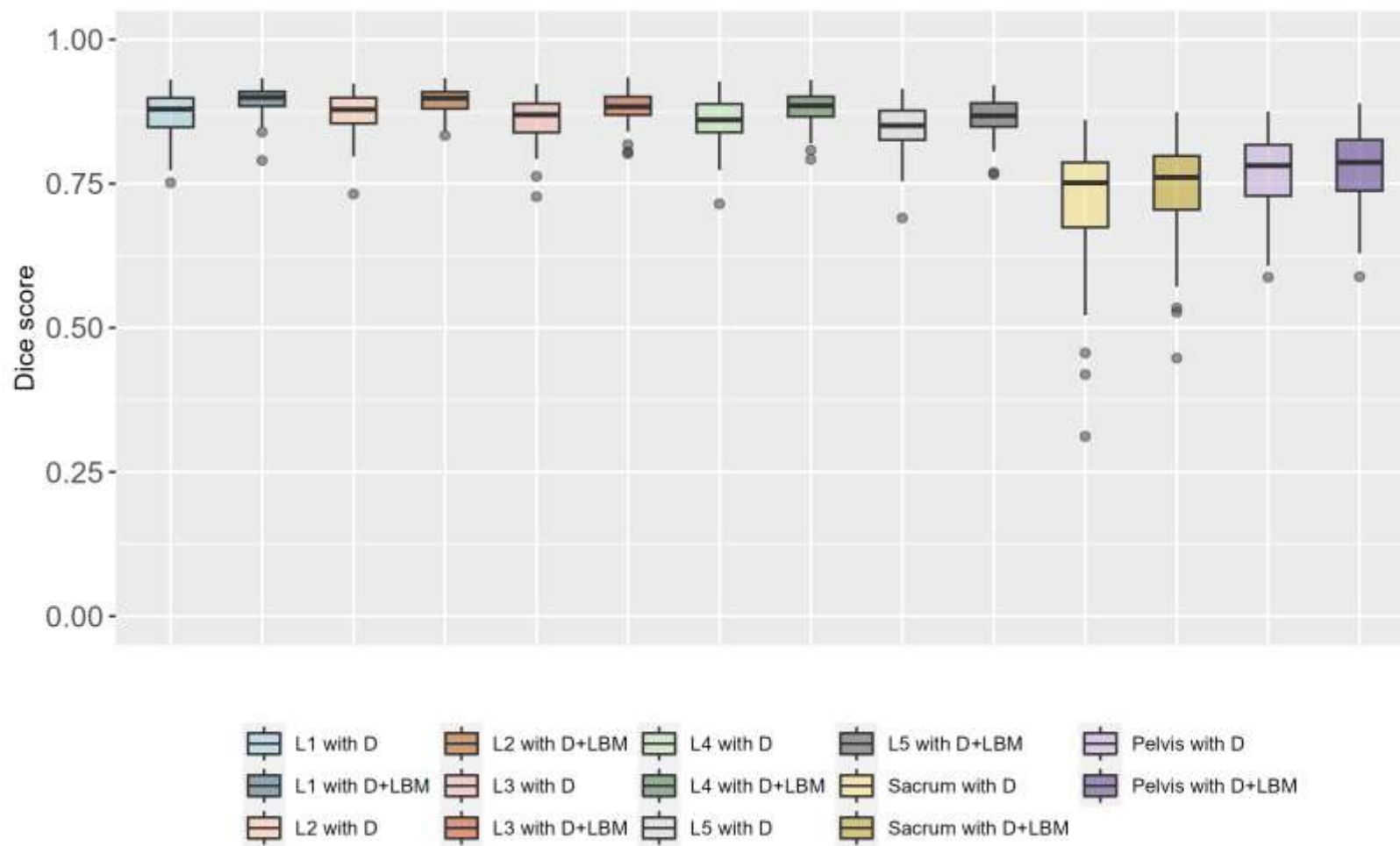
Figure 37: Dice score between CT reconstructed and SSM predicted single bones for only with demographics (D) and with demographics and linear bone measurements (D+LBM)

4.2. Combined pelvis and sacrum analysis

4.2.1. PCA

For combined pelvis and sacrum bones, the first PC described the pelvis height and coccyx inclination variation (61%). The second PC accounted for the sacral ala and ischium width variation (7%) and third PC indicated the sacral plateau height and iliac crest width variation (6%) (Figure 38).
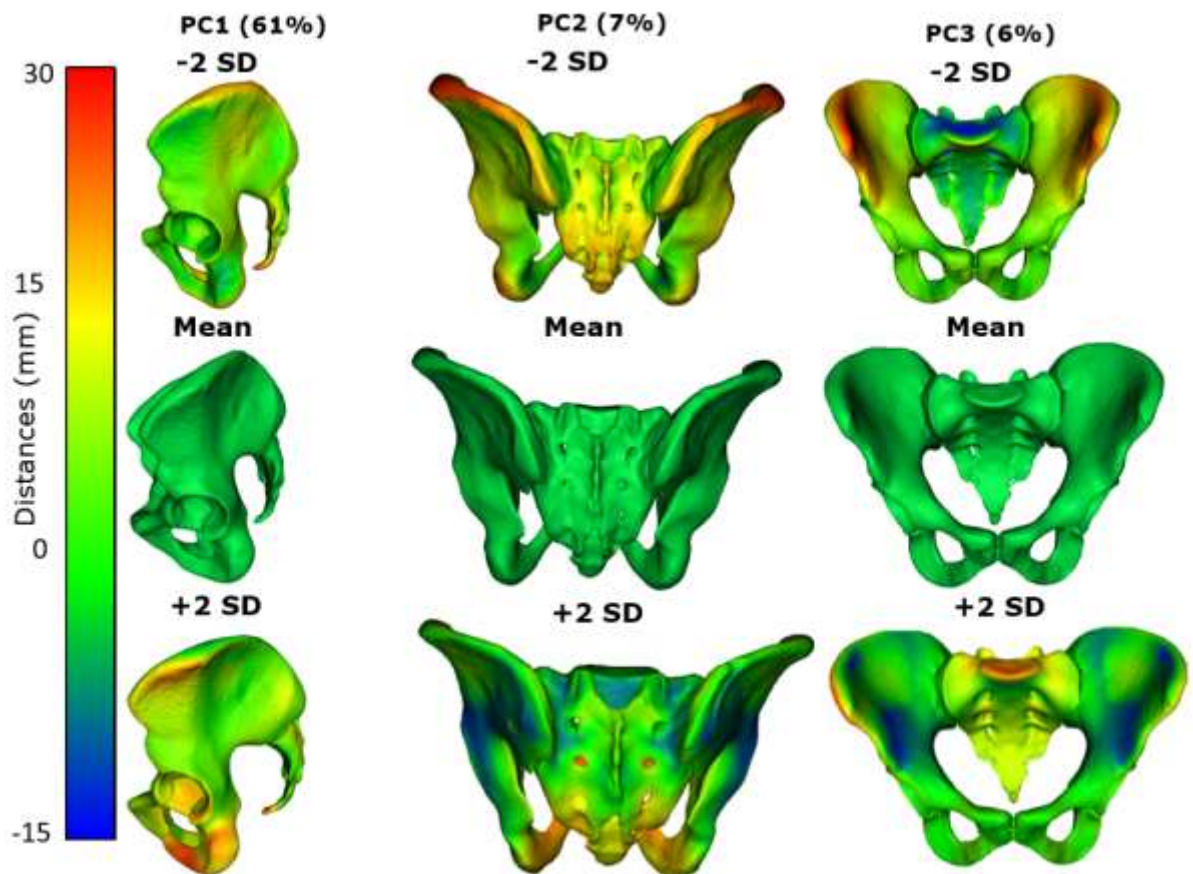
Figure 38: Mean ± 2 SD meshes for PC1 to PC3 for combined pelvis and sacrum (where PC1 shows lateral view, PC2 shows anterior view and PC3 shows the posterior view of combined pelvis and sacrum)

4.3. Combined lumbar spine analysis

4.3.1. PCA

4.3.1.1. Unscaled lumbar spine model

For the unscaled model, the first PC (52%) accounted for the pelvic tilt and coccyx inclination variation (Figure 39). The second PC (11%) described the lumbar spine curvature and pelvic tilt variation (Figure 40). The third (6%) PC explained the variation of the lumbar vertebrae's posterior arch, sacral crest and pubis width (Figure 41).
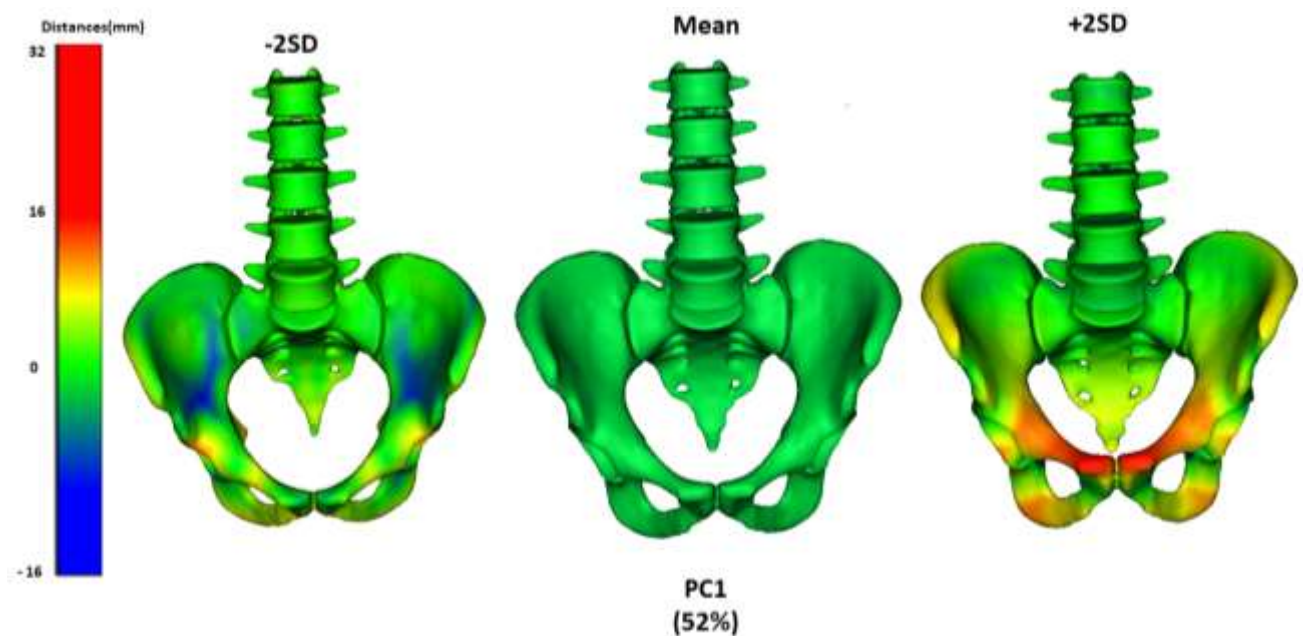
Figure 39: Mean mesh and ± 2 standard deviation meshes for PC1 (where PC1 shows the anterior view of unscaled lumbar spine model)
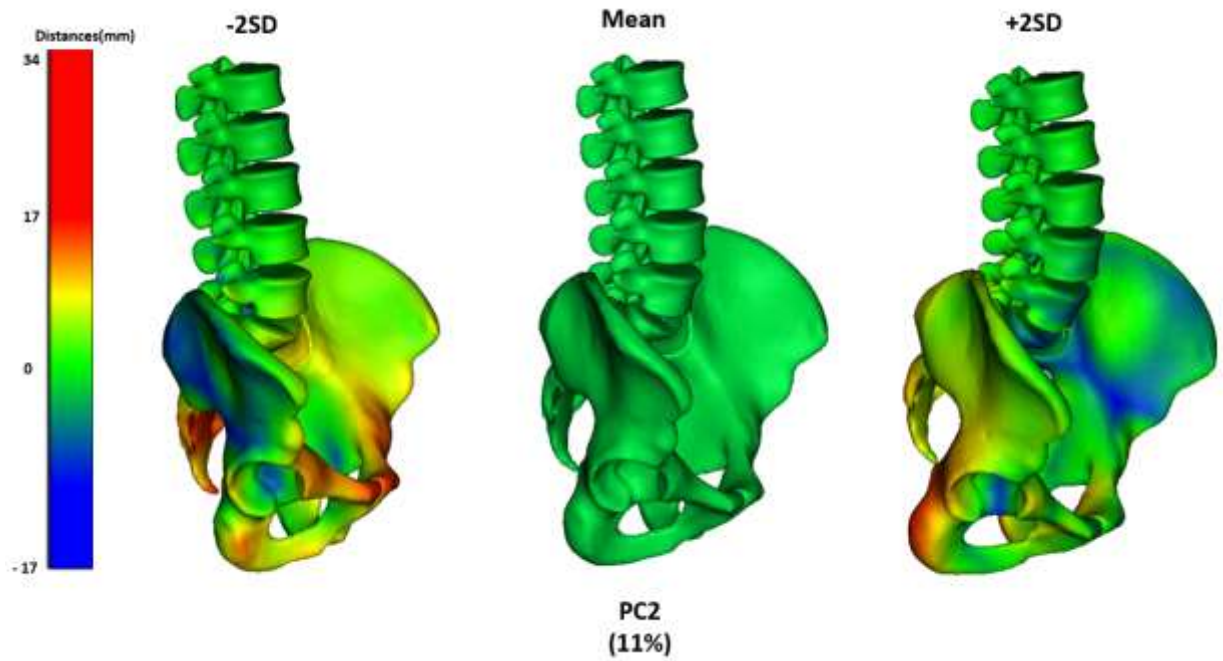
Figure 40: Mean mesh and ± 2 standard deviation meshes for PC2 (where PC2 shows the lateral view of unscaled lumbar spine model)
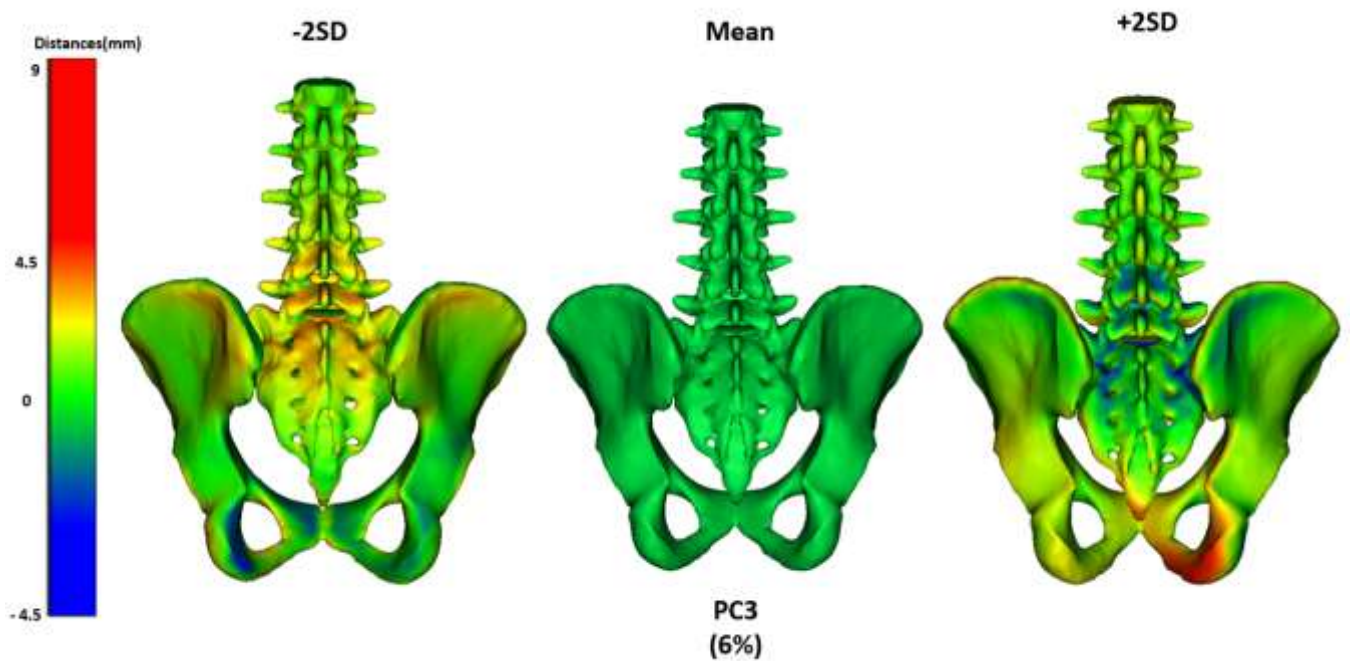
Figure 41: Mean mesh and ± 2 standard deviation meshes for PC3 (where PC3 shows the posterior view of unscaled lumbar spine model)

4.3.1.2 Scaled lumbar spine model

In the Procrustes analysis, the first PC (25%) accounted for the lumbar curvature and pelvic tilt variation in the sagittal plane (Figure 42). The second PC of the scaled model (18%) described the lumbar curvature variation (mainly in L1-L2 level) and iliac, and pubic width variation (Figure 43). The third (8%) PC explained the variation of the lumbar vertebrae's (L3, L4, and L5) posterior arch, sacral crest and pubic width (Figure 44).
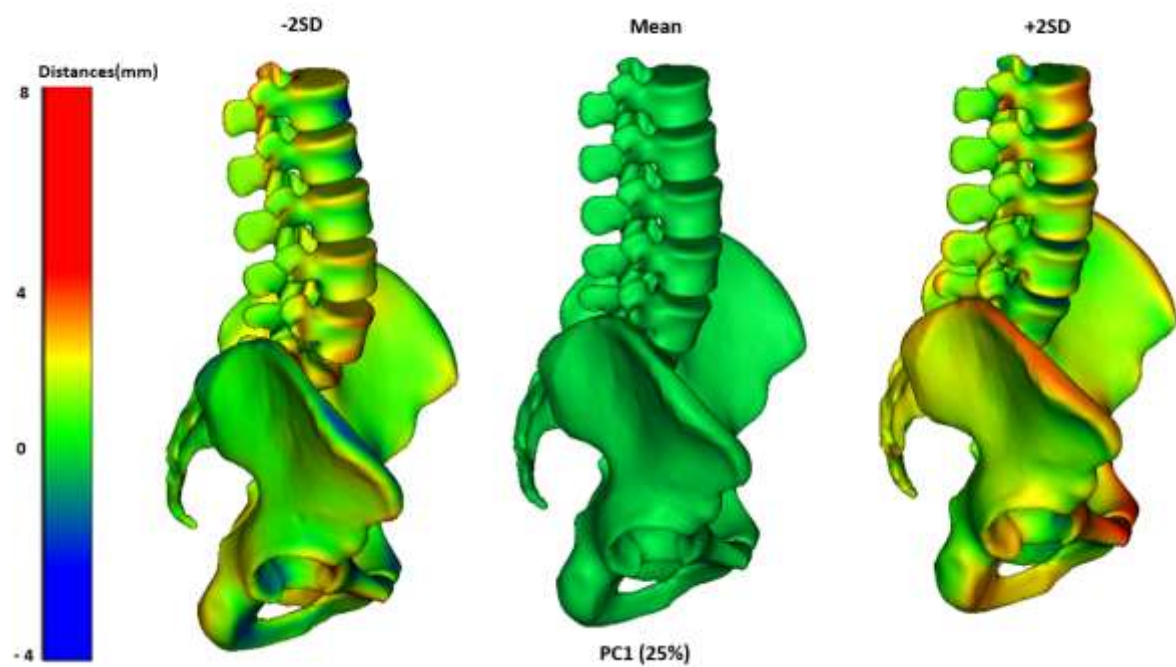
Figure 42: Mean mesh and ± 2 standard deviation meshes for PC1(where PC1 shows the lateral view of the scaled lumbar spine model)
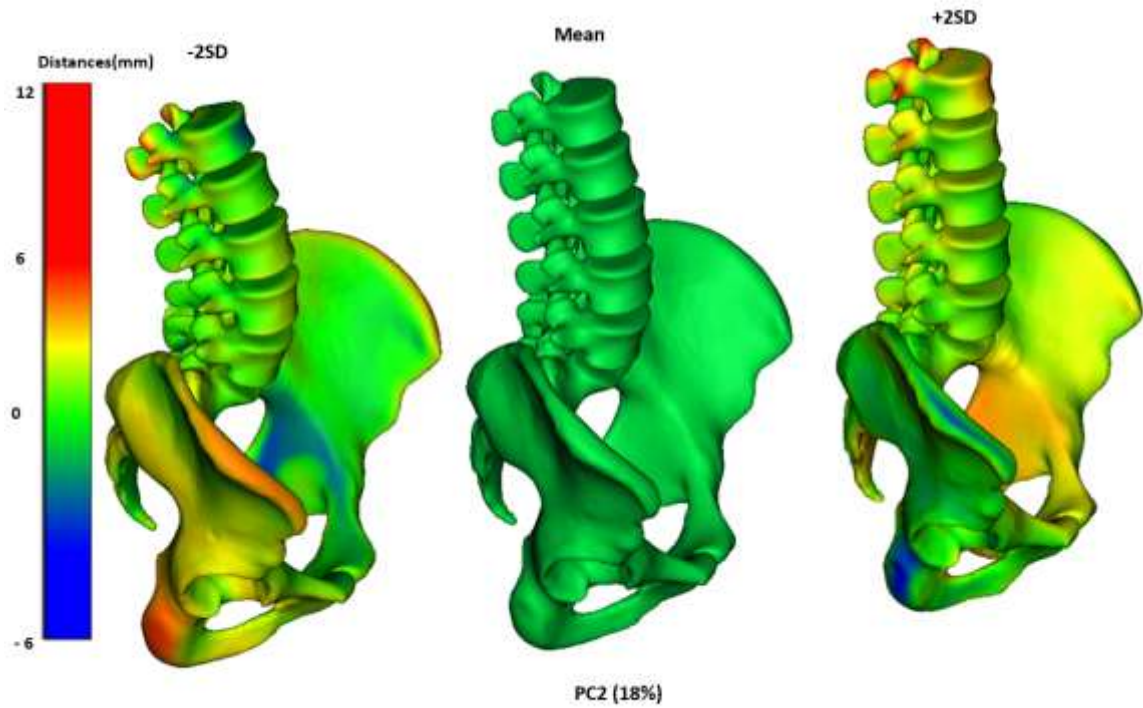
Figure 43: Mean mesh and ± 2 standard deviation meshes for PC2 (where PC2 shows the lateral view of the scaled lumbar spine model)
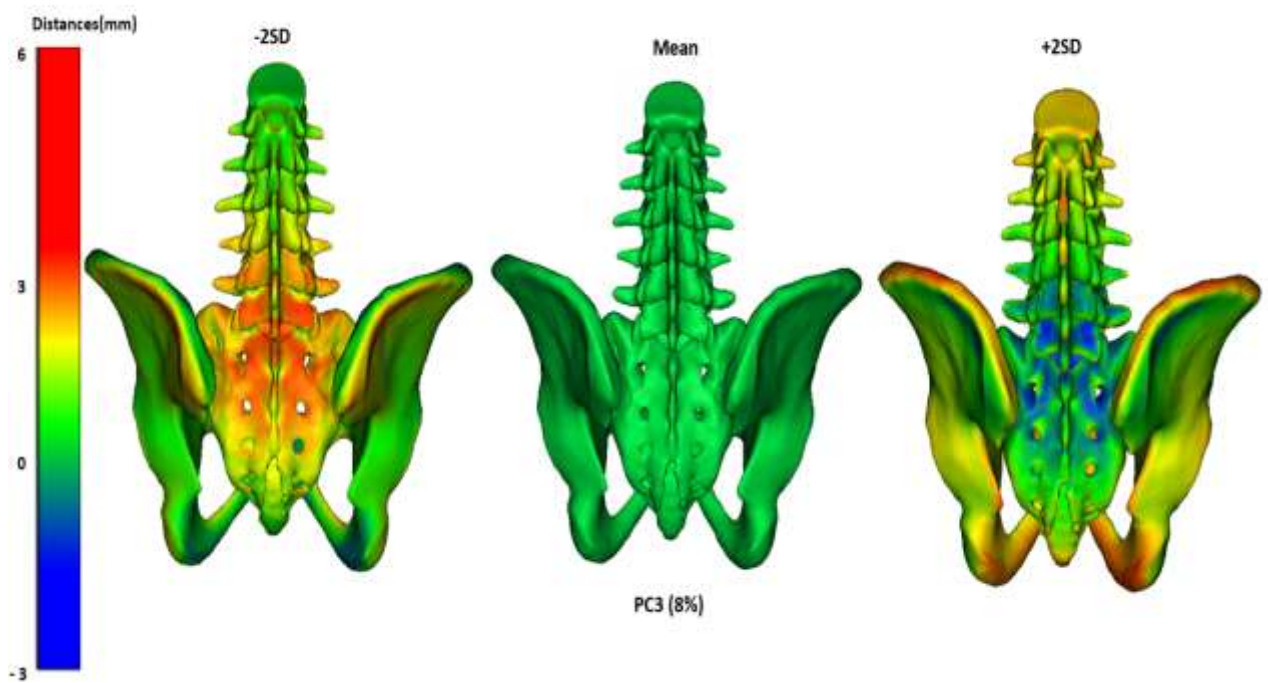
Figure 44: Mean mesh and ± 2 standard deviation meshes for PC3 (where PC3 shows the posterior view of the scaled lumbar spine model)

4.3.2 Prediction Accuracy of the lumbar spine SSM:

4.3.2.1. Fitting error:

The whole lumbar spine's fitting error (RMSE) was 0.67mm.

4.3.2.2. Model Compactness:

4.3.2.2.1 Unscaled lumbar spine model

The first and most predominant mode of the whole lumbar spine accounted for size variation (52%) in the unscaled model. The first 10 PCs defined 95% of the data variation within the population in the unscaled lumbar spine model (Figure 45).

4.3.2.2.2 Scaled lumbar spine model

In the case of the scaled model, the first PC captured only 25% variation. Since in the scaled model, the size variation was ignored, the variation captured by the PCS were lesser compared to the unscaled model. The first 35 PCs accounted for 95% of data variation (Figure 46).
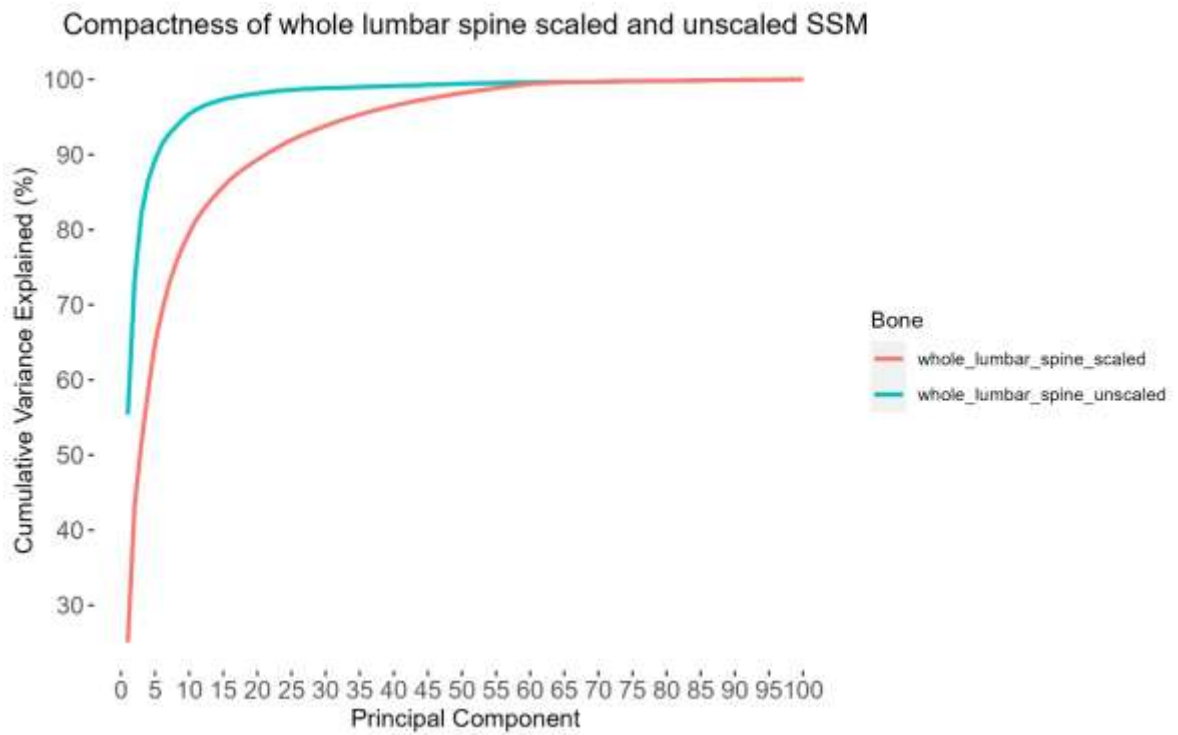
Figure 45: Whole lumbar spine unscaled and scaled model variation explained by PCA

4.3.2.3. Specificity:

In the case of the whole lumbar spine (Figure 46), 26 PCs are required to reach the RMSE value of 8.58 mm.
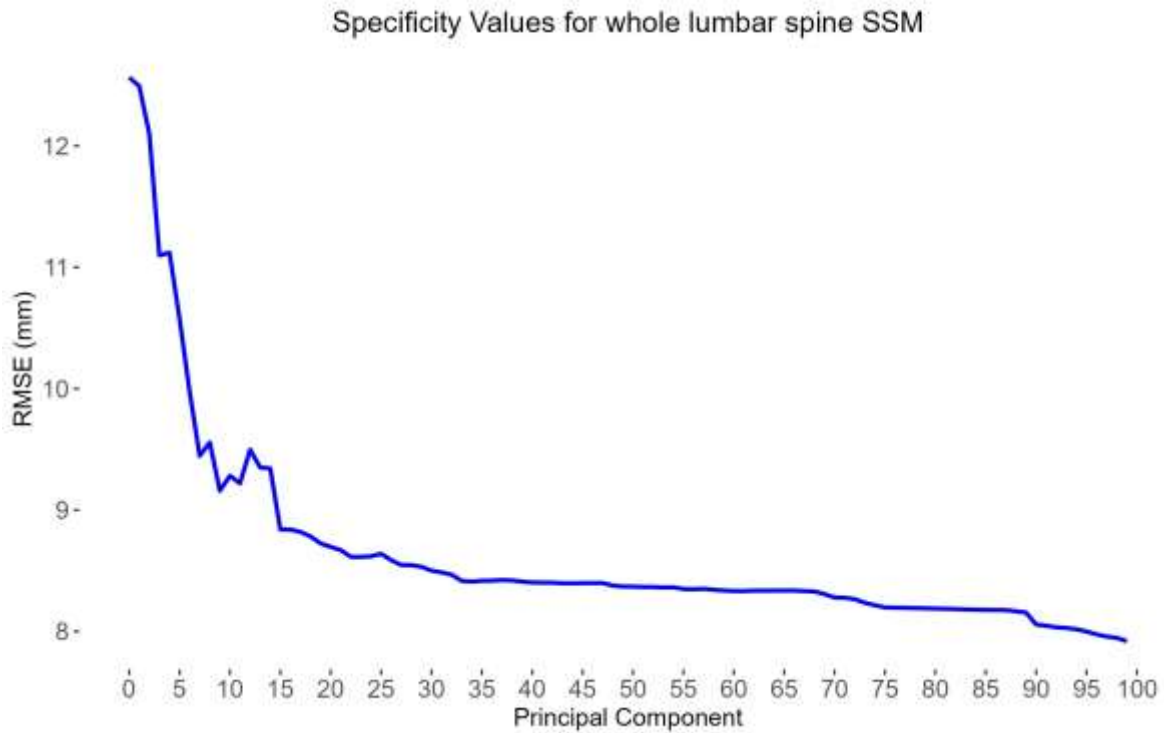
Figure 46: Specificity of whole lumbar spine SSM

4.3.2.4. Leave one out analysis:

The predictive capability for whole lumbar spine SSMs was quantified with the computation of RMSE value and Dice score between the CT reconstructed and SSM predicted bones. The RMSE values for whole lumbar spine integrating lumbosacral angles and bone measurements were around 9.21 ± 4.1 mm. The dice score value between the CT reconstructed and SSM predicted whole lumbar spine were around 0.63.

4.4. Prediction Accuracy of whole lumbar spine model for 1 participant

4.4.1. Prediction using anatomical landmarks and few PCs

The comparison of the whole lumbar spine predicted shape (using anatomical landmarks from CT scans and 3 PCs) with the CT reconstructed shape for a specific patient is shown in Figure 47. In this figure, the gray lumbar spine is the CT reconstructed (ground truth) shape and the shape in the forms of point-clouds is the SSM predicted shape.
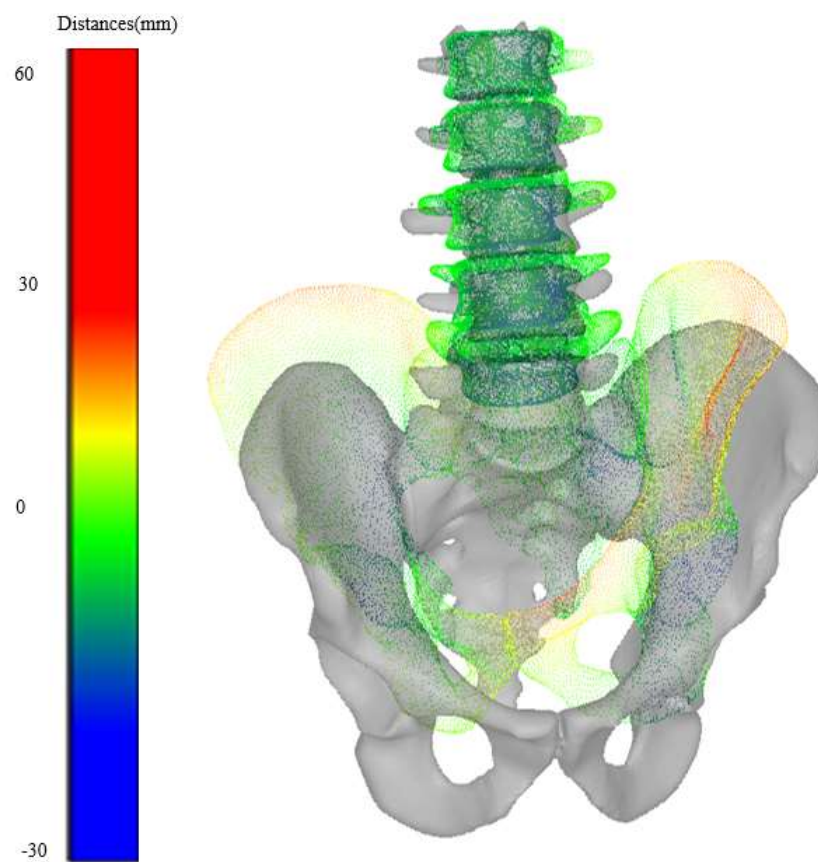
Figure 47: Comparison of whole lumbar spine prediction (with only the landmarks) with the CT reconstructed mesh (anterior view)

4.4.2. Prediction using patient-specific bone measurements and lumbosacral angles obtained from landmarks

The comparison of shape between the CT reconstructed and predicted shape with integration of patient-specific bone measurements and angles is shown in Figure 48. In this figure, the original shape of the patient-specific lumbar spine is shown in Gray colour. The average error between these two shapes were 14mm. From the colour bar we can see that the prediction errors exist in spinous processes and pelvis.
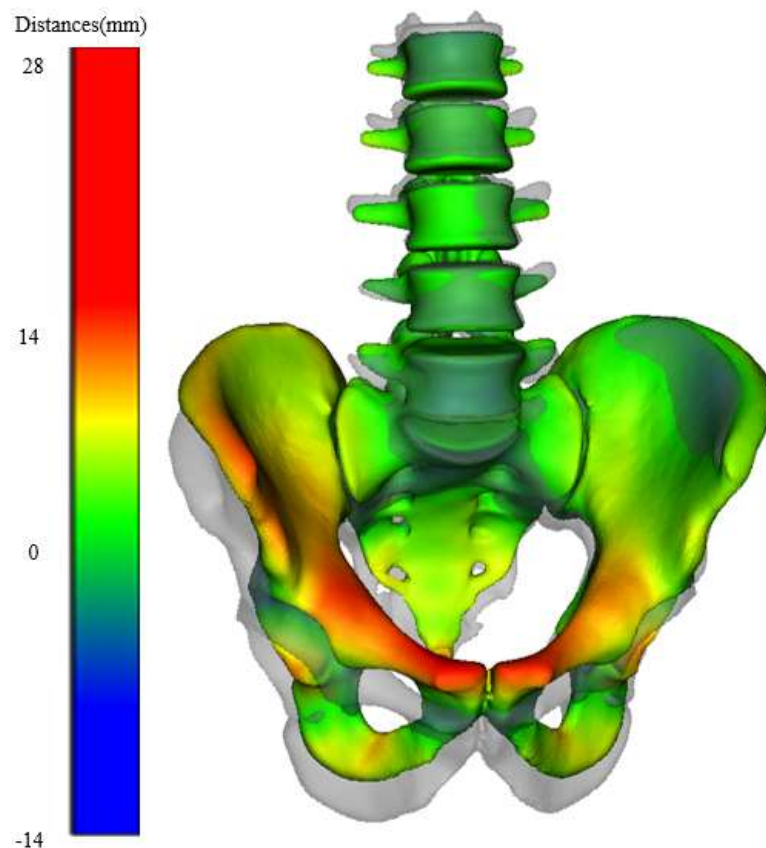
Figure 48: Comparison of whole spine prediction (with the patient-specific bone and lumbosacral angles) with the CT reconstructed mesh (anterior view)

Then, for detailed understanding of the maximum error between the predicted and the CT reconstructed shape we excluded the pelvis. The maximum error decreased from 28 to 22mm, found in the sacrum and coccyx (Figure 49).
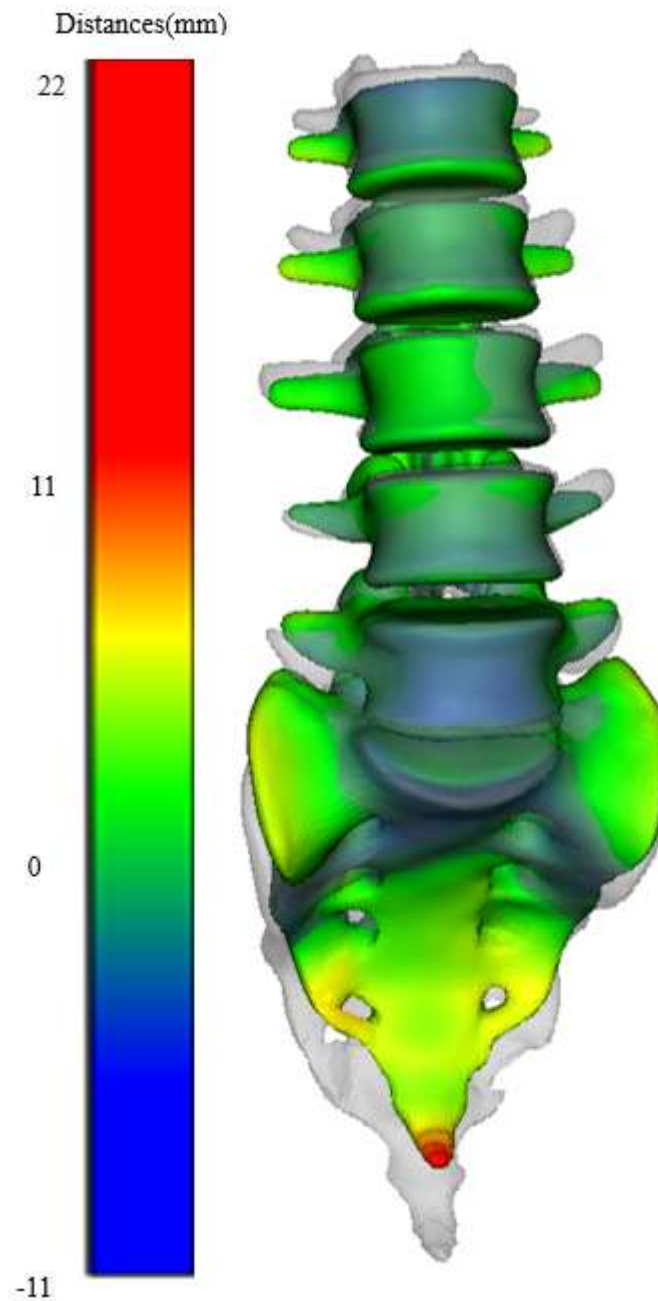
Figure 49: Comparison of lumbar spine (without pelvis) prediction with the CT reconstructed mesh (anterior view)

Finally, we wanted to understand the maximum error in the vertebrae between the CT reconstructed and the SSM predicted shape. From the colour bar of Figure 50 the maximum shape error in lumbar vertebrae occurred in the posterior arch. Additionally, by excluding the sacrum the maximum error decreased from 22 to 9 mm.
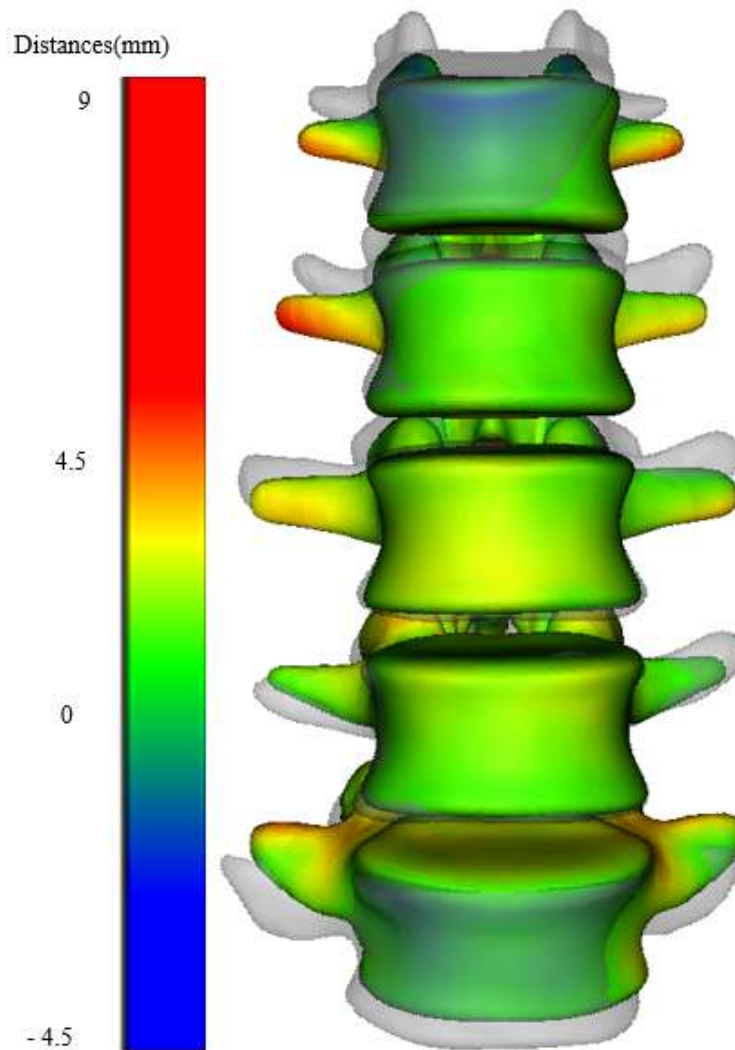
Figure 50: Comparison of lumbar vertebrae (without pelvis and sacrum) prediction with the CT reconstructed mesh (anterior view)

4.5. Relationship between 2D and 3D sacropelvic parameters:

From the paired sample t-test no statistically significant differences were found between the 2D and 3D sacropelvic angles measured from the fitted SSM meshes (Table 5) however, the crest-pubic distance and inlet outlet distances showed statistically significant differences ($p<0.001$).

Table 5: Mean ± SD of sacropelvic angles (º) and distances (mm) calculated in 3 dimension (3D) and measured in 2D slices.

*** $p<0.001$

	APA	PI	STA	PA	FSPA	PSA	CPD ***	CSD ***	ID ***	OD***
2D	20 ± 3	51 ± 9	102 ± 6	18 ±11	69 ± 10	42 ±15	89 ±11	99 ± 9	120 ± 9	115 ± 9
3D	20 ± 4	50 ± 10	103 ± 6	18 ± 12	68 ± 9	42 ± 14	94 ± 11	103 ± 9	127 ± 9	123 ± 9

Where APA = Anterior Pelvic angle, PI = Pelvic Incidence, STA = Sacral Table angle, PA = Projection angle, FSPA = Femorosacropelvic angle, PSA = Pelvisacral angle, CPD = Crest pubic distance, CSD = Crest sacrum distance, ID = Inlet distance and OD = Outlet distance

4.6. Correlation between individual pelvis, sacrum, fused pelvis and sacrum, whole lumbar spine shape & sacropelvic parameters:

The Pearson correlation coefficient value measured between the sacral plateau width (PC2) and pelvic incidence showed a medium correlation ($r = 0.54$) (Table 6). Furthermore, Pearson correlation coefficient between the anterior pelvic angle and the sacral ala and ischium width (PC2) also showed negative medium correlation ($r = - 0.55$) (Table 7). However, no significant correlations were observed between

102

the other sacropelvic parameters (angles and distances) and pelvis, sacrum and fused pelvis and sacrum bone shape.

Table 6: The relationship between Pearson correlation coefficient value and bone variations for sacrum, where Orange= Medium correlation (± 0.51 and ± 0.70), Blue= Weak correlation (± 0.31 and 0.50), Yellow= Negligible (0 to 0.3). Range obtained from (Miot 2018)

r value	PI	PA	PSA	STA	APA
PC1	0.23	0.05	0.31	0.32	0.24
PC2	0.54	0.03	0.05	0.03	0.03
PC3	0.19	0.21	0.14	0.12	0.13

Where APA = Anterior Pelvic angle, PI = Pelvic Incidence, STA = Sacral Table angle, PA = Projection angle, PSA = Pelvisacral angle

Table 7: The relationship between r value and bone variations for fused pelvis and sacrum where Orange= Medium correlation (± 0.51 and ± 0.70), Blue= Weak correlation (± 0.31 and 0.50), Yellow= Negligible (0 to 0.3). Range obtained from (Miot 2018)

r value	PI	PA	PSA	STA	APA
PC1	0.15	-0.09	-0.15	-0.12	-0.008
PC2	0.43	0.06	-0.07	0.03	-0.55
PC3	0.07	-0.26	-0.43	-0.03	-0.26

Where APA = Anterior Pelvic angle, PI = Pelvic Incidence, STA = Sacral Table angle, PA = Projection angle, PSA = Pelvisacral angle

The unscaled model of whole lumbar spine PCA was described elsewhere (Section 4.3.1.1). For neglecting the size variation, a scaled model of whole lumbar spine was also developed (Section 4.3.1.2). Since 95% of the data variation within the population was captured by first 10 PCs in the unscaled model, and first 35 PCs in the scaled model, these projected weights were taken into consideration for the statistical analysis.

The coefficient of determination (R^2) between the individual PC projected weights (PC1 to PC10 for unscaled model & PC1 to PC35 for scaled model) obtained from the whole lumbar spine SSM showed no significant correlation with the previously calculated 3D sacropelvic parameters. For the unscaled model, the multivariate regression on combined PC1-PC10 weights and FSPA, LL showed medium correlation (Table 8). Other sacropelvic parameters such as PI, PA, CSD, APA, CSD, In-out angle, SK and L5-Sacrum angle showed weak correlation. In the scaled model, the multivariate regression on combined PC1-PC35 weights showed weak and negligible correlation on the 3D sacropelvic parameters (Table 8).

Table 8: The relationship between spinopelvic parameters and bone variations for scaled and unscaled whole lumbar spine where Green= Very strong correlation (<± 0.9), Red= Strong correlation (± 0.71 and ± 0.9) Orange= Medium correlation (± 0.51 and ± 0.70), Blue= Weak correlation (± 0.31 and 0.50), Yellow= Negligible (0 to 0.3)

Spinopelvic parameters	R² values combined pc weights	
	Unscaled model	Scaled model
PI	0.31	0.26
APA	0.42	0.32
PA	0.35	0.23
FSPA	0.53	0.33
CPD	0.41	0.38
CSD	0.35	0.30
ID	0.45	0.38
LL	0.57	0.47

Where APA = Anterior Pelvic angle, PI = Pelvic Incidence, PA = Projection angle, FSPA = Femorosacropelvic angle, LL = Lumbar lordosis, CPD = Crest pubic distance, CSD = Crest sacrum distance, and ID = Inlet distance.

4.6. Understanding sex differences on 3D spinopelvic parameters:

The simple main effects analysis indicated sex did not have a statistically significant difference (p = 0.909) on all the spinopelvic parameters. In the one-way Anova test, a statistically significant difference

(p < 0.05) was found in mean anterior pelvic angle, pelvic incidence angle and lumbar lordosis angle between sexes (Table 9).

Table 9: Mean ± SD of sacropelvic angles (°) and distances (mm) calculated in 3 dimensions (3D) between male and female

** p<0.05

	APA **	PI **	STA	PA	FSPA	PSA	CPD	CSD	SAO	LL **
Male	21 ± 3	48 ± 9	102 ± 6	21 ± 9	66 ± 9	42 ± 9	89 ±10	97 ± 9	53 ± 8	47± 10
Female	18 ± 2	51 ± 7	103 ± 6	21 ± 8	67 ± 7	40 ± 7	91 ± 11	100 ± 8	52 ± 6	53 ± 8

Where APA = Anterior Pelvic angle, PI = Pelvic Incidence, STA = Sacral Table angle, PA = Projection angle, FSPA = Femorosacropelvic angle, PSA = Pelvisacral angle, CPD = Crest pubic distance, CSD = Crest sacrum distance, SAO = Sacral anatomic orientation angle, LL= Lumbar lordosis

4.7. FE model

4.7.1. Bone Material property Validation:

The bone material property validation consisted of comparing the maximum Von Mises stress with prior FE vertebral studies (Jovanovic et al. 2010; Nabhani et al. 2002; Nguyen et al. 2018). Cortical bone material property was assigned to L2, and we replicated the loading and boundary conditions of the other FE modelling studies. The maximum Von Mises stress obtained for L2 was 2.8 MPa (Figure 51) which was in the range of previous FE studies who found 4.77 MPa (Nguyen et al. 2018), 4.04 MPa (Jovanovic et al. 2010) and 1.92 MPa (Nabhani et al. 2002).(Table 10).
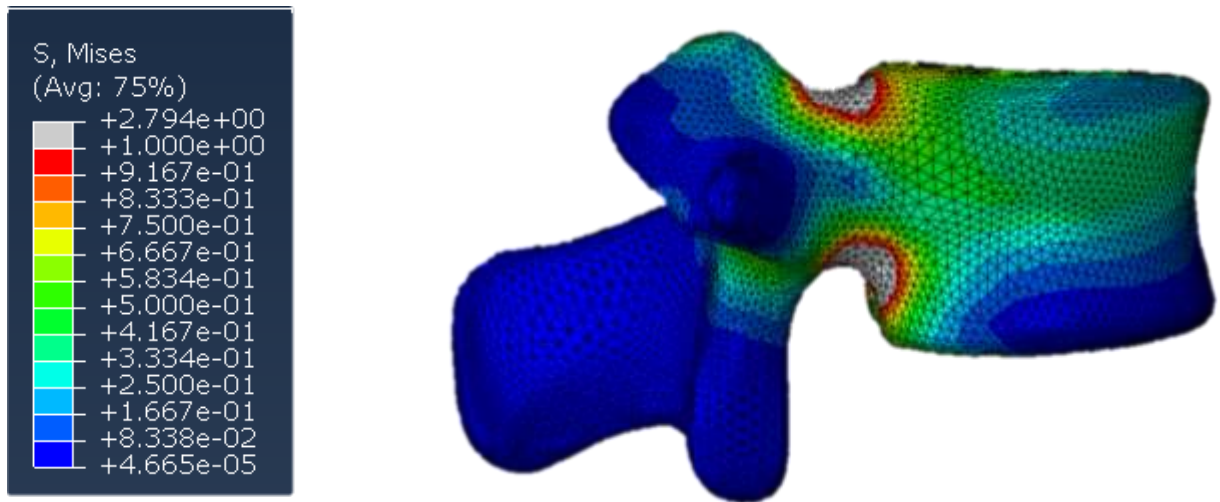
Figure 51: Von Mises stress distribution in L2 in MPa

Table 10: Maximum Von Mises stress (Mpa) analysis between our individual vertebrae (L2) FE model and other published individual vertebrae models

Model Name	Material property assignment	Maximum Von Mises stress (MPa)
Nabhani et al. (2002)	Previous literature values	1.92
Jovanovic et al. (2010)	CT-based material property	4.04
Nguyen et al. (2018)	CT-based material property	4.77
Our individual vertebrae (L2) model	Previous literature values	2.8

4.7.2. FE Model mesh convergence analysis:

For understanding the effect of mesh resolution on the prediction (average von mises stress values) of our individual vertebrae (L2) model, we performed the mesh convergence analysis on the tetrahedral mesh. We ran 5 simulations with five different mesh sizes such as 0.5, 1, 2, 3, and 4 mm and then we computed the average von mises stress at the L2 vertebral body. From Figure 52, it is observed that around 2 mm mesh size, the model predictions changed less than 5%. Therefore, we consider the mesh size of 2mm being converged (Aytruk et al. 2011) and we have used this mesh size in all of our subsequent FE simulations. The element numbers according to each mesh element size is summarized in Table 11.

Table 11: Element numbers of different mesh element sizes

Mesh element size (mm)	Element numbers
0.5	642761
1	136059
2	107196
3	8274
4	5586
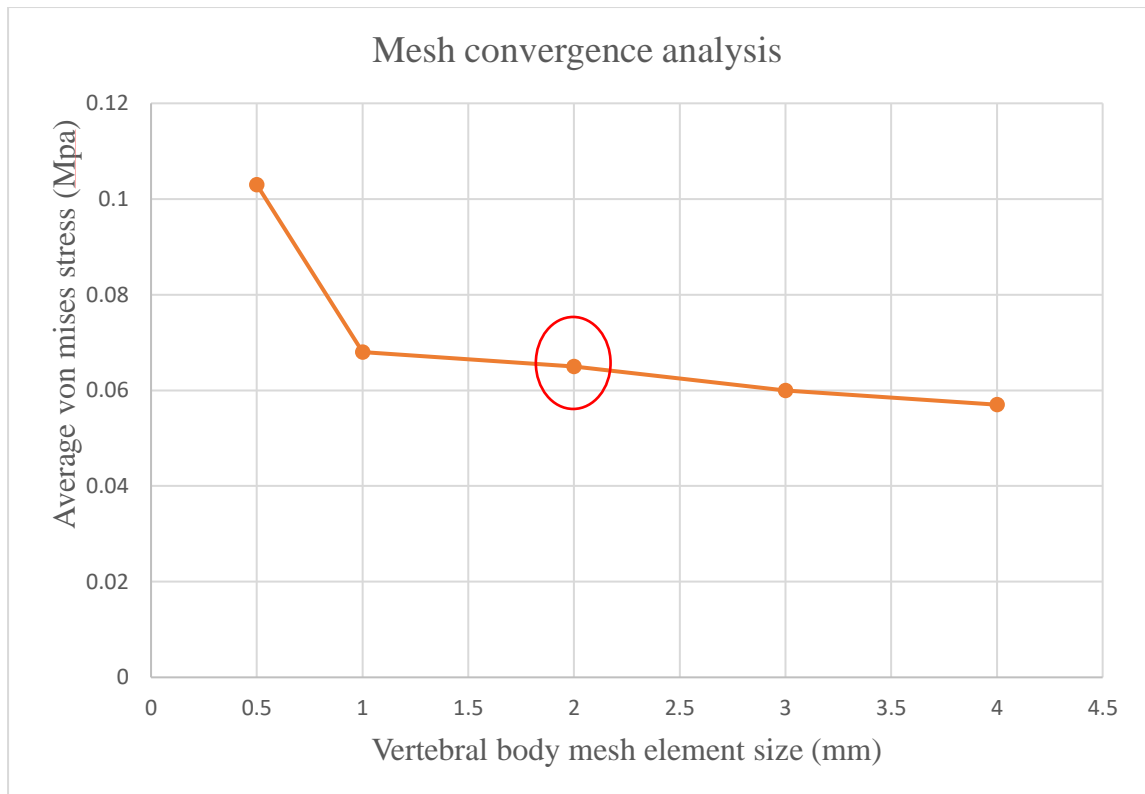
Figure 52: Mesh convergence analysis for tetrahedral mesh used in our FE study

4.7.3. Disc Material Property Validation:

In this step, the disc material property was validated with previous FE studies (Kuo et al. 2010; Ranu et al. 1979; Shirazi-Adl et al. 1984) by analyzing the intradiscal pressure in the standing position with the FE Model which consisted of L1-L2 FSU and intervertebral disc (IVD). For this IVD model, the intra-discal pressure (IDP) was computed at L1-L2 vertebral level under the load of 300N, 460N and 600N and compared with the previous ex-vivo and FE studies (Kuo et al. 2010; Ranu et al. 1979; Shirazi-Adl et al. 1984). The results indicated that the IDP obtained from the disc model (shown in yellow in Figure 53) was much lower than the previous FE studies (Kuo et al. 2010; Ranu et al. 1979; Shirazi-Adl et al. 1984). For the disc model, the IDP value was 0.08 MPa, 0.12 MPa and 0.16 MPa under the load of 300, 400 and 600N.

4.7.4. Lumbar ligaments Property Validation:

Spring ligaments

The IDP value obtained from the model where ligaments were modelled as linear spring was also lower compared to other works (Kuo et al. 2010; Ranu et al. 1979; Shirazi-Adl et al. 1984). Although it is seen from Figure 53, the IDP value increased compared to the disc model, still it was not in the range. From the spring ligament model, the IDP values were 0.13, 0.16 and 0.26 mm while subjected to the axial load of 300N, 460N and 600N.

Connector ligaments

In the ligaments as connector's model, the IDP value at L1-L2 level further increased to 0.28mm, 0.33mm and 0.38mm which was in the good agreement with other prior studies (Kuo et al. 2010; Ranu et al. 1979; Shirazi-Adl et al. 1984). Moreover, the data indicated in each model, the IDP increased linearly with increasing compressive load (Figure 53).
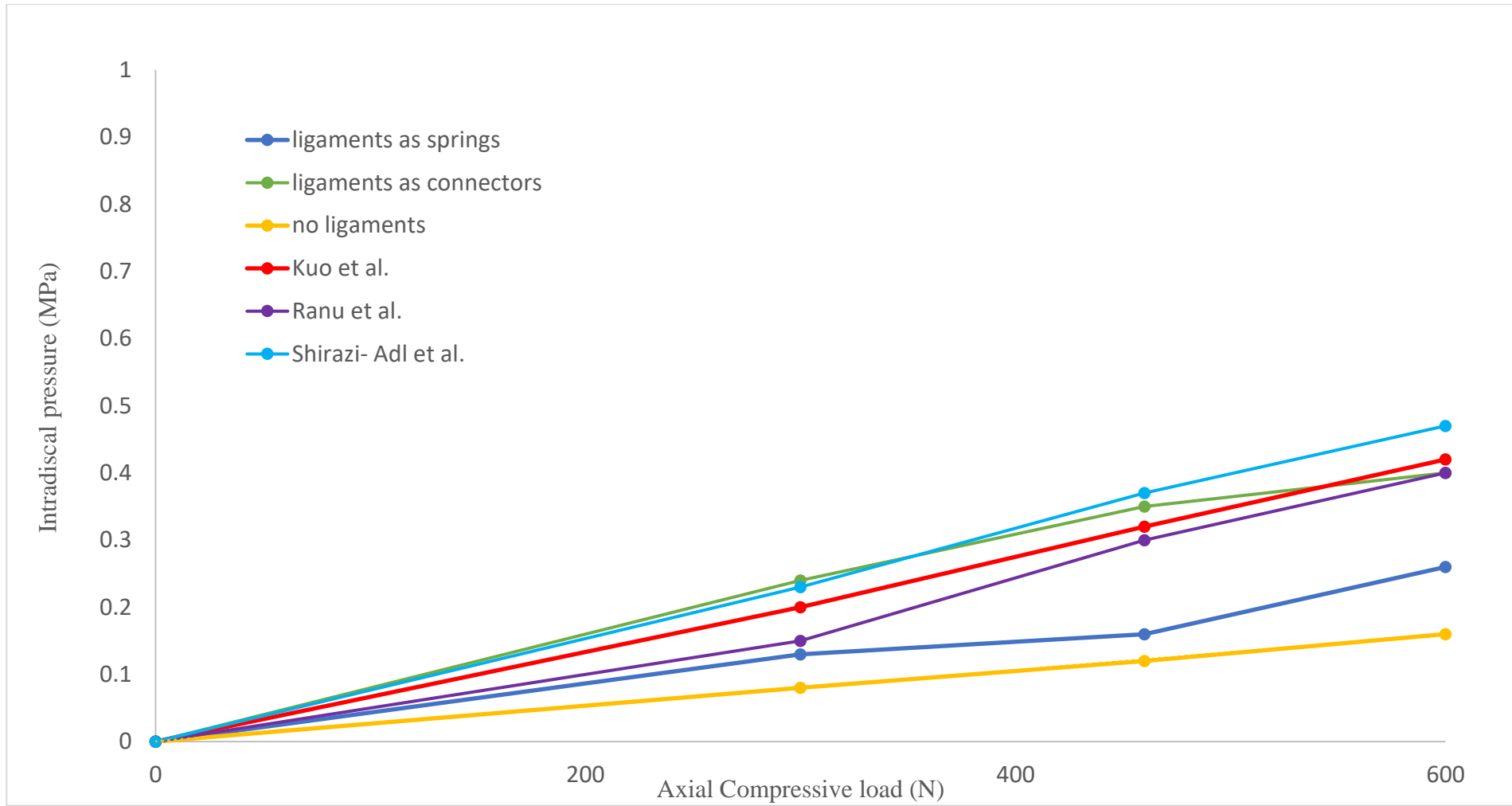
Figure 53: Validation of IVD and ligament material property by comparing the intradiscal pressure with previous studies

4.7.5. Functional spinal unit (without IVD) Validation:

This validation was conducted to find the most accurate property of the intervertebral disc without modelling the disc in our FE model. Therefore, a sensitivity analysis was performed on disc stiffness and clearance parameters (at which contact pressure is zero) for our FSU model (L1, L2, without IVD, ligaments as connectors). We wanted to achieve the average Von Mises stress and the displacement of L1 in this model which was in the range of the validated model (with the IVD and ligaments).We observed while the stiffness was constant (0 N/mm) and the disc clearance was increased, the average Von Mises stress at L1 also increased. Similarly, while the disc clearance was set to constant (highest clearance 7), by increasing the stifness from 0 to 200 N/mm, the average Von Mises stress at L1 was also increased. Then, we compared the displacement at L1, with the clearance and displacement values (Table 12). Since the IDP value of FE model (with IVD and ligaments as connectors) was validated with previous studies (Figure 52), the average Von Mises stress, L1 displacement, stress pattern in L1 & L2 and computational time of Model without IVD was computed and was compared with Model with IVD (Table 13). For simplicity, we defined model with IVD as Model 1 and model without IVD as Model 2. It was found that in Model 2 at 50 N/mm disc stiffness and clearance value of 6, the avereage Von Mises stress, displacement at a node in L1 and stress pattern (Figure 54) exhibited similarity with Model 1(Table 13). However, Model 2 was 7 times more time efficient compared to the Model 1.

Table 12: Sensitivity analysis between the Model 1 (disc and ligament validated model) and disc stiffness and clearance parameters of Model 2 (FE model without the IVD)

	Stiffness (N/mm)	Clearance value	Nodal displacement in L1	Avg Von Mises stress (Mpa)	Computational time (mins)
Model 1 (with IVD and ligaments)	N/A	N/A	0.94 mm	L1: 0.81 ± 0.78 Mpa L2: 0.86 ± 0.87 Mpa	20
Model 2 (without IVD)	200	7	1.64 mm	L1: 0.88 ± 0.82 Mpa L2: 0.90 ± 0.88 Mpa	6
	125	7	1.63 mm	L1: 0.87 ± 0.82 Mpa L2: 0.90 ± 0.88 Mpa	6
	100	7	1.61mm	L1: 0.87 ± 0.81 Mpa L2: 0.89 ± 0.88 Mpa	5
	100	6	1.30 mm	L1: 0.82 ± 0.80 Mpa L2: 0.84 ± 0.84 Mpa	4
	50	6	1.19 mm	L1: 0.79 ± 0.80 Mpa L2: 0.80 ± 0.84 Mpa	4
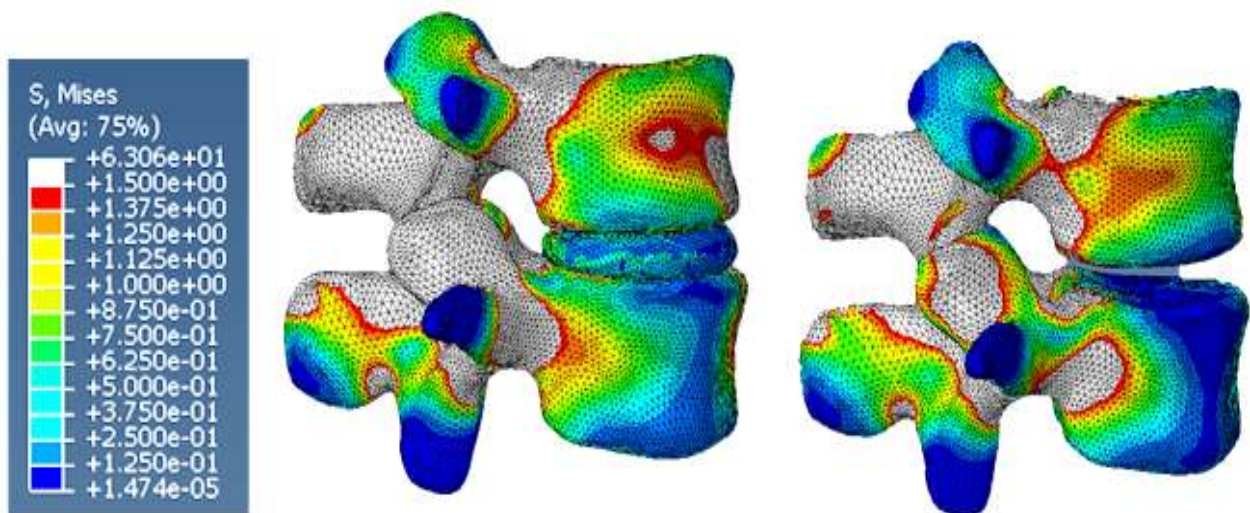
Figure 54: Stress distribution of Model 1 (left) & Model 2 (right)

Table 13: Comparison of different parameters between Model 1 & Model 2

Model Name	Avg. ± s.d. Von Mises stress (Mpa)	Displacement at a node in L1 (mm)	Computational time (mins)
Model 1 (with IVD)	L1: 0.81 ± 0.78 L2: 0.86 ± 0.87	0.94	29
Model 2 (without IVD)	L1: 0.79 ± 0.80 L2: 0.80 ± 0.84	1.19	4

Where Avg= Average, SD = standard deviation, IVD= Intervertebral disc

4.7.6. Average Von Mises stress from the whole lumbar spine:

Finally, we extended the Model 2 by integrating the other lumbar vertebrae (L3, L4, and L5), the lumbar ligaments at each vertebral level and sacropelvic ligaments. From this FE model, the average Von Mises stress and maximum Von Mises stress was computed at each vertebral level (Table 14). It was noticed that average and the maximum Von Mises stress increased along downward direction (Figure 54) which

114

is consistent with the literature (Kuo et al. 2010). For better visualization of stress distribution in lumbar vertebrae, the pelvis and sacropelvic ligaments were hidden (Figure 55). In the L5, the maximum Von Mises stress recorded was 10 Mpa is in good agreement with previous study (Kuo et al. 2010).

Table 14: Average, Max Von Mises stress, and computational time in the whole lumbar spine FE model (without IVD)

Model Name	Bone level	Avg ± SD Von Mises Stress (Mpa)	Max. Von Mises Stress (Mpa)	Computational time (mins)
Whole lumbar spine FE model without IVD	L1	0.45 ± 0.7	4	240
	L2	0.51 ± 0.78	4.5	
	L3	0.53 ± 0.75	6	
	L4	0.55 ± 0.81	8	
	L5	0.57 ± 0.83	10	
	Sacrum	0.60 ± 0.85	14	

Where Avg= Average, SD= standard deviation, IVD= Intervertebral disc
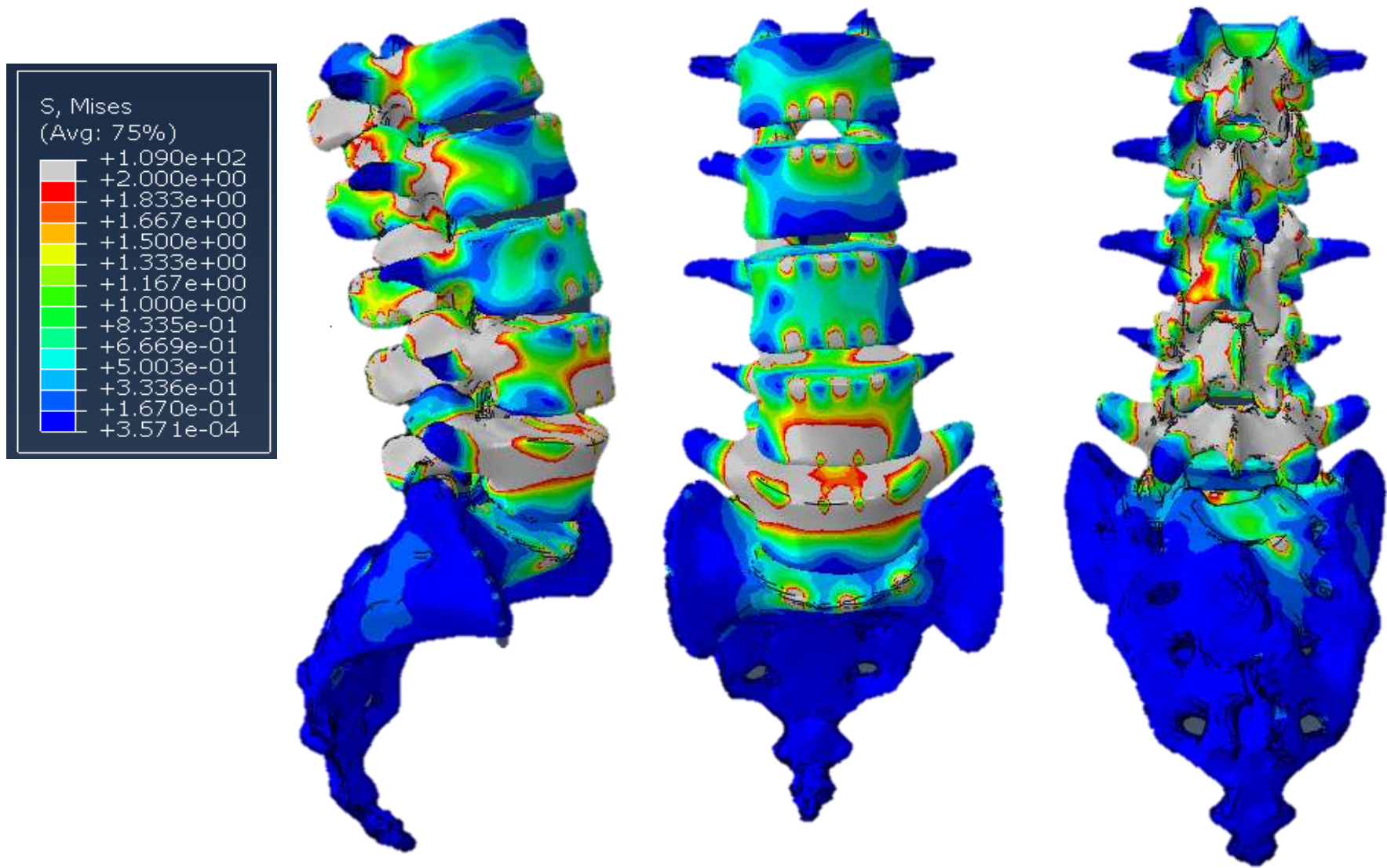
Figure 55: Von Mises Stress distribution in Model 6, Sagittal (A), Frontal (B) & Posterior (C) view in the whole lumbar spine

Chapter 5: Discussion

The first aim of our study was to create a personalized, automated and population based whole lumbar spine model from an adult healthy population. The creation of a personalized, population-based lumbar spine model shows the feasibility and potential utility of such an approach in clinical practice. The characterization of bone shape variation provides valuable insights into the morphological diversity within the population, essential for personalized healthcare interventions.

The second aim of our study was to investigate the differences between the spinopelvic parameters measured on CT scans from 2D slices and the 3D reconstruction of the spine and to understand the correlation between the 3D spinopelvic parameters and the bone shape. The observed correlations between 3D spinopelvic parameters and bone shape assessed the interconnectedness of anatomical structures in the lumbar spine, evaluating the importance of comprehensive modelling approaches.

The third aim of our study was to create a computationally time efficient lumbar spine finite element model which could be used for clinical purposes. In terms of FE modelling, the exploration of material properties and ligament modelling strategies contributes to the refinement of computational models, aiming to achieve a balance between accuracy and computational efficiency. The assessment of FE model accuracy with and without disc modelling provides valuable insights into the necessity of incorporating disc properties in biomechanical simulations.

5.1. Statistical Shape Modelling (SSM)

The development of statistical shape models (SSMs) for the individual lumbar vertebrae, pelvis, sacrum, and whole lumbar spine represented a significant contribution to the field of spine biomechanics and personalized healthcare. Our research aimed to comprehensively characterize bone shape variation in a healthy adult population aged 17-84, providing valuable insights into lumbar spine morphology and its implications for clinical practice.

Our study successfully applied principal component analysis (PCA) to capture shape variations across various anatomical structures of the lumbar spine. Notably, the first PC of the lumbar vertebrae model predominantly accounted for vertebral height variation, consistent with previous literature findings

Hollenbeck et al. (2018). Similarly, the variation in posterior lumbar elements was captured by the second and third PCs, aligning with prior research results (Hollenbeck et al. 2018, Haq et al. 2020).

For the whole lumbar spine, we introduced two SSM models: scaled and unscaled, each focused on distinct purposes in understanding shape variations. The scaled model effectively removed size variation, enabling focused analysis of shape changes across different regions of the lumbar spine. The first PC of our whole lumbar spine unscaled model captured the variation of the lumbar spine size, which is similar to prior L1-L5 models (Campbell and Petrella 2016; Hollenbeck et al. 2018; Rasoulian et al. 2013). The second PC described the variation in lumbar spine curvature, which is comparable to prior SSM of the whole lumbar spine (Ali et al. 2012; Campbell and Petrella 2016; Rasoulian et al. 2013). For our scaled model, the first PC captured the lumbar curvature variation which was difficult to visualise in the unscaled model. Moreover, the percentage variation (25%) captured by the first pc in the scaled model was lesser compared to the unscaled model (52%). The second and third PC of the scaled model demonstrated iliac width and sacral crest shape changes, which was not prominent in the unscaled model. This shows the development of scaled model was crucial to understand the shape variation of every part of the lumbar spine other than size. To our knowledge, no studies have studied the scaled whole lumbar spine shape. Therefore, the PCA results of the scaled whole lumbar spine shape model cannot be compared with the previous work.

Additionally, my study uniquely explored shape variations in the whole lumbar spine, including the pelvis and sacrum, offering novel insights into spinopelvic interactions. Prior studies (Ahrend et al. 2020; Arand et al. 2019), have also investigated the 3D shape variation of the pelvic ring and pelvic bone for the generic Asian population. In these studies, the first and second PC demonstrated size and shape variation of the pelvis, similar to our study.

Assessment of the SSM model's accuracy through measures such as compactness, generalization, and specificity demonstrated the robustness of our models in capturing shape variations within the healthy adult population. Notably, our larger sample size enabled a more comprehensive characterization of bone shape variation compared to previous studies (Hollenbeck et al. 2018). In our study, for the individual vertebrae (L1-L5), the maximum shape variation occurred in the anterior part of the vertebral body. Our ultimate research goal was to develop a personalized FEM from the SSM model of the lumbar spine. Since we found most of the shape variation in the anterior part of the vertebrae, in our FEM, we did not model the posterior part of the vertebrae separately.

For our pelvis and sacrum model, the first PC accounted for 39% and 34% shape variation, similar to (Meller and Kalender 2004). Considering compactness factor, 95% of the shape variation within the

population in our work was defined by the first 39 PCs in L1, 37 PCs in L2, 38 PCs in L3, 43 PCs in L4, 41 PCs in L5, 35 PCs in the pelvis, and 47 PCs in the sacrum. Meller et al. (2004) reported 24 out of 39 modes were required to capture the 95% shape variation in the pelvis. Meyen et al. (2020) required 25 out of 90 modes for capturing 95% variation in pelvic discontinuity. The difference in compactness (percentages of shape variation) in different studies could be influenced by the difference in population size, age range and ethnicity. In our study, the maximum fitting error was observed in pelvis and sacrum compared to individual vertebrae. These fitting errors were similar to Meyen et al. (2020). The maximum fitting error was observed in pelvis and sacrum due to the bone size. Moreover, some participants had different number of sacral foramina and coccyx shape compared to the template mesh. However, the number of sacral foramina and coccyx shape consideration was not crucial for our FEM purposes. To the best of our knowledge, no studies have quantified the individual vertebrae's generalization and specificity errors. The prior studies have limitations with their sample size, restricted age range, or gender selection. The novel aspect of our SSM work is representing the bone shape variation of individual lumbar vertebrae, whole lumbar spine, pelvis, and sacrum in an extensive range of healthy adult populations, which is ideal for characterizing the morphological differences across the entire population.

For our whole lumbar spine unscaled SSM, 95% data variation within the population was defined by the first 10 PCs. In our scaled model, first 35 pcs captured 95% of the shape variation. Since in our scaled model, the most dominant factor size was removed, more number of PCs were required to capture 95% data variation. Campbell et al. (2016) and Rasoulian et al. (2013) demonstrated that 12 modes were sufficient to capture 95% variation in L1-L5 shape However, one key difference between our whole lumbar spine SSM and other SSMs is that, in our study, the pelvis and sacrum were also included with the L1-L5 vertebrae. To our knowledge, no studies have developed a whole lumbar spine model for a healthy adult population. Since, in our work we wanted to understand the influence of spinopelvic angles and distances in the whole lumbar spine shape for pre-surgery planning, we included pelvis and sacrum in our SSM.

Rasoulian et al. (2013) considered shape and pose modes separately in their SSM. Whereas, in our study, pose and shape variations were combined, consistent with other studies (Campbell and Petrella 2016; Hollenbeck et al. 2018). The selection of considering pose and shape together or differently relies on the application of the analysis. In our study, the SSM of the whole lumbar spine were used in FE simulation in weight-bearing condition, considering pose was important. Consequently, we fit this SSM to weight-bearing FEM. As, lumbar posture in supine and weight bearing condition will be different, an articulated

shape model that can accurately capture the shape and pose of the lumbar spine would be a good option for future work.

Furthermore, we developed our SSM based on healthy participants. However, the patients that need surgery are usually older and have pathological conditions in terms of posture and loading conditions. In the older population, while the bone shape may exhibit similarities, the spine curvature might be different compared to the healthy population. To account for this, employing the articulated shape model to the participant dataset in future is a good alternative to effectively capture of the spinal curvature within the population.

In the current whole lumbar spine SSM, the specificity error was 8.63 mm, including 25 out of 100 modes. The error value increased compared to other works (Campbell and Petrella 2016; Rasoulian et al. 2013), due to presence of the pelvis and sacrum in our SSM.

The predictive capability of our SSMs was evaluated using root mean square error (RMSE) and dice score, providing valuable insights into the models' performance in predicting bone shapes. The RMSE value for our individual vertebrae models (averaged across all the vertebrae) with bone measurements were 1.92 ± 0.68 mm, which was higher than the RMSE, i.e., 1.06 ± 0.19 mm (for 52 participants) reported by Hollenbeck et al. (2018). The higher RMSE value in our study might be attributed to the presence of unusual transverse process or flatter spinous process shapes in some of our participants. Incorporating bone measurements significantly improved predictive accuracy, emphasizing the importance of comprehensive anthropometric data in SSM development.

For our pelvis and sacrum model, the RMSE value were 5.75 ± 1.76 mm and 4.28 ± 1.29 mm. An earlier study by Ahrend et al. (2020) developed a CT-based 3D statistical pelvic bone model to investigate the generic Asian population for 100 participants. They performed a leave-one-out test to measure the fitness of their reconstruction process. With 30 CT scans, they obtained a mean distance error of 5.24 ± 2.62 mm, which are in the range of our results. According to our understanding, as the pelvis is a big bone compared to the lumbar vertebrae, the prediction error is also bigger for the pelvis. To the best of our knowledge, we are unaware of any SSM model of the sacrum where the RMSE computation for prediction accuracy is reported. In our sacrum SSM, most of the errors were present either in sacral foramen or in coccyx. However, the RMSE value found in sacral foramen or coccyx was not the focus of our FE

120

analysis. Since the pelvic incidence value depends on the orientation of sacral endplate, we were only interested to understand the stress distribution in sacral endplate during weight-bearing for our FE analysis.

We have computed the dice score for the volume similarity comparison between our predicted model and the original (ground truth model). Our dice score for the individual lumbar vertebrae, pelvis and sacrum SSM was similar to adult cochlea (Noble et al. 2017), liver (Spinczyk et al. 2018) and prostate (Karimi et al. 2019) SSMs. When the bone measurements were included in the bone volume prediction, the prediction improved by only 2-3% for individual lumbar vertebrae, pelvis, and sacrum. Therefore, we can conclude that the bone height, length, width, pelvis ASIS and PSIS distances and sacral plateau length and width did not improve the volume prediction by a significant amount.

Despite these advancements, several limitations were identified, including the lack of certain demographic information and ethnicity considerations in the dataset. For the SSM study, the knowledge of ethnicity is imperative for evaluating its potential influence on the population. The presence of shape outliers in the dataset often leads to higher errors in the leave-one-out validation. In case of vertebrae shape prediction, the outliers occurred from unusual transverse process or flatter spinous process shapes present in some participants. In case of pelvis, some participants had a fused pubic symphysis. For sacrum, the coccyx inclination and sacral foramen was different for many participants. Therefore, the LOO unable to predict these shape changes for these participants accurately. In future, by integrating more landmarks in the posterior arch of vertebrae, pubic symphysis and coccyx we could mitigate these outliers.

For our whole lumbar spine model, we predicted the whole lumbar spine shape for 2 participants by fitting the mean lumbar spine model, three PCs and patient-specific CT landmark coordinates. For achieving this prediction, we have used our in-house (GIAS2) library. This library was originally developed for the prediction of the lower limb bones. However, for the whole lumbar spine shape prediction this library needed more modification in terms of adding correspondence between the landmarks of source and target meshes. In our work, we have limited option to modify the previously developed library or create a new library. Therefore, this method did not perform well for whole lumbar spine shape prediction. Our results indicated that this workflow could not capture the shape of the whole lumbar spine curvature in the frontal plane and posterior part of the lumbar spine, pelvis, and sacrum. By excluding the pelvis and sacrum from the whole lumbar spine prediction, the maximum error between the predicted and CT reconstructed shape

121

decreased by 16mm. The main drawback of this workflow was the lack of corresponding bone landmarks between the template mesh (source mesh) and the participant's CT landmark coordinates (target mesh). Moreover, our SSM did not consider the articulating joints between each vertebra. The number of landmarks used for the pelvis and sacrum was minimal considering the size of the bones. With this approach, we predicted the shape of two participants, which is inadequate for the bone prediction in a population. All these factors contribute to errors in the whole lumbar spine shape prediction.

For improving the whole lumbar spine shape prediction, we then integrated the anthropological predictors (age, sex), a few spinopelvic angles (mono-segmental lordosis angle, pelvic incidence, and L5- sacrum angle), and different bone measurements (height, length, and width of each lumbar vertebrae) which can be easily measured from the bone landmark selected previously on the CT images. In this approach, the mono-segmental angle, the total lumbar lordosis angle, angle between pelvis and sacrum were input for the bone prediction. Restoration of these angles between each bone are very crucial for the whole lumbar spine shape definition. Therefore, this approach matched the lumbar shape more accurately than the previous approach (prediction using mean shape, 3 pcs and landmarks). The RMSE value for the whole lumbar spine was 9.21 ± 4.55 mm (for 100 participants). No prior studies have predicted the shape of the whole lumbar spine (including the pelvis and sacrum). For our whole lumbar spine SSM the dice score was 0.63. The dice score reduced compared to the individual vertebrae (0.88 across all vertebrae). The reduction of the dice score could be influenced by the exclusion of pose. Moreover, the volume of posterior arch, coccyx and pubic symphysis and articulating facet joints prediction is notoriously difficult in the whole lumbar spine SSM.

Our development of statistical shape models (SSMs) for various components of the lumbar spine offers significant potential for clinical applications. By characterizing bone shape variations in a healthy adult population, our models provide clinicians with valuable insights into the natural morphological variability of the lumbar spine. This understanding is crucial for personalized treatment planning, particularly in cases where surgical interventions are considered. With the ability to accurately predict bone shapes using our SSMs, clinicians can better anticipate anatomical variations and tailor surgical approaches accordingly. For example, in spinal fusion procedures, understanding individualized bone morphology can inform decisions regarding implant selection, sizing, and placement, ultimately optimizing surgical outcomes and reducing the risk of complications.

Moreover, our study sheds light on the importance of incorporating comprehensive anthropometric data, such as age, sex, and bone measurements, into predictive models. By leveraging this information, clinicians can enhance the accuracy of preoperative assessments and improve patient-specific treatment

plans. For instance, knowledge of spinopelvic angles and distances can aid in evaluating spinal alignment and biomechanical stability, guiding decisions regarding surgical approaches and postoperative rehabilitation strategies.

5.2. 2D and 3D Sacropelvic parameters comparison

The next objective of our study aimed to investigate the relationship between 3D spinopelvic parameters and bone shape variation in the lumbar spine and pelvis. Our research goal was to provide valuable insights that could inform clinical decision-making and improve patient care in the context of spinal surgery and treatment planning.

Schwab et al. (2013) have shown that restoration of spinopelvic alignment is vital for successful spinal fusion surgery. Sagittal spinopelvic alignment is defined by the interaction between static (Pelvic incidence (PI) and dynamic pelvic parameters (Pelvic tilt (PT), Sacral slope (SS) and spinal curvatures (Lumbar lordosis (LL). PI is a static parameter that does not vary after skeletal maturity and does not change with the rotation of the pelvis in the sagittal plane. PI is also the summation of PT and SS. PT is the angle formed by the line connecting the midpoint of the sacral endplate to the bicoxofemoral axis and a vertical reference line. SS is the angle formed by the superior sacral endplate and a horizontal reference line. PT and SS are directly associated with pelvic positioning, and it varies. The inability to restore spinal curvature post-surgery leads to disability, pain, adjacent segment degeneration, and revision surgery. Therefore, the relationship between pelvic incidence (PI) and other sacropelvic parameters such as lumbar lordosis (LL), sacral slope (SS), Pth (pelvic thickness), pelvic tilt (PT), and Sacral kyphosis (SK) are well explored in prior works (Glassman et al 2010.; Okamoto et al. 2020; Schwab et al. 2013; Tardieu et al. 2013). Beaupere et al. (1992) have shown a correlation between PI and SS (r=0.8), LL and TK (r=0.59), and SS and LL (r=0.87). Legaye et al. (1998) and Vialle et al. (2005) also demonstrated a strong correlation between SS and LL (r=0.86). Okamoto et al. (2020) found that TK, LL, PI, and SS increase with the decreasing sacral height. Our findings between the sacropelvic parameter and sacrum shape suggest that sacrum width is moderately correlated with PI and APA. Since the PI angle defines the sacrum position in the sagittal plane w.r.t femoral heads, the result of our study is consistent with the anatomy.

5.3. Correlation between the bone shape and 3D spinopelvic parameters

Since spinal fusion surgery is performed to restore the spine's natural curvature, a detailed analysis of lumbar spine shape in 3D and its contribution to pelvic morphology is crucial. Since the lumbar lordosis varies hugely in proximal (L1-L3) and distal vertebral level (L4-L5), Anwar et al. (2015), Pesenti et al. (2018) and Baker et al. (2020) initially investigated the distribution of monosegmental mean lordosis in the total lumbar lordosis. Baker et al. (2020) and Pesenti et al. (2018) determined that the distal vertebral bodies (L4-L5) contribute to 81 % and 62% of total lumbar lordosis, respectively. Then, the authors studied the influence of PI in proximal and distal LL. Baker et al. (2020) found out the PI value is more strongly correlated with the monosegmental lordosis obtained from proximal vertebral bodies (L1-L3). These findings were consistent with other studies by Anwar et al. (2015) and Pesenti et al. (2018). Although these studies aimed to understand the spine shape considering proximal and distal lordosis, it is not enough to accurately understand the complex morphological spine shape in 3D. Therefore, our work correlated the 3D sacropelvic parameters with the shape modes of the whole lumbar spine. Our study analysed the shape modes with various 3D sacropelvic parameters such as PI, LL, APA, PA, FSPA, PSA, Pth, CPD, and CSD. Our findings suggested that there is a moderate correlation between lumbar spine shape and sacropelvic parameters due to the structural complexity of the spine. Prior studies have demonstrated PI determines SS, which in turn influences LL. However, what predicts PI is still unclear. Since PI is a fixed morphological parameter, pre- and post-surgery, we wanted to understand if there is a strong correlation between the lumbar shape and the PI or other sacropelvic parameters. The correlation between the bone shapes and sacropelvic parameters can inform clinicians in pre-surgery planning for spinal deformities. To the best of our knowledge, this is the first study to explore the relationship between bone shape and sacropelvic parameters.

The limitation of our study is the imaging modality used to collect the imaging data. The participants analyzed in our study were in CT supine positions. However, the lumbar spine curvature variation can be assessed accurately if the participants are in a standing X-ray scan. In the future, the SSM model of the lumbar spine used in this study should be fitted to an upright X-ray to capture the lumbar curvature variation more accurately.

5.4. Understanding the effect of sex on 3D spinopelvic parameters

Furthermore, my study revealed significant sex-related differences in 3D spinopelvic parameters, among a healthy adult population. Previous studies have investigated sex-related changes in 3D spinopelvic parameters to understand the morphological variation between sexes. Tardieu et al. (2013), Janssen et al. (2009), and Thiong et al. (2011) did not find any statistically significant difference between SS, PT, and PI. However, our results demonstrated statistically significant differences in APA, PI, and LL measurements between sexes, which is consistent with studies by Vialle et al. (2005) and Anon et al. 2015). The difference in lumbar lordosis might occur due to a higher PI in average in women compared to men. Additionally, some researchers (Bailey et al. 2016; Janssen et al. 2009) found that the lumbar lordosis angle in the female lumbar spine has larger curvature and is more posteriorly inclined to adapt to the centre of gravity change during pregnancy. The simple main effects analysis indicated that sex did not have a statistically significant difference (p = 0.909) on all the spinopelvic parameters. Most of these prior works (Boulay et al. 2006; Legaye et al. 1998; Vialle et al. 2005) have quantified the sacropelvic parameter in standing sagittal X-rays, which simplifies the complex morphology of the spine and pelvis. Therefore, the evaluation of the spinopelvic parameter from the sagittal radiograph does not describe the morphology of the population accurately. To our knowledge, only Janssen et al. (2009) have quantified the spinopelvic parameters in a small cohort of 60 adults' European population aged 20-42. They did not find any statistically significant differences in LL and PI between men and women. Our study has 100 healthy adult participants (36 F) aged 17-84. Moreover, the participants in our study were analysed in a CT supine position. Therefore, comparing our result with this study (Janssen et al. 2009) is not appropriate. Due to a lack of standardized definition of LL in literature, LL was measured by 4 different definitions in different publications (Frenkel et al. 2018). In our research, LL was measured between L1-L5 (Vialle et al. 2005), which is not in accordance with the L1-S1 measurement of LL in other work (Boulay et al. 2006). These findings emphasize on the importance of considering sex-specific variations in spinal morphology when developing personalized treatment strategies. By accounting for these differences, clinicians can tailor interventions to individual patient needs more effectively, ultimately improving surgical outcomes and patient satisfaction.

The limitation of our study is the small number of female participants compared to males. Moreover, we analysed the participants in CT supine position, which might not be able to distinguish LL accurately between sexes. Bailey et al. (2016) reported that the LL value differs significantly between standing and

supine position. Therefore, a study from the same participant in different postures (standing, sitting, and supine) in 3D would be more informative in understanding the 3D spinopelvic parameters. Furthermore, if different ethnicities could be included, then the analysis would be more robust.

Moreover, our investigation into the differences between spinopelvic parameters measured on 2D CT scans and 3D reconstructions offers valuable insights into the reliability and accuracy of different imaging modalities. Most spinopelvic parameters are measured on 2D sagittal/frontal X-rays pre-surgery. The information obtained from the projection of 2D angles is supposedly limited compared to the parameters calculated in 3D, highlighting the limitations of traditional radiographic techniques in capturing the full complexity of spinal anatomy. This information is crucial for optimizing preoperative imaging protocols and enhancing the precision of diagnostic assessments in clinical practice. Hu et al. (2021) reported that the sacropelvic measurement, such as Thoracic Kyphosis (TK), the sagittal vertical axis (SVA), LL, PI, and PT, between 2D and 3D, is similar. Imai et al. (2020) investigated the correlation between spinopelvic parameters and sacral slope in female patients with developmental hip dysplasia and concluded that the measurements were similar in 2D and 3D. In our study, the sacropelvic angles in 2D and 3D were identical, while the sacropelvic distances, such as CSD and CPD, showed significant differences. This difference is likely due to two reasons. First, the SSM calculated distances are taken in 3D space, which will always be larger than when projected onto a 2D plane. Second, the 2D calculated distances highly depend on the CT scan slice chosen for measurements. These results look promising to use the SSM with a regression algorithm to predict clinical angles without requiring extensive scans. To the best of our knowledge, no work has compared the 2D and 3D sacropelvic distances. Our result also demonstrates the reliability of 2D measures from the surgeons when compared with the 3D reconstructions.

In terms of clinical implications, our findings have several important implications for surgical planning and patient management. By elucidating the relationship between spinopelvic parameters and bone shape variation, our research provides clinicians with valuable tools for predicting and optimizing surgical outcomes. Additionally, our identification of sex-related differences in spinal morphology describes the importance of personalized approaches to treatment and highlights the need for sex-specific considerations in surgical decision-making.

5.5. Finite Element Model (FEM)

My research aimed to develop a computationally time-efficient 3D lumbar spine finite element (FE) model suitable for clinical use, addressing several key aspects of model validation and simplification for practical application. We employed tetrahedral meshing for its robustness in capturing complex lumbar vertebrae geometry, following the previous studies (Fan et al. (2019), Kuo et al. (2010) , Salsabili et al. (2019). This choice ensured accurate representation while maintaining computational efficiency.

Prior works have modelled the vertebral bodies with single (Nabhani and Wake 2002; Shin et al. 2018) or two distinct material properties (Charriere et al. 2003; Shirazi-Adl et al. 1984) for cortical and trabecular region, or CT data-based subject-specific material (Jovanovic and Miomir 2010; Nguyen et al. 2018; Sylvestre, Villemure, and Aubin 2007) property. Concerning bone material property, in our model we have used only cortical bone property to the whole vertebrae for simplicity and computational cost efficiency. The maximum Von Mises (VM) stress obtained from our study was a bit lower compared to the other similar studies (Jovanovic and Miomir 2010; Nabhani and Wake 2002; Nguyen et al. 2018). This difference in stress could be due to the CT based material property assignment in prior studies. The maximum VM stress comparison may not be ideal because it is highly subject-specific. Since these studies did not report the average VM stress, we could not compare the stress values. However, the VM stress pattern between our study and prior works (Jovanovic and Miomir 2010; Nguyen et al. 2018) were comparable.

Some studies (Noailly et al. 2005; Renner et al. 2007; Schmidt et al. 2006) have modelled the anisotropic fibers and ground substance of the intervertebral disc (IVD) in a composite structure. On the contrary, other researchers (Elliott and Setton 2001; Wagner and Lotz 2004; Wut et al. 2006.) have employed isotropic hyperelastic law, without isolating the fibers and ground substances. Both approaches are complex, labour intensive and not suitable for clinical use. Therefore, in our IVD modelling, we neglected the annulus fibers modelling similar to other studies (Raheem and Aljanabi 2020; Z. Zhang et al. 2018). The intradiscal pressure (IDP) obtained from our study (without the ligament), under the load of 300N, 460N, and 600N was relatively lower than previous ex-vivo and FE studies (Kuo et al. 2010; Ranu et al. 1979; Shirazi-Adl et al. 1984). One key difference between our study and these studies are the absence of annulus fibers. Kuo et al. (2010) has shown that the intradiscal pressure of IVD is highly dependent on the annulus fibers mechanical properties. The IDP increased subsequently after integrating the lumbar ligaments in our model.

For understanding the mechanical behaviour of ligaments, we have modelled the lumbar ligaments both with connectors and springs. Since the linear tension only spring does not take into account the non-linear behaviour of the ligaments, the FE model with ligament modelled as spring is more computationally time efficient. Many researchers (Coogan et al. 2016; Fan et al. 2019; Guan et al. 2006) have assumed the lumbar ligaments as linear in their FE modelling. Our results indicate that the IDP obtained from the linear ligament model was much lower than in other studies (Kuo et al. 2010; Ranu et al. 1979). For example, in case of 460N, the IDP value in linear ligament model was 0.16 MPa, whereas in previous studies it was around 0.3 MPa. In contrast, when we considered the slack length and non-linear property of the ligaments the IDP value increased to 0.33 MPa (in case 460N) which was in the range of other studies (Kuo et al. 2010; Ranu et al. 1979; Shirazi-Adl et al. 1984) (Figure 49). Therefore, in our FE model we have modelled the ligaments as connectors since it represents the biomechanical behaviour of spinal ligaments more realistically. Moreover, in our FE models, we have considered the pre-stress conditions of the IDP to mimic the physiological behaviour of the IVD, since the IVD has a 'pre-stress' condition without the action of muscles and ligaments. This approach aligns with biomechanical reality and enhances the clinical relevance of our model.

In our final FE model, we removed the IVD to reduce computational time and replaced with contact pressure overclosure relationship. The contact pressure overclosure relationship was selected by sensitivity analysis to accurately mimic the IVD property. To the best of our knowledge, this is the first study which developed a simple yet realistic, computationally time efficient FE model without compromising the accurate biomechanical properties of each component. Our FE analysis demonstrated that the average VM stress, stress pattern and displacement in our FE model with and without IVD is similar. Also, our model without IVD, is almost 8 times more computationally time efficient. Therefore, we can conclude that our simplified model has a good potential for clinical use. We also extracted the average and maximum VM stress from our whole lumbar spine model including pelvis and sacrum. Kuo et al. (2010) had developed a similar FE model for the standing position with similar loading and boundary conditions. However, in their model, they did not model the pelvis and the sacropelvic ligaments for stability. Moreover, they only reported the range of VM stress in L5 vertebral body which is similar to our result. Furthermore, the stress pattern obtained in their FE model for each vertebral body is also comparable to our result as the average VM stress in our FE model also increased towards the downwards in the lumbar spine. Our final FE model enhances the feasibility of the clinical application by achieving a balance between the accuracy and efficiency.

Our FE model has several limitations such as simplifying the material properties of bone, IVD and ligaments. Although the simplification was needed for our research objective, it might not represent the
128

actual geometry of the lumbar spine. Most of the components in our study and other researchers (Zhong et al. 2006, Kim et al. 2010, Shin et al. 2017) assumed the FE components as linear and elastic, which is a contradiction to the reality. Moreover, we have not modelled the muscles in this study which is present in the lumbar spine for stability. Also, we have modelled only one participant in the study which is not ideal to validate the geometry of each and every subject. While our model simplifications were necessary for efficiency, future research could explore parameterized models tailored to individual patient anatomy and biomechanics, further enhancing clinical relevance and personalized treatment strategies. Future research should focus on developing a fully parameterized FE model by fitting the SSM model of lumbar spine to the patient-specific landmarks. Validation studies comparing our simplified FE model to clinical outcomes and imaging data will be essential to establish its reliability and effectiveness in real-world applications.

Chapter 6: Conclusion and Future work

Our research was able to develop a personalised 3D lumbar spine finite element model which could be used in clinical environment in future. Initially we developed statistical shape model of individual lumbar vertebrae, pelvis, sacrum, combined pelvis and sacrum and the whole lumbar spine to quantify bone shape variations within an adult healthy population of wide age range (17-84). We developed the SSM of different bones in our study from the participants who were in supine position during CT scan. However, the lumbar curvature will vary on supine and standing position. Therefore, in future an articulated shape model of whole lumbar spine should be developed to consider different postures of the participants. Moreover, the prediction could be improved in future by collecting more demographic parameters such as height, weight, and a greater number of landmarks in pelvis and sacrum.

In our study, we also successfully investigated the difference between 2D and 3D sacropelvic parameters. Our research validated the sacropelvic parameters measured by the surgeon pre-surgery in 2D is accurate when compared to the 3D measurement. We also evaluated the contribution of these 3D sacropelvic parameters in the pelvis, sacrum, fused pelvis sacrum and whole lumbar spine bone shape. Our research has indicated the sacropelvic parameters are moderately correlated with bone shape due to structural complexity of the bone shapes. In this work also the participants analyzed were in CT supine position. This can lead to inaccurate representation of lumbar spine curvature. Therefore, in future a SSM should be developed from the weight-bearing X-ray participants to understand the correlation between the sacropelvic parameters more robustly. We also studied the 3D sacropelvic parameter differences between male and female. This work can be used to inform in pre-surgery planning, forensic science, and musculoskeletal modelling. However, in our study the number of male vs female were not sufficient. In future, for quantifying sex differences in sacropelvic parameters a good ratio between male and female population should be achieved.

Finally, we developed a personalised FE model in our study which is computationally time-efficient, simple yet accurate. In our work, we have developed only one FE model, which is not ideal for validating the stress distribution in the lumbar spine. In future, more FE model should be developed by fitting the mean SSM of lumbar spine to the patient-specific landmarks. Moreover, the effect of lumbar fusion

implant placement in the FE model should be also investigated and validated by the clinicians or retrospective patient's outcomes.

Since we are interested in developing a 3D lumbar spine personalised model for clinical use, in future a 2D to 3D registration algorithm should be developed. 3D shape reconstruction of lumbar spine from 2D biplanar unscaled X-ray image is a challenge due to the structural complexity. Moreover, during CT scans the participants are exposed to more radiation and it is more expensive in a clinical setting. The reconstruction process also requires prior information about the shape. In future, our mean lumbar spine SSM could be deformed until the information (contours, edges, and landmarks) extracted from the X-ray images are matched with the deformed 3D shape.

In conclusion, my research contributes to bridging the gap between biomechanical modelling and clinical practice, providing clinicians with valuable tools for personalized treatment planning and optimization of patient outcomes in lumbar spine pathology. The pipeline generated in my study can be used as a foundation for the future development of bioengineering tool. This tool would enable surgeons to visualise the 3D lumbar spine geometry and assess spinopelvic parameters as well as stress- strain distribution, derived from patient-specific bone geometry. This tool can minimize the failure of the spinal fusion surgery and helps to improve the clinical performance of patients.

Local and International Conference Abstracts:

Nikita Ghosh, Justin Fernandez, Joe Baker, Ju Zhang, Peter Robertson and Julie Choisne."Development of a simplified computationally time efficient clinical Finite element model." submitted to SpineWeek, May 2023.

Nikita Ghosh, Justin Fernandez, Joe Baker, Ju Zhang, Peter Robertson and Julie Choisne "Understanding sex differences in spinopelvic parameters for pre-surgery planning" Queenstown Research Week, Queenstown, New Zealand, August 2022.

Nikita Ghosh, Justin Fernandez, Joe Baker, Ju Zhang, Peter Robertson, and Julie Choisne "Is lumbar spine shape variation influenced by spinopelvic parameters" 9th World Congress of Biomechanics, Taipei, July 2022.

Nikita Ghosh, Justin Fernandez, Joe Baker, Ju Zhang, Peter Robertson, and Julie Choisne " The relationship between 2D and 3D sacropelvic parameters" 28th Congress of the International Society of Biomechanics, Stockholm, July 2021.

Nikita Ghosh, Justin Fernandez, Joe Baker, Ju Zhang, Peter Robertson, and Julie Choisne "Lumbar and pelvis statistical shape model to characterize population shape variations" 28th Congress of the International Society of Biomechanics, Stockholm, July 2021

Nikita Ghosh, Justin Fernandez, Joe Baker, Ju Zhang, Peter Robertson, and Julie Choisne " Lumbar spine shape variation among healthy adult", Regional Australasian Biomechanics conference, Auckland, New Zealand, Feb 2021.

Appendix
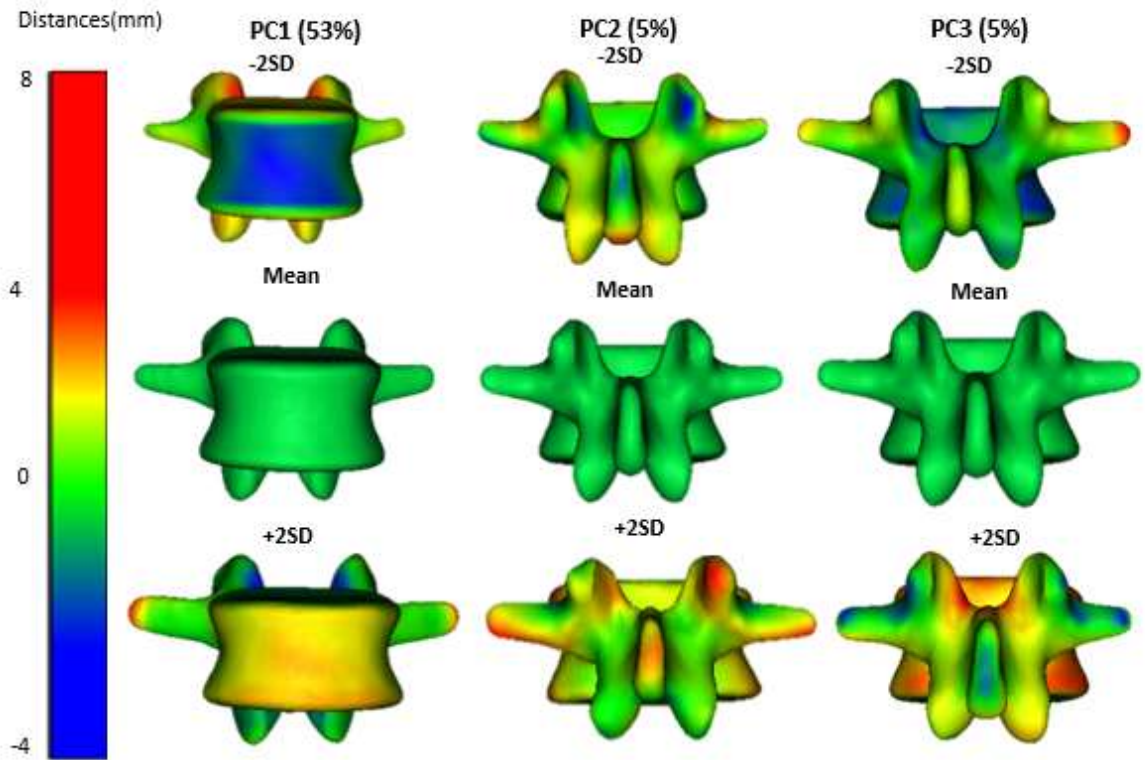
Figure A1: Average shape ± 2SD in each direction for PC1, PC2 and PC3 for L2
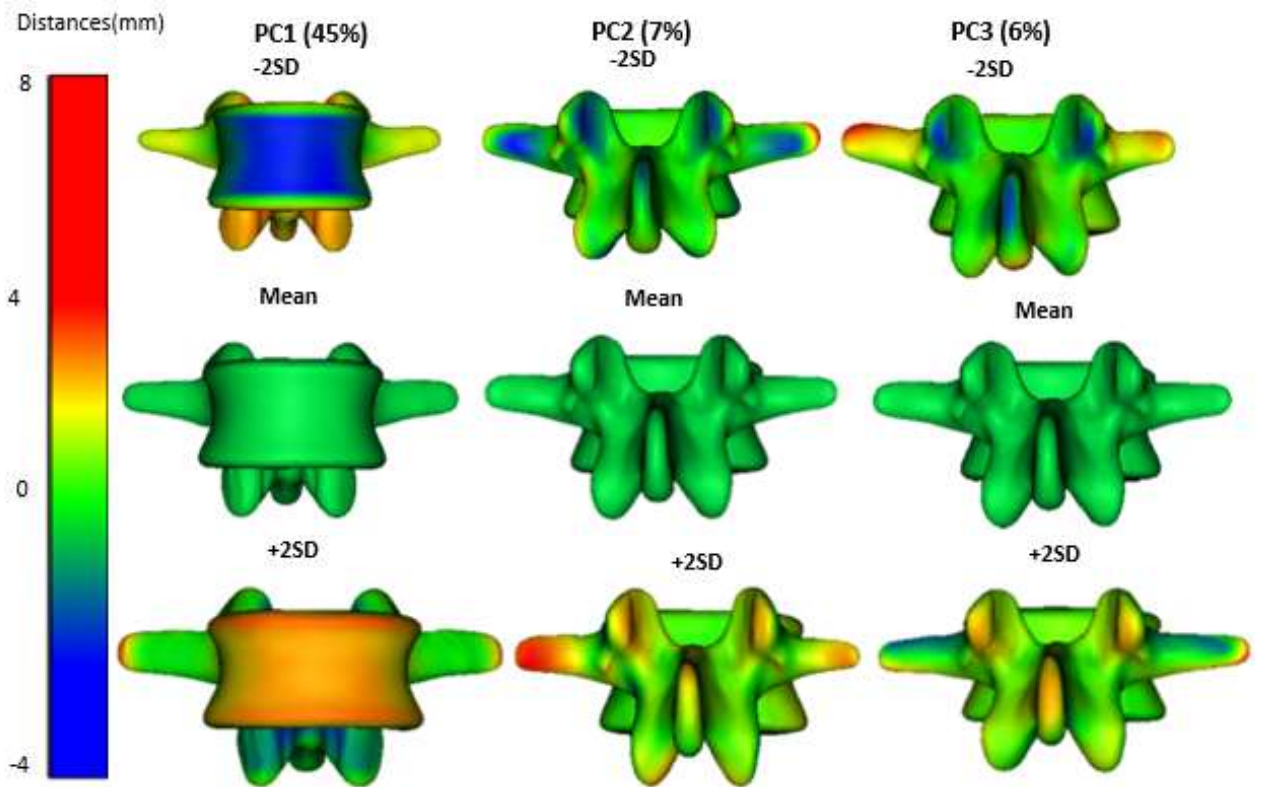
Figure A2: Average shape ± 2SD in each direction for PC1, PC2 and PC3 for L3
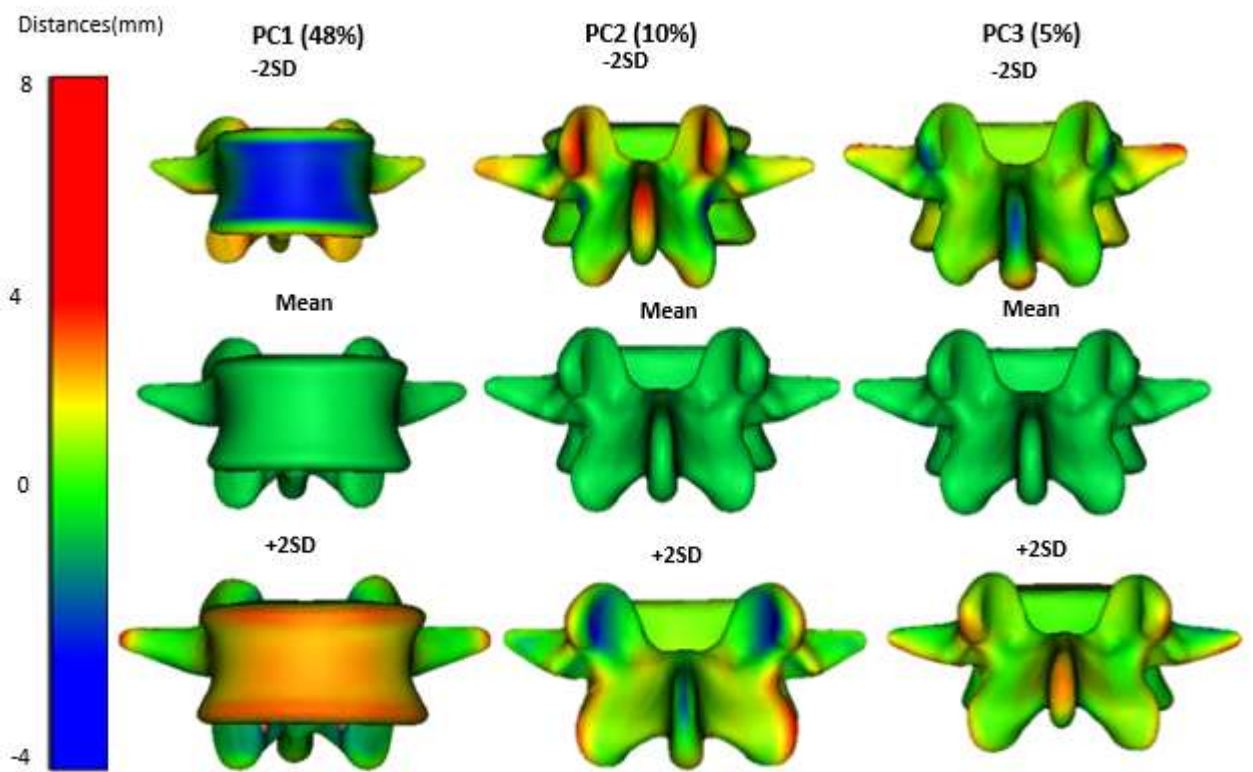
Figure A3: Average shape ± 2SD in each direction for PC1, PC2 and PC3 for L4
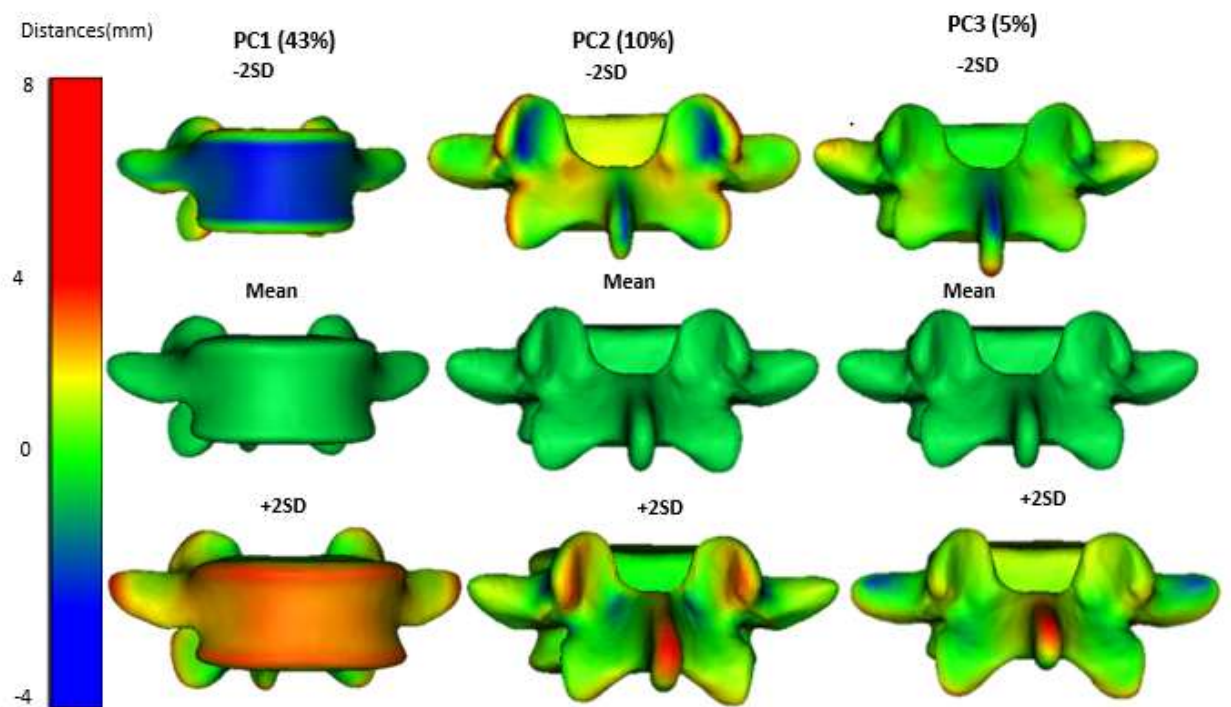
Figure A4: Average shape ± 2SD in each direction for PC1, PC2 and PC3 for L5

135

References:

Adams, M. A., & Hutton, W. C. (1985). Gradual disc prolapse. *Spine*, *10*(6), 524-531.

Adams, M. A. (2004). Biomechanics of back pain. *Acupuncture in medicine*, *22*(4), 178-188.

Ahrend, M. D., Noser, H., Shanmugam, R., Burr, F., Kamer, L., Kamarul, T., & Gueorguiev-Rüegg, B. (2020). Development of generic Asian pelvic bone models using CT-based 3D statistical modelling. *Journal of orthopaedic translation*, *20*, 100-106.

Ali, A. H., Cowan, A. B., Gregory, J. S., Aspden, R. M., & Meakin, J. R. (2012). The accuracy of active shape modelling and end-plate measurements for characterising the shape of the lumbar spine in the sagittal plane. *Computer methods in biomechanics and biomedical engineering*, *15*(2), 167-172.

A. Chagnon, C.-E. Aubin, and I. Villemure, "Biomechanical influence of disk properties on the load transfer of healthy and degenerated disks using a poroelastic finite element model.," J. Biomech. Eng., vol. 132, no. 11, p. 111006, 2010.

Andersson, G. B. (1999). Epidemiological features of chronic low-back pain. *The lancet*, *354*(9178), 581-585.

Anwar, Hanny A., Joseph S. Butler, Tejas Yarashi, Karthig Rajakulendran, and Sean Molloy. 2015. "Segmental Pelvic Correlation (SPeC): A Novel Approach to Understanding Sagittal Plane Spinal Alignment." *Spine Journal* 15(12):2518–23. doi: 10.1016/j.spinee.2015.09.021.

Aoki, Yasuchika, Arata Nakajima, Hiroshi Takahashi, Masato Sonobe, Fumiaki Terajima, Masahiko Saito, Kazuhisa Takahashi, Seiji Ohtori, Atsuya Watanabe, Takayuki Nakajima, Makoto Takazawa, Sumihisa Orita, Yawara Eguchi, and Koichi Nakagawa. 2015. "Influence of Pelvic Incidence-Lumbar Lordosis Mismatch on Surgical Outcomes of Short-Segment Transforaminal Lumbar Interbody Fusion." *BMC Musculoskeletal Disorders* 16(1). doi: 10.1186/s12891-015-0676-1.

Arand, Charlotte, Daniel Wagner, Robert Geoff Richards, Hansrudi Noser, Lukas Kamer, Takeshi Sawaguchi, and Pol M. Rommens. 2019. "3D Statistical Model of the Pelvic Ring – a CT-Based Statistical Evaluation of Anatomical Variation." *Journal of Anatomy*. doi: 10.1111/joa.12928.

Audenaert, E. A., C. Pattyn, G. Steenackers, J. de Roeck, D. Vandermeulen, and P. Claes. 2019. "Statistical Shape Modeling of Skeletal Anatomy for Sex Discrimination: Their Training Size, Sexual Dimorphism, and Asymmetry." *Frontiers in Bioengineering and Biotechnology* 7(November):1–11. doi: 10.3389/fbioe.2019.00302.

Ayturk, Ugur M., and Christian M. Puttlitz. 2011. "Parametric Convergence Sensitivity and Validation of a Finite Element Model of the Human Lumbar Spine." *Computer Methods in Biomechanics and Biomedical Engineering* 14(8):695–705. doi: 10.1080/10255842.2010.493517.

Bailey, Jeannie F., Carolyn J. Sparrey, Ella Been, and Patricia A. Kramer. 2016. "Morphological and Postural Sexual Dimorphism of the Lumbar Spine Facilitates Greater Lordosis in Females." *Journal of Anatomy* 229(1):82–91. doi: 10.1111/joa.12451.

Baker, Joseph F., and Peter A. Robertson. 2020. "Segmental Contributions to Lumbar Lordosis: A Computed Tomography Study." 14(6):949–55.

Baldwin, Mark A., Joseph E. Langenderfer, Paul J. Rullkoetter, and Peter J. Laz. 2010a. "Development of Subject-Specific and Statistical Shape Models of the Knee Using an Efficient Segmentation and Mesh-Morphing Approach." *Computer Methods and Programs in Biomedicine* 97(3):232–40. doi: 10.1016/j.cmpb.2009.07.005.

Baldwin, Mark A., Joseph E. Langenderfer, Paul J. Rullkoetter, and Peter J. Laz. 2010b. "Development of Subject-Specific and Statistical Shape Models of the Knee Using an Efficient Segmentation and Mesh-Morphing Approach." *Computer Methods and Programs in Biomedicine*. doi: 10.1016/j.cmpb.2009.07.005.

Ben-Hatira, Fafa, Kaouthar Saidane, and Abdelfatah Mrabet. 2012. "A Finite Element Modeling of the Human Lumbar Unit Including the Spinal Cord." *Journal of Biomedical Science and Engineering*. doi: 10.4236/jbise.2012.53019.

Benzley, S. E., E. Perry, K. Merkley, B. Clark, and G. Sjaardema. 1995. "A Comparison of All-Hexahedral and All-Tetrahedral Finite Element Meshes for Elastic and Elasto-Plastic Analysis." *4th International Meshing Roundtable, Sandia National Laboratories* (December 2014):179–91.

Bernick, Sol, and Rene Cailliet. 1982. "Vertebral End-Plate Changes with Aging of Human Vertebrae." *Spine*. doi: 10.1097/00007632-198203000-00002.

Bertagnoli, Rudolf, and Selva Kumar. 2011. "Indications for Full Prosthetic Disc Arthroplasty: A Correlation of Clinical Outcome against a Variety of Indications." in *Arthroplasty of the Spine*.

Bevers, Melissa S. A. M., Caroline E. Wyers, Anne M. Daniels, Emmanuel A. Audenaert, Sander M. J. van Kuijk, Bert van Rietbergen, Piet P. M. M. Geusens, Sjoerd Kaarsemaker, Heinrich M. J. Janzing, Pascal F. W. Hannemann, Martijn Poeze, and Joop P. van den Bergh. 2021. "Association between Bone Shape and the Presence of a Fracture in Patients with a Clinically Suspected Scaphoid Fracture." *Journal of Biomechanics* 128. doi: 10.1016/j.jbiomech.2021.110726.

Bischoff, Jeffrey E., Yifei Dai, Casey Goodlett, Brad Davis, and Marc Bandi. 2014. "Incorporating Population-Level Variability in Orthopedic Biomechanical Analysis: A Review." *Journal of Biomechanical Engineering*. doi: 10.1115/1.4026258.

Bogduk, Nikolai, and Twomey, Lance T. Clinical Anatomy of the Lumbar Spine. United Kingdom, Churchill Livingstone, 1991.

Boisvert, Jonathan, Farida Cheriet, Xavier Pennec, Hubert Labelle, and Nicholas Ayache. 2008. "Geometric Variability of the Scoliotic Spine Using Statistics on Articulated Shape Models." *IEEE Transactions on Medical Imaging*. doi: 10.1109/TMI.2007.911474.

Bono, Christopher M., and Casey K. Lee. 2004. "Critical Analysis of Trends in Fusion for Degenerative Disc Disease over the Past 20 Years: Influence of Technique on Fusion Rate and Clinical Outcome." *Spine*. doi: 10.1097/01.BRS.0000090825.94611.28.

Bono, Christopher M., and Casey K. Lee. 2005. "The Influence of Subdiagnosis on Radiographic and Clinical Outcomes after Lumbar Fusion for Degenerative Disc Disorders: An Analysis of the Literature from Two Decades." *Spine*.

Boulay, C., C. Tardieu, J. Hecquet, C. Benaim, B. Mouilleseaux, C. Marty, D. Prat-Pradal, J. Legaye, G. Duval-Beaupère, and J. Pélissier. 2006. "Sagittal Alignment of Spine and Pelvis Regulated by Pelvic Incidence: Standard Values and Prediction of Lordosis." *European Spine Journal* 15(4):415–22. doi: 10.1007/s00586-005-0984-5.

Bredbenner, Todd L., Travis D. Eliason, W. Loren Francis, John M. McFarland, Andrew C. Merkle, and Daniel P. Nicolella. 2014. "Development and Validation of a Statistical Shape Modeling-Based Finite Element Model of the Cervical Spine under Low-Level Multiple Direction Loading Conditions." *Frontiers in Bioengineering and Biotechnology* 2(NOV):1–12. doi: 10.3389/fbioe.2014.00058.

Brown, Ian E., Stephen H. Scott ~, and Gerald E. Loeb. 1996. *Mechanics of Feline Soleus: II Design and Validation of a Mathematical Model*. Vol. 17.

Bruce, Olivia L., Michael Baggaley, Lauren Welte, Michael J. Rainbow, and W. Brent Edwards. 2022. "A Statistical Shape Model of the Tibia-Fibula Complex: Sexual Dimorphism and Effects of Age on Reconstruction Accuracy from Anatomical Landmarks." *Computer Methods in Biomechanics and Biomedical Engineering* 25(8):875–86. doi: 10.1080/10255842.2021.1985111.

Bryan, Rebecca, P. Surya Mohan, Andrew Hopkins, Francis Galloway, Mark Taylor, and Prasanth B. Nair. 2010. "Statistical Modelling of the Whole Human Femur Incorporating Geometric and Material Properties." *Medical Engineering and Physics* 32(1):57–65. doi: 10.1016/j.medengphy.2009.10.008.

Buckley, Jenni M., Kenneth Loo, and Julie Motherway. 2007. "Comparison of Quantitative Computed Tomography-Based Measures in Predicting Vertebral Compressive Strength." *Bone* 40(3):767–74. doi: 10.1016/j.bone.2006.10.025.

Campbell, J. Q., and A. J. Petrella. 2016. "Automated Finite Element Modeling of the Lumbar Spine: Using a Statistical Shape Model to Generate a Virtual Population of Models." *Journal of Biomechanics*. doi: 10.1016/j.jbiomech.2016.05.013.

Campbell, Julius Quinn, and Anthony J. Petrella. 2015. "An Automated Method for Landmark Identification and Finite-Element Modeling of the Lumbar Spine." *IEEE Transactions on Biomedical Engineering*. doi: 10.1109/TBME.2015.2444811.

Cassidy, J. David, Linda J. Carroll, and Pierre Côté. 1998. "The Saskatchewan Health and Back Pain Survey: The Prevalence of Low Back Pain and Related Disability in Saskatchewan Adults." *Spine*. doi: 10.1097/00007632-199809010-00012.

Charriere, E., F. Sirey, and P. K. Zysset. 2003. "A Finite Element Model of the L5-S1 Functional Spinal Unit: Development and Comparison with Biomechanical Tests in Vitro." *Computer Methods in Biomechanics and Biomedical Engineering* 6(4):249–61. doi: 10.1080/10255840310001606099.

Chazal, J., A. Tanguy, M. Bourges, G. Gaurel, G. Escande, M. Guillot, and G. Vanneuville. 1985. "Biomechanical Properties of Spinal Ligaments and a Histological Study of the Supraspinal Ligament in Traction." *Journal of Biomechanics* 18(3):167–76. doi: 10.1016/0021-9290(85)90202-7.

Chiang, Ming Fu, Zheng Cheng Zhong, Chen Sheng Chen, Cheng Kung Cheng, and Shih Liang Shih. 2006. "Biomechanical Comparison of Instrumented Posterior Lumbar Interbody Fusion with One or Two Cages by Finite Element Analysis." *Spine* 31(19):682–89. doi: 10.1097/01.brs.0000232714.72699.8e.

Choi, Jisoo, Dong Ah Shin, and Sohee Kim. 2017. "Biomechanical Effects of the Geometry of Ball-and-Socket Artificial Disc on Lumbar Spine." *Spine* 42(6):E332–39. doi: 10.1097/BRS.0000000000001789.

Coogan, Jessica S., W. Loren Francis, Travis D. Eliason, Todd L. Bredbenner, Brian D. Stemper, Narayan Yoganandan, Frank A. Pintar, and Daniel P. Nicolella. 2016. "Finite Element Study of a Lumbar Intervertebral Disc Nucleus Replacement Device." *Frontiers in Bioengineering and Biotechnology* 4(DEC):1–11. doi: 10.3389/fbioe.2016.00093.

Cootes, T. F., C. J. Taylor, D. H. Cooper, and J. Graham. 1995. "Active Shape Models - Their Training and Application." *Computer Vision and Image Understanding*. doi: 10.1006/cviu.1995.1004.

Crawford, R. Paul, Christopher E. Cann, and Tony M. Keaveny. 2003. "Finite Element Models Predict in Vitro Vertebral Body Compressive Strength Better than Quantitative Computed Tomography." *Bone*. doi: 10.1016/S8756-3282(03)00210-2.

Damm, Nicolas, Robert Rockenfeller, and Karin Gruber. 2020. "Lumbar Spinal Ligament Characteristics Extracted from Stepwise Reduction Experiments Allow for Preciser Modeling than Literature Data." *Biomechanics and Modeling in Mechanobiology* 19(3):893–910. doi: 10.1007/s10237-019-01259-6.

Devereaux MW. Anatomy and examination of the spine. Neurol Clin. 2007 May;25(2):331-51

Dmitriev, Anton E., Norman W. Gill, Timothy R. Kuklo, and Michael K. Rosner. 2008. "Effect of Multilevel Lumbar Disc Arthroplasty on the Operative- and Adjacent-Level Kinematics and Intradiscal Pressures: An in Vitro Human Cadaveric Assessment." *Spine Journal*. doi: 10.1016/j.spinee.2007.10.034.

Don, A. S., & Carragee, E. (2008). A brief overview of evidence-informed management of chronic low back pain with surgery. *The Spine Journal*, *8*(1), 258-265.

Dooris, Andrew P., Vijay K. Goel, Nicole M. Grosland, Lars G. Gilbertson, and David G. Wilder. 2001. "Load-Sharing Between Anterior and Posterior Elements in a Lumbar Motion Segment Implanted With an Artificial Disc." *Spine*. doi: 10.1097/00007632-200103150-00004.

Dreischarf, M., T. Zander, A. Shirazi-Adl, C. M. Puttlitz, C. J. Adam, C. S. Chen, V. K. Goel, A. Kiapour, Y. H. Kim, K. M. Labus, J. P. Little, W. M. Park, Y. H. Wang, H. J. Wilke, A. Rohlmann, and H. Schmidt. 2014. "Comparison of Eight Published Static Finite Element Models of the Intact Lumbar Spine: Predictive Power of Models Improves When Combined Together." *Journal of Biomechanics*. doi: 10.1016/j.jbiomech.2014.04.002.

Dunlop, R. B., M. A. Adams, and W. C. Hutton. 1984. "Disc Space Narrowing and the Lumbar Facet Joints." *Journal of Bone and Joint Surgery - Series B* 66(5):706–10. doi: 10.1302/0301-620x.66b5.6501365.

Duval-Beaupere, G., Schmidt, C., & Cosson, P. H. (1992). A Barycentremetric study of the sagittal shape of spine and pelvis: the conditions required for an economic standing position. *Annals of biomedical engineering*, *20*, 451-462.

Ellingson, A. M., Shaw, M. N., Giambini, H., & An, K. N. (2016). Comparative role of disc degeneration and ligament failure on functional mechanics of the lumbar spine. *Computer methods in biomechanics and biomedical engineering*, *19*(9), 1009-1018.

Elliott, Alison M., Blair H. Smith, Kay I. Penny, W. Cairns Smith, and W. Alastair Chambers. 1999. "The Epidemiology of Chronic Pain in the Community." *Lancet*. doi: 10.1016/S0140-6736(99)03057-3.

Elliott, D. M., and L. A. Setton. 2001. "Anisotropic and Inhomogeneous Tensile Behavior of the Human Anulus Fibrosus: Experimental Measurement and Material Model Predictions." *Journal of Biomechanical Engineering* 123(3):256–63. doi: 10.1115/1.1374202.

Fan, Yunpeng, Shaobo Zhou, Tao Xie, Zefeng Yu, Xiao Han, and Liulong Zhu. 2019. "Topping-off Surgery vs Posterior Lumbar Interbody Fusion for Degenerative Lumbar Disease: A Finite Element Analysis." *Journal of Orthopaedic Surgery and Research* 14(1):1–15. doi: 10.1186/s13018-019-1503-4.

Farcy, Jean Pierre C., and Frank J. Schwab. 1997. "Management of Flatback and Related Kyphotic Decompensation Syndromes." *Spine*. doi: 10.1097/00007632-199710150-00025.

Frenkel, Mark B., Casey D. Frey, Jaclyn J. Renfrow, Stacey Q. Wolfe, Alexander K. Powers, and Charles L. Branch. 2018. "A Call for Consistent Radiographic Definition of Lumbar Lordosis." *Journal of Neurosurgery: Spine* 29(2):231–34.

Fritzell, Peter, Olle Hägg, Dick Jonsson, Anders Nordwall, O. Andréen, G. Appelgren, S. Berg, B. Branth, C. G. Cederlund, P. Elkan, R. Hedlund, O. Hägg, H. Kogler, C. Leufvén, G. Németh,

P. Neumann, M. Nilsson, K. Nordenström, A. Ohlin, G. Ordeberg, T. Reigo, T. Sahlstrand, R. Sandberg, L. Skogland, B. Strömqvist, H. Tropp, T. Tullberg, T. Wikström, and J. Willén. 2004. "Cost-Effectiveness of Lumbar Fusion and Nonsurgical Treatment for Chronic Low Back Pain in the Swedish Lumbar Spine Study: A Multicenter, Randomized, Controlled Trial from the Swedish Lumbar Spine Study Group." *Spine*. doi: 10.1097/01.BRS.0000102681.61791.12.

Fritzell, Peter, Olle Hägg, Per Wessberg, and Anders Nordwall. 2001. "2001 Volvo Award Winner in Clinical Studies: Lumbar Fusion versus Nonsurgical Treatment for Chronic Low Back Pain. A Multicenter Randomized Controlled Trial from the Swedish Lumbar Spine Study Group." *Spine*. doi: 10.1097/00007632-200112010-00002.

Galbusera, Fabio, Chiara Maria Bellini, Federica Anasetti, Cristina Ciavarro, Alessio Lovi, and Marco Brayda-Bruno. 2011. "Rigid and Flexible Spinal Stabilization Devices: A Biomechanical Comparison." *Medical Engineering and Physics*. doi: 10.1016/j.medengphy.2010.11.018.

Ghiselli, Gary, Jeffrey C. Wang, Wellington K. Hsu, and Edgar G. Dawson. 2003. "L5-S1 Segment Survivorship and Clinical Outcome Analysis after L4-L5 Isolated Fusion." *Spine*. doi: 10.1097/01.BRS.0000065566.24152.D3.

Gilchrist RV, Frey ME, Nadler SF. Muscular control of the lumbar spine. Pain Physician. 2003 Jul;6(3):361-8.

Gillet, Philippe. 2003. "The Fate of the Adjacent Motion Segments after Lumbar Fusion." *Journal of Spinal Disorders and Techniques*. doi: 10.1097/00024720-200308000-00005.

Glassman, Steven D., Sigurd Berven, Keith Bridwell, William Horton, and John R. Dimar. n.d. *Correlation of Radiographic Parameters and Clinical Symptoms in Adult Scoliosis*. Vol. 30.

Goel, Vijay K., Jonathan N. Grauer, Tushar Ch Patel, Ashok Biyani, Koichi Sairyo, Sri Lakshmi Vishnubhotla, Aaron Matyas, Ian Cowgill, Miranda Shaw, Rebecca Long, David Dick, Manohar M. Panjabi, and Hassan Serhan. 2005. "Effects of Charité Artificial Disc on the Implanted and Adjacent Spinal Segments Mechanics Using a Hybrid Testing Protocol." *Spine*. doi: 10.1097/01.brs.0000195897.17277.67.

Goel, Vijay K., B. T. Monroe, L. G. Gilbertson, and P. Brinckmann. 1995. "Interlaminar Shear Stresses and Laminae Separation in a Disc: Finite Element Analysis of the L3-L4 Motion Segment Subjected to Axial Compressive Loads." *Spine*. doi: 10.1097/00007632-199503150-00010.

Grant, Tamara M., Laura E. Diamond, Claudio Pizzolato, Bryce A. Killen, Daniel Devaprakash, Luke Kelly, Jayishni N. Maharaj, and David J. Saxby. 2020. "Development and Validation of Statistical Shape Models of the Primary Functional Bone Segments of the Foot." *PeerJ* 2020(2). doi: 10.7717/peerj.8397.

Guan, Yabo, Narayan Yoganandan, Jiangyue Zhang, Frank A. Pintar, Joesph F. Cusick, Christopher E. Wolfla, and Dennis J. Maiman. 2006. "Validation of a Clinical Finite Element Model of the Human Lumbosacral Spine." *Medical and Biological Engineering and Computing*. doi: 10.1007/s11517-006-0066-9.

Haddas, Ram, Ming Xu, Isador Lieberman, and James Yang. 2018. "Finite Element Analysis of Pre and Post Lumbar Fusion for Adult Degenerative Scoliosis Patients." in *Lecture Notes in Bioengineering*.

Hao, Zhixiu, Chao Wan, Xiangfei Gao, and Tao Ji. 2011. "The Effect of Boundary Condition on the Biomechanics of a Human Pelvic Joint under an Axial Compressive Load: A Three-Dimensional Finite Element Model." *Journal of Biomechanical Engineering* 133(10):1–9. doi: 10.1115/1.4005223.

Haq, Rabia, Jérôme Schmid, Roderick Borgie, Joshua Cates, and Michel A. Audette. 2020. "Deformable Multisurface Segmentation of the Spine for Orthopedic Surgery Planning and Simulation." *Journal of Medical Imaging* 7(01):1. doi: 10.1117/1.jmi.7.1.015002.

Harrysson, Ola L. A., Yasser A. Hosni, and Jamal F. Nayfeh. 2007. "Custom-Designed Orthopedic Implants Evaluated Using Finite Element Analysis of Patient-Specific Computed Tomography Data : Femoral-Component Case Study." 10(iv):1–10. doi: 10.1186/1471-2474-8-91.

Hegazy, Abdelmonem A., and Raafat A. Hegazy. 2014. "Midsagittal Anatomy of Lumbar Lordosis in Adult Egyptians: MRI Study." *Anatomy Research International* 2014:1–12. doi: 10.1155/2014/370852.

Heuer, Frank, Hendrik Schmidt, Zdenek Klezl, Lutz Claes, and Hans Joachim Wilke. 2007. "Stepwise Reduction of Functional Spinal Structures Increase Range of Motion and Change Lordosis Angle." *Journal of Biomechanics* 40(2):271–80. doi: 10.1016/j.jbiomech.2006.01.007.

Hollenbeck, Justin F. M., Christopher M. Cain, Jill A. Fattor, Paul J. Rullkoetter, and Peter J. Laz. 2018. "Statistical Shape Modeling Characterizes Three-Dimensional Shape and Alignment

Variability in the Lumbar Spine." *Journal of Biomechanics*. doi: 10.1016/j.jbiomech.2018.01.020.

Hu, Zongshan, Claudio Vergari, Laurent Gajny, Zhen Liu, Tsz Ping Lam, Zezhang Zhu, Yong Qiu, Gene C. W. Man, Kwong Hang Yeung, Winnie C. W. Chu, Jack C. Y. Cheng, and Wafa Skalli. 2021. "Comparison of 3D and 2D Characterization of Spinal Geometry from Biplanar X-Rays: A Large Cohort Study." *Quantitative Imaging in Medicine and Surgery* 11(7):3306–13. doi: 10.21037/qims-20-861.

Hyun, Seung Jae, and Seung Chul Rhim. 2010. "Clinical Outcomes and Complications after Pedicle Subtraction Osteotomy for Fixed Sagittal Imbalance Patients: A Long-Term Follow-up Data." *Journal of Korean Neurosurgical Society*. doi: 10.3340/jkns.2010.47.2.95.

Imai, Norio, Hayato Suzuki, Atsushi Sakagami, Yuki Hirano, and Naoto Endo. 2020. "Correlation of the Anatomical Sacral Slope with Pelvic Incidence in Female Patients with Developmental Hip Dysplasia: A Retrospective Cross-Sectional Study." *Journal of Orthopaedic Surgery and Research* 15(1):1–6. doi: 10.1186/s13018-020-02022-9.

Institute of Medicine (U.S.). Committee on Advancing Pain Research, Care. 2011. *Relieving Pain in America : A Blueprint for Transforming Prevention, Care, Education, and Research*. National Academies Press.

Janssen, Michiel M. A., Xavier Drevelle, Ludovic Humbert, Wafa Skalli, and René M. Castelein. 2009. "Differences in Male and Female Spino-Pelvic Alignment in Asymptomatic Young Adults: A Three-Dimensional Analysis Using Upright Low-Dose Digital Biplanar X-Rays." *Spine* 34(23). doi: 10.1097/BRS.0b013e3181a9fd85.

Jayson, The Lumbar Spine and Back Pain. United Kingdom, Pitman Medical, 1980.

J.E. Crouch. 1978. *Functional Human Anatomy*. ISBN 0-812. Henry Kimpton Publishers.

Jones, Alison C., and Ruth K. Wilcox. 2008. "Finite Element Analysis of the Spine: Towards a Framework of Verification, Validation and Sensitivity Analysis." *Medical Engineering and Physics*.

Jovanovic, J. D., and Lj Jovanovic Miomir. 2010. "Finite Element Modeling of the Vertebra With Geometry and Material Properties Retreived From Ct-Scan Data." *Facta Universitatis-Series: Mechanical Engineering* 8(1):19–26.

Jóźwiak, Marek, Michał Rychlik, Bartosz Musielak, Brian Po Jung Chen, Maciej Idzior, and Andrzej Grzegorzewski. 2015. "An Accurate Method of Radiological Assessment of Acetabular Volume and Orientation in Computed Tomography Spatial Reconstruction." *BMC Musculoskeletal Disorders* 16(1):1–10. doi: 10.1186/s12891-015-0503-8.

Karimi, Davood, Qi Zeng, Prateek Mathur, Apeksha Avinash, Sara Mahdavi, Ingrid Spadinger, Purang Abolmaesumi, and Septimiu E. Salcudean. 2019. "Accurate and Robust Deep Learning-Based Segmentation of the Prostate Clinical Target Volume in Ultrasound Images." *Medical Image Analysis* 57:186–96. doi: 10.1016/j.media.2019.07.005.

Kassab-Bachi, Amin, Nishant Ravikumar, Ruth K. Wilcox, Alejandro F. Frangi, and Zeike A. Taylor. 2022. "Contribution of Shape Features to Intradiscal Pressure and Facets Contact Pressure in L4/L5 FSUs: An In-Silico Study." *Annals of Biomedical Engineering*. doi: 10.1007/s10439-022-03072-2.

Keast, Meghan, Jason Bonacci, and Aaron Fox. n.d. "Geometric Variation of the Human Tibia-Fibula: A Public Dataset of Tibia-Fibula Surface Meshes and Statistical Shape 2 Model 3." doi: 10.1101/2022.08.04.502722.

Kendall, D. G. 1977. "The Diffusion of Shape." *Advances in Applied Probability*. doi: 10.2307/1426091.

Keyak, J. H., J. M. Meagher, H. B. Skinner, and C. D. Mote. 1990. "Automated Three-Dimensional Finite Element Modelling of Bone: A New Method." *Journal of Biomedical Engineering*. doi: 10.1016/0141-5425(90)90022-F.

Kim, Ki Tack, Sang Hun Lee, Kyung Soo Suk, Jung Hee Lee, and Bi O. Jeong. 2010. "Biomechanical Changes of the Lumbar Segment after Total Disc Replacement: Charite®, Prodisc® and Maverick® Using Finite Element Model Study." *Journal of Korean Neurosurgical Society* 47(6):446–53. doi: 10.3340/jkns.2010.47.6.446.

Kim, Yongjung J., Keith H. Bridwell, Lawrence G. Lenke, Gene Cheh, and Christine Baldus. 2007. "Results of Lumbar Pedicle Subtraction Osteotomies for Fixed Sagittal Imbalance: A Minimum 5-Year Follow-up Study." *Spine*. doi: 10.1097/BRS.0b013e31814b8371.

Kirby, Michael Christopher, and Hukins, D. W.L. Spinal Ligaments: A Determination of Their Structure and Function. N.p., University of Manchester., 1989.

Klop, C., A. G. Becking, C. Klop, J. H. Koolstra, N. H. J. Lobé, T. J. J. Maal, C. S. Mulder, J. W. Nolte, R. Schreurs, and V. Vespasiano. 2021. "A Three-Dimensional Statistical Shape Model of the Growing Mandible." *Scientific Reports* 11(1):1–10. doi: 10.1038/s41598-021-98421-x.

Kuo, Ching Sung, Hsuan Teh Hu, Ruey Mo Lin, Kuo Yuan Huang, Po Chun Lin, Zheng Cheng Zhong, and Mu Lin Hseih. 2010. "Biomechanical Analysis of the Lumbar Spine on Facet Joint Force and Intradiscal Pressure - A Finite Element Study." *BMC Musculoskeletal Disorders*. doi: 10.1186/1471-2474-11-151.

Lamecker, Hans, Martin Seebass, Hans-Christian Hege, and Peter Deuflhard. 2004. "A 3D Statistical Shape Model of the Pelvic Bone for Segmentation." in *Medical Imaging 2004: Image Processing*.

Lavaste, Francois, Wafa Skalli, Stéphane Robin, Raymond Roy-Camille, and Christian Mazel. 1992. "Three-Dimensional Geometrical and Mechanical Modelling of the Lumbar Spine." *Journal of Biomechanics*. doi: 10.1016/0021-9290(92)90071-8.

Legaye, J., G. Duval-Beaupère, J. Hecquet, and C. Marty. 1998. "Pelvic Incidence: A Fundamental Pelvic Parameter for Three-Dimensional Regulation of Spinal Sagittal Curves." *European Spine Journal*. doi: 10.1007/s005860050038.

Le Huec, J. C., Mathews, H., Basso, Y., Aunoble, S., Hoste, D., Bley, B., & Friesem, T. (2005). Clinical results of Maverick lumbar total disc replacement: two-year prospective follow-up. *Orthopedic Clinics*, *36*(3), 315-322.

Lorenz, Cristian, and Nils Krahnstöver. 2000. "Generation of Point-Based 3D Statistical Shape Models for Anatomical Objects." *Computer Vision and Image Understanding*. doi: 10.1006/cviu.1999.0814.

Lu, Yuan Chiao, and Costin D. Untaroiu. 2013. "Statistical Shape Analysis of Clavicular Cortical Bone with Applications to the Development of Mean and Boundary Shape Models." *Computer Methods and Programs in Biomedicine* 111(3):613–28. doi: 10.1016/j.cmpb.2013.05.017.

Mac-Thiong, Jean Marc, P. Roussouly, E. Berthonnaud, and P. Guigui. 2011. "Age- and Sex-Related Variations in Sagittal Sacropelvic Morphology and Balance in Asymptomatic Adults." *European Spine Journal : Official Publication of the European Spine Society, the European Spinal Deformity Society, and the European Section of the Cervical Spine Research Society* 20 Suppl 5:572–77. doi: 10.1007/s00586-011-1923-2.

Martin, Brook I., Sohail K. Mirza, Gary M. Franklin, Jon D. Lurie, Todd A. MacKenzie, and Richard A. Deyo. 2013. "Hospital and Surgeon Variation in Complications and Repeat Surgery Following Incident Lumbar Fusion for Common Degenerative Diagnoses." *Health Services Research*. doi: 10.1111/j.1475-6773.2012.01434. x.

Más, Yolanda, Luis Gracia, Elena Ibarz, Sergio Gabarre, Diego Peña, and Antonio Herrera. 2017. "Finite Element Simulation and Clinical Followup of Lumbar Spine Biomechanics with Dynamic Fixations." *PLoS ONE* 12(11). doi: 10.1371/journal.pone.0188328.

Mathur, V., and Dragomir-Daescu. 2012. "Hexahedral vs. Tetrahedral Finite Element Models of the Proximal Femur." *ORS 2012 Annual Meeting* (1020):27065.

Maurel, Nathalie, F. Lavaste, and W. Skalli. 1997. "A Three-Dimensional Parameterized Finite Element Model of the Lower Cervical Spine. Study of the Influence of the Posterior Articular Facets." *Journal of Biomechanics*. doi: 10.1016/S0021-9290(97)00056-0.

Mazzoli, Alida, Michele Germani, and Roberto Raffaeli. 2009. "Direct Fabrication through Electron Beam Melting Technology of Custom Cranial Implants Designed in a PHANToM-Based Haptic Environment." *Materials and Design* 30(8):3186–92. doi: 10.1016/j.matdes.2008.11.013.

Meakin, Judith R., Jennifer S. Gregory, Richard M. Aspden, Francis W. Smith, and Fiona J. Gilbert. 2009. "The Intrinsic Shape of the Human Lumbar Spine in the Supine, Standing and Sitting Postures: Characterization Using an Active Shape Model." *Journal of Anatomy* 215(2):206–11. doi: 10.1111/j.1469-7580.2009.01102.x.

Meakin, Judith R., Thomas W. Redpath, and David W. L. Hukins. 2001. "The Effect of Partial Removal of the Nucleus Pulposus from the Intervertebral Disc on the Response of the Human Annulus Fibrosus to Compression." *Clinical Biomechanics*. doi: 10.1016/S0268-0033(00)00075-9.

Meijer, Gerdine J. M., Jasper Homminga, Albert G. Veldhuizen, and Gijsbertus J. Verkerke. 2011. "Influence of Interpersonal Geometrical Variation on Spinal Motion Segment Stiffness: Implications for Patient-Specific Modeling." *Spine*. doi: 10.1097/BRS.0b013e3181fd7f7f.

Meller, Sebastian, and Willi A. Kalender. 2004. "Building a Statistical Shape Model of the Pelvis." *International Congress Series*. doi: 10.1016/j.ics.2004.03.295.

Merck, Derek, Gregg Tracton, Rohit Saboo, Joshua Levy, Edward Chaney, Stephen Pizer, and Sarang Joshi. 2008. "Training Models of Anatomic Shape Variability." *Medical Physics*. doi: 10.1118/1.2940188.

Meynen, Alexander, Harold Matthews, Nele Nauwelaers, Peter Claes, Michiel Mulier, and Lennart Scheys. 2020. "Accurate Reconstructions of Pelvic Defects and Discontinuities Using Statistical Shape Models." *Computer Methods in Biomechanics and Biomedical Engineering* 23(13):1026–33. doi: 10.1080/10255842.2020.1784404.

Miot, Hélio Amante. 2018. "Correlation Analysis in Clinical and Experimental Studies." *Jornal Vascular Brasileiro* 17(4):275–79. doi: 10.1590/1677-5449.174118.

Mobbs, Ralph J., Aji Loganathan, Vivian Yeung, and Prashanth J. Rao. 2013. "Indications for Anterior Lumbar Interbody Fusion." *Orthopaedic Surgery*. doi: 10.1111/os.12048.

Moramarco, V., A. Pérez del Palomar, C. Pappalettere, and M. Doblaré. 2010. "An Accurate Validation of a Computational Model of a Human Lumbosacral Segment." *Journal of Biomechanics*. doi: 10.1016/j.jbiomech.2009.07.042.

Murrie, Vanessa L., A. K. Dixon, W. Hollingworth, H. Wilson, and T. A. C. Doyle. 2003. "Lumbar Lordosis: Study of Patients with and without Low Back Pain." *Clinical Anatomy* 16(2):144–47. doi: 10.1002/ca.10114.

Nabhani, F., and M. Wake. 2002. "Computer Modelling and Stress Analysis of the Lumbar Spine." *Journal of Materials Processing Technology*. doi: 10.1016/S0924-0136(02)00195-4.

Nguyen, Ho Quang, Tien Tuan Dao, Alain Rassineux, and Marie Christine Ho Ba Tho. 2018. "Material-Driven Mesh of the Lumbar Spine Derived from CT Data." *Computer Methods in Biomechanics and Biomedical Engineering: Imaging and Visualization*. doi: 10.1080/21681163.2016.1188729.

Nicolella, Daniel P., and Todd L. Bredbenner. 2012. "Development of a Parametric Finite Element Model of the Proximal Femur Using Statistical Shape and Density Modelling." *Computer Methods in Biomechanics and Biomedical Engineering* 15(2):101–10. doi: 10.1080/10255842.2010.515984.

Noailly, Jérôme, Luigi Ambrosio, K. Elizabeth Tanner, Josep A. Planell, and Damien Lacroix. 2012. "In Silico Evaluation of a New Composite Disc Substitute with a L3-L5 Lumbar Spine Finite Element Model." *European Spine Journal*. doi: 10.1007/s00586-011-1716-7.

Noailly, Jérôme, Damien Lacroix, and Josep A. Planell. 2005. "Finite Element Study of a Novel Intervertebral Disc Substitute." *Spine*. doi: 10.1097/01.brs.0000182319.81795.72.

Noble, Jack H., René H. Gifford, Robert F. Labadie, and Benoît M. Dawant. n.d. *Statistical Shape Model Segmentation and Frequency Mapping of Cochlear Implant Stimulation Targets in CT*.

Nolte, Daniel, Siu Teing Ko, Anthony M. J. Bull, and Angela E. Kedgley. 2020. "Reconstruction of the Lower Limb Bones from Digitised Anatomical Landmarks Using Statistical Shape Modelling." *Gait and Posture*. doi: 10.1016/j.gaitpost.2020.02.010.

Nolte, L. P., Panjabi, M. M., & Oxland, T. R. (1990). Biomechanical properties of lumbar spinal ligaments. *Clinical implant materials, advances in biomaterials*, *9*, 663-668.

Okamoto, Masashi, Kazuhiro Hasegawa, Shun Hatsushikano, Kei Watanabe, Haruka Shimoda, Koichi Kobayashi, and Makoto Sakamoto. 2020. "Relative Position of Sacral Base in the Pelvis and Its Correlation with Spino-Pelvic Parameters." *European Spine Journal* 29(3):446–54. doi: 10.1007/s00586-019-06118-7.

Okuda, Shin'ya, Motoki Iwasaki, Akira Miyauchi, Hiroyuki Aono, Masahiro Morita, and Tomio Yamamoto. 2004. "Risk Factors for Adjacent Segment Degeneration after PLIF." *Spine*. doi: 10.1097/01.BRS.0000131417.93637.9D.

Panjabi, Manohar M., Vijay K. Goel, and Koichiro Takata. 1982. "1981 Volvo Award in Biomechanics: Physiologic Strains in the Lumbar Spinal Ligaments: An in Vitro Biomechanical Study." *Spine* 7(3):192–203.

Panjabi, Manohar, George Malcolmson, Edward Teng, Yasuhiro Tominaga, Gweneth Henderson, and Hassan Serhan. 2007. "Hybrid Testing of Lumbar CHARITI Discs versus Fusions." *Spine*. doi: 10.1097/01.brs.0000260792.13893.88.

Park, Won Man, Kyungsoo Kim, and Yoon Hyuk Kim. 2013. "Effects of Degenerated Intervertebral Discs on Intersegmental Rotations, Intradiscal Pressures, and Facet Joint Forces of the Whole Lumbar Spine." *Computers in Biology and Medicine* 43(9):1234–40. doi: 10.1016/j.compbiomed.2013.06.011.

Pavlova, Anastasia v., Fiona R. Saunders, Stella G. Muthuri, Jennifer S. Gregory, Rebecca J. Barr, Kathryn R. Martin, Rebecca J. Hardy, Rachel Cooper, Judith E. Adams, Diana Kuh, and Richard M. Aspden. 2017. "Statistical Shape Modelling of Hip and Lumbar Spine Morphology and Their Relationship in the MRC National Survey of Health and Development." *Journal of Anatomy*. doi: 10.1111/joa.12631.

Pekkanen, Liisa, Marko H. Neva, Hannu Kautiainen, Joost Dekker, Kirsi Piitulainen, Marko Wahlman, and Arja Häkkinen. 2013. "Disability and Health-Related Quality of Life in Patients Undergoing Spinal Fusion: A Comparison with a General Population Sample." *BMC Musculoskeletal Disorders*. doi: 10.1186/1471-2474-14-211.

Peloquin, John M., Jonathon H. Yoder, Nathan T. Jacobs, Sung M. Moon, Alexander C. Wright, Edward J. Vresilovic, and Dawn M. Elliott. 2014. "Human L3L4 Intervertebral Disc Mean 3D Shape, Modes of Variation, and Their Relationship to Degeneration." *Journal of Biomechanics* 47(10):2452–59. doi: 10.1016/j.jbiomech.2014.04.014.

Pesenti, Sebastien, Renaud Lafage, Daniel Stein, Jonathan C. Elysee, Lawrence G. Lenke, Frank J. Schwab, Han Jo Kim, and Virginie Lafage. 2018. "The Amount of Proximal Lumbar Lordosis Is Related to Pelvic Incidence." *Clinical Orthopaedics and Related Research* 476(8):1603–11. doi: 10.1097/CORR.0000000000000380.

Phillips, A. T. M., P. Pankaj, C. R. Howie, A. S. Usmani, and A. H. R. W. Simpson. 2007. "Finite Element Modelling of the Pelvis: Inclusion of Muscular and Ligamentous Boundary Conditions." *Medical Engineering and Physics* 29(7):739–48. doi: 10.1016/j.medengphy.2006.08.010.

Pintar, Frank A., Narayan Yoganandan, Thomas Myers, Ali Elhagediab, and Anthony Sances. 1992. "Biomechanical Properties of Human Lumbar Spine Ligaments." *Journal of Biomechanics*. doi: 10.1016/0021-9290(92)90290-H.

Prescher, Andreas. 1998. "Anatomy and Pathology of the Aging Spine." *European Journal of Radiology*. doi: 10.1016/S0720-048X(97)00165-4.

Putzer, Michael, Stefan Auer, William Malpica, Franz Suess, and Sebastian Dendorfer. 2016. "A Numerical Study to Determine the Effect of Ligament Stiffness on Kinematics of the Lumbar Spine during Flexion." *BMC Musculoskeletal Disorders* 17(1):1–7. doi: 10.1186/s12891-016-0942-x.

R. Mellano, Chris, and Andrew I. Spitzer. 2015. "How Does Pelvic Rotation or Tilt Affect Radiographic Measurement of Acetabular Component Inclination Angle during THA?" *Journal of Orthopaedics* 12(4):222–27. doi: 10.1016/j.jor.2015.05.009.

Raheem, Hassan Mansour, and Mohanad Aljanabi. 2020. "Finite Element Modeling of the Functional Spinal Unit under Compression Loads." *Procedia Structural Integrity* 28:1755–60. doi: 10.1016/j.prostr.2020.10.151.

Ranu, H. S., R. A. Denton, and A. I. King. 1979. "Pressure Distribution under an Intervertebral Disc-An Experimental Study." *Journal of Biomechanics* 12(10):807–12. doi: 10.1016/0021-9290(79)90166-0.

Rasoulian, Abtin, Robert Rohling, and Purang Abolmaesumi. 2013. "Lumbar Spine Segmentation Using a Statistical Multi-Vertebrae Anatomical Shape+pose Model." *IEEE Transactions on Medical Imaging*. doi: 10.1109/TMI.2013.2268424.

Renner, Susan M., Raghu N. Natarajan, Avinash G. Patwardhan, Robert M. Havey, Leonard I. Voronov, Bev Y. Guo, Gunnar B. J. Andersson, and Howard S. An. 2007. "Novel Model to Analyze the Effect of a Large Compressive Follower Pre-Load on Range of Motions in a Lumbar Spine." *Journal of Biomechanics*. doi: 10.1016/j.jbiomech.2006.05.019.

Rohlmann, Antonius, Anke Mann, Thomas Zander, and Georg Bergmann. 2009. "Effect of an Artificial Disc on Lumbar Spine Biomechanics: A Probabilistic Finite Element Study." *European Spine Journal*. doi: 10.1007/s00586-008-0836-1.

Rohlmann, Antonius, Thomas Zander, Hendrik Schmidt, Hans Joachim Wilke, and Georg Bergmann. 2006. "Analysis of the Influence of Disc Degeneration on the Mechanical Behaviour of a Lumbar Motion Segment Using the Finite Element Method." *Journal of Biomechanics*. doi: 10.1016/j.jbiomech.2005.07.026.

Rothenfluh, Dominique A., Daniel A. Mueller, Esin Rothenfluh, and Kan Min. 2015. "Pelvic Incidence-Lumbar Lordosis Mismatch Predisposes to Adjacent Segment Disease after Lumbar Spinal Fusion." *European Spine Journal*. doi: 10.1007/s00586-014-3454-0.

Salsabili, Neda, Joaquín Santiago López, and María Isabel Prieto Barrio. 2019. "Simplifying the Human Lumbar Spine (L3/L4) Material in Order to Create an Elemental Structure for the Future Modeling." *Australasian Physical and Engineering Sciences in Medicine*. doi: 10.1007/s13246-019-00768.

Schmidt, Hendrik, Frank Heuer, Joerg Drumm, Zdenek Klezl, Lutz Claes, and Hans Joachim Wilke. 2007. "Application of a Calibration Method Provides More Realistic Results for a Finite Element Model of a Lumbar Spinal Segment." *Clinical Biomechanics*. doi: 10.1016/j.clinbiomech.2006.11.008.

Schmidt, Hendrik, Frank Heuer, Ulrich Simon, Annette Kettler, Antonius Rohlmann, Lutz Claes, and Hans Joachim Wilke. 2006. "Application of a New Calibration Method for a Three-Dimensional Finite Element Model of a Human Lumbar Annulus Fibrosus." *Clinical Biomechanics* 21(4):337–44. doi: 10.1016/j.clinbiomech.2005.12.001.

Schmidt, Hendrik, Aboulfazl Shirazi-Adl, Fabio Galbusera, and Hans Joachim Wilke. 2010. "Response Analysis of the Lumbar Spine during Regular Daily Activities-A Finite Element Analysis." *Journal of Biomechanics*. doi: 10.1016/j.jbiomech.2010.03.035.

Schwab, Frank J., Benjamin Blondel, Shay Bess, Richard Hostin, Christopher I. Shaffrey, Justin S. Smith, Oheneba Boachie-Adjei, Douglas C. Burton, Behrooz A. Akbarnia, Gregory M. Mundis, Christopher P. Ames, Khaled Kebaish, Robert A. Hart, Jean Pierre Farcy, and Virginie Lafage. 2013. "Radiographical Spinopelvic Parameters and Disability in the Setting of Adult Spinal Deformity: A Prospective Multicenter Analysis." *Spine*. doi: 10.1097/BRS.0b013e318292b7b9.

Sengupta, D. K. (2004). Dynamic stabilization devices in the treatment of low back pain. *Orthopedic Clinics*, *35*(1), 43-56.

Serhan, Hassan A., Gus Varnavas, Andrew P. Dooris, Avinash Patwardhan, and Michael Tzermiadianos. 2008. "Biomechanics of the Posterior Lumbar Articulating Elements." *Neurosurgical Focus*. doi: 10.3171/foc.2007.22.1.1.

Shahraki, Narjes Momeni, Ali Fatemi, Vijay K. Goel, and Anand Agarwal. 2015. "On the Use of Biaxial Properties in Modeling Annulus as a Holzapfel-Gasser-Ogden Material." *Frontiers in Bioengineering and Biotechnology* 3(JUN):1–9. doi: 10.3389/fbioe.2015.00069.

Shim, Chan Shik, Sang Ho Lee, Ho Dong Shin, Han Sug Kang, Won Chul Choi, Byungjoo Jung, Gun Choi, Yong Ahn, Seungcheol Lee, and Ho Yeon Lee. 2007. "CHARITI versus ProDisc: A Comparative Study of a Minimum 3-Year Follow-Up." *Spine*. doi: 10.1097/01.brs.0000260795. 57798.a0.

Shin, Jong Ki, Tae Sik Goh, Myung Sung Kim, Keunyoung Kim, Myung Jun Shin, Seung Min Son, Hee Jin Lee, Jung Sub Lee, and Chi Seung Lee. 2018. "Stress and Strain Analyses of Single and Segmental Lumbar Spines Based on an Accurate Finite Element Model for Vertebrae." *Biomedical Research (India)*. doi: 10.4066/biomedicalresearch.29-17-763.

Shin, Jong Ki, Tae Sik Goh, Myung Sung Kim, Keunyoung Kim, Myung Jun Shin, Seung Min Son, Hee Jin Lee, Jung Sub Lee, and Chi Seung Lee. 2018b. "Stress and Strain Analyses of Single and Segmental Lumbar Spines Based on an Accurate Finite Element Model for Vertebrae." *Biomedical Research (India)*. doi: 10.4066/biomedicalresearch.29-17-763.Shirazi-Adl, A. 1994. "Analysis of Role of Bone Compliance on Mechanics of a Lumbar Motion Segment." *Journal of Biomechanical Engineering* 116(4):408–12. doi: 10.1115/1.2895791.

Shirazi-Adl, S. A., S. C. Shrivastava, and A. M. Ahmed. 1984. "Stress Analysis of the Lumbar Disc-Body Unit in Compression. A Three-Dimensional Nonlinear Finite Element Study." *Spine*. doi: 10.1097/00007632-198403000-00003.

Siepe, Christoph J., H. Michael Mayer, Karsten Wiechert, and Andreas Korge. 2006. "Clinical Results of Total Lumbar Disc Replacement with ProDisc II: Three-Year Results for Different Indications." *Spine*. doi: 10.1097/01.brs.0000228780.06569.e8.

Sigal, Ian A., Hongli Yang, Michael D. Roberts, and J. Crawford Downs. 2010. "Morphing Methods to Parameterize Specimen-Specific Finite Element Model Geometries." *Journal of Biomechanics*. doi: 10.1016/j.jbiomech.2009.08.036.

Singh, R., Yadav, S. K., Sood, S., Yadav, R. K., & Rohilla, R. (2018). Spino-pelvic radiological parameters in normal Indian population. *SICOT-J,4*.

Sinigaglia, Riccardo, Albert Bundy, Sandro Costantini, Ugo Nena, Francesco Finocchiaro, and Daniele A. Fabris Monterumici. 2009. "Comparison of Single-Level L4-L5 versus L5-S1 Lumbar Disc Replacement: Results and Prognostic Factors." *European Spine Journal*. doi: 10.1007/s00586-009-0992-y.

S.J. Hall. 1995. *Basic Biomechanics*. ISBN 0-815.

Spinczyk, Dominik, and Agata Krasoń. 2018. "Automatic Liver Segmentation in Computed Tomography Using General-Purpose Shape Modeling Methods." *BioMedical Engineering Online* 17(1). doi: 10.1186/s12938-018-0504-6.

Sprent, P., and F. L. Bookstein. 2006. "The Measurement of Biological Shape and Shape Change." *Biometrics*. doi: 10.2307/2530360.

Sudhir, G., Shankar Acharya, Kalra K.l, and Rupinder Chahal. 2015. "Radiographic Analysis of the Sacropelvic Parameters of the Spine and Their Correlation in Normal Asymptomatic Subjects." *Global Spine Journal* 6(2):169–75. doi: 10.1055/s-0035-1558652.

Sylvestre, Pierre Luc, Isabelle Villemure, and Carl Éric Aubin. 2007. "Finite Element Modeling of the Growth Plate in a Detailed Spine Model." *Medical and Biological Engineering and Computing* 45(10):977–88. doi: 10.1007/s11517-007-0220-z.

Tadepalli, Srinivas C., Ahmet Erdemir, and Peter R. Cavanagh. 2011. "Comparison of Hexahedral and Tetrahedral Elements in Finite Element Analysis of the Foot and Footwear." *Journal of Biomechanics* 44(12):2337–43. doi: 10.1016/j.jbiomech.2011.05.006.

Tardieu, Christine, Noémie Bonneau, Jér Ôme Hecquet, Christophe Boulay, Catherine Marty, Jean Legaye, and Geneviève Duval-Beaupère. 2013. "How Is Sagittal Balance Acquired during Bipedal Gait Acquisition? Comparison of Neonatal and Adult Pelves in Three Dimensions. Evolutionary Implications." *Journal of Human Evolution* 65(2):209–22. doi: 10.1016/j.jhevol.2013.06.002.

Taylor, James. The Lumbar Spine: An Atlas of Normal Anatomy and the Morbid Anatomy of Ageing and Injury. Netherlands, Elsevier Health Sciences, 2020.

Thompson, J. P., R. H. Pearce, M. T. Schechter, M. E. Adams, I. K. Tsang, and P. B. Bishop. 1990. "Preliminary Evaluation of a Scheme for Grading the Gross Morphology of the Human Intervertebral Disc." *Spine*.

Thompson, Paul M., Tyrone D. Cannon, Katherine L. Narr, Theo van Erp, Veli Pekka Poutanen, Matti Huttunen, Jouko Lönnqvist, Carl Gustaf Standertskjöld-Nordenstam, Jaakko Kaprio, Mohammad Khaledy, Rajneesh Dail, Chris I. Zoumalan, and Arthur W. Toga. 2001. "Genetic Influences on Brain Structure." *Nature Neuroscience*. doi: 10.1038/nn758.

Tropiano, Patrick, Russel C. Huang, Federico P. Girardi, and Thierry Marnay. 2003. "Lumbar Disc Replacement: Preliminary Results with Prodisc II after a Minimum Follow-up Period of 1 Year." *Journal of Spinal Disorders and Techniques*. doi: 10.1097/00024720-200308000-00008.

Vaccaro, Alexander R. Fractures of the Cervical, Thoracic, and Lumbar Spine. United Kingdom, CRC Press, 2002.

Vadapalli, S., Sairyo, K., Goel, V. K., Robon, M., Biyani, A., Khandha, A., & Ebraheim, N. A. (2006). Biomechanical rationale for using polyetheretherketone (PEEK) spacers for lumbar interbody fusion–a finite element study. *Spine*, *31*(26), E992-E998.

Vialle Levassor, Rillardon Templier,.Skalli & Guigui, (2005). Radiographic analysis of the sagittal alignment and balance of the spine in asymptomatic subjects. *JBJS*, *87*(2), 260-267.

Vresilovic, E., J. Peloquin, J. Yoder, N. Jacobs, S. Moon, A. Wright, and D. Elliott. 2012. "A Model for Intervertebral Disk Shape Variation in a Population Including the Effect of Degeneration." *Global Spine Journal*. doi: 10.1055/s-0032-1320010.

Wagner, Diane R., and Jeffrey C. Lotz. 2004. "Theoretical Model and Experimental Results for the Nonlinear Elastic Behavior of Human Annulus Fibrosus." *Journal of Orthopaedic Research* 22(4):901–9. doi: 10.1016/j.orthres.2003.12.012.

Wai, Gordon, Wan Rusli, Shaaz Ghouse, David C. Kieser, Angela Kedgley, and Nicolas Newell. 2022. "Statistical Shape Modelling of the Thoracic Spine for the Development of Pedicle Screw Insertion Guides." Biomechanics and Modeling in Mechanobiology. doi: 10.1007/s10237-022-01636-8.

Wang, Z. L., J. C. M. Teo, C. K. Chui, S. H. Ong, C. H. Yan, S. C. Wang, H. K. Wong, and S. H. Teoh. 2005. "Computational Biomechanical Modelling of the Lumbar Spine Using Marching-Cubes Surface Smoothened Finite Element Voxel Meshing." Computer Methods and Programs in Biomedicine. doi: 10.1016/j.cmpb.2005.06.006.

Waxenbaum JA, Reddy V, Williams C, Futterman B. StatPearls [Internet]. StatPearls Publishing; Treasure Island (FL): Jul 30, 2023. Anatomy, Back, Lumbar Vertebrae.

Wilke, Hans Joachim, Frank Heuer, and Hendrik Schmidt. 2009. "Prospective Design Delineation and Subsequent in Vitro Evaluation of a New Posterior Dynamic Stabilization System." *Spine*. doi: 10.1097/BRS.0b013e3181920e9c.

Winther, Flemming, Corinne Vigouroux, André Fayt, Veli-Matti Horneman, and Rauno Anttila. 2002. "Letter To the Editor." *Journal of Molecular Spectroscopy* 212(2):223–24. doi: 10.1006/jmsp.2002.8528.

Wu, Aimin, Lyn March, Xuanqi Zheng, Jinfeng Huang, Xiangyang Wang, Jie Zhao, Fiona M. Blyth, Emma Smith, Rachelle Buchbinder, and Damian Hoy. 2020. "Global Low Back Pain Prevalence and Years Lived with Disability from 1990 to 2017: Estimates from the Global Burden of Disease Study 2017." *Annals of Translational Medicine* 8(6):299–299. doi: 10.21037/atm.2020.02.175.

Yann Philippe Charles, Lucas Venancio Pires Carvalho Lima, Sylvain Persohn, Philippe Rouch, Jean-Paul Steib, Wafa Skalli," Influence of an auxiliary facet system on intervertebral discs and adjacent facet joints", The Spine Journal,Volume 13, Issue 10, 2013, Pages 1293-1300, ISSN 1529-9430, https://doi.org/10.1016/j.spinee.2013.06.019.

Zhang, Ju, David Ackland, and Justin Fernandez. 2018. "Point-Cloud Registration Using Adaptive Radial Basis Functions." Computer Methods in Biomechanics and Biomedical Engineering 21(7):498–502. doi: 10.1080/10255842.2018.1484914.

Zhang, Ju, Duane Malcolm, Jacqui Hislop-Jambrich, C. David L. Thomas, and Poul M. F. Nielsen. 2014. "An Anatomical Region-Based Statistical Shape Model of the Human Femur." *Computer Methods in Biomechanics and Biomedical Engineering: Imaging and Visualization*. doi: 10.1080/21681163.2013.878668.

Zhang, Zhenjun, Guy R. Fogel, Zhenhua Liao, Yitao Sun, and Weiqiang Liu. 2018. "Biomechanical Analysis of Lumbar Interbody Fusion Cages with Various Lordotic Angles: A Finite Element Study." *Computer Methods in Biomechanics and Biomedical Engineering* 21(3):247–54. doi: 10.1080/10255842.2018.1442443.

Zhong, Z. C., Wei, S. H., Wang, J. P., Feng, C. K., Chen, C. S., & Yu, C. H. (2006). Finite element analysis of the lumbar spine with a new cage using a topology optimization method. *Medical engineering & physics*, *28*(1), 90-98.